

Harnessing haplotype sharing information from low coverage sequencing and sparsely genotyped data

Sam Morris

A dissertation submitted in partial fulfillment
of the requirements for the degree of
Doctor of Philosophy
of
University College London.

UCL Genetics Institute
University College London

September 17, 2021

I, Sam Morris, confirm that the work presented in this thesis is my own. Where information has been derived from other sources, I confirm that this has been indicated in the work.

Abstract

Acknowledgements

Acknowledge all the things!

Contents

1	Introduction	25
1.1	Chromopainter and ancient DNA	25
1.2	Methods used to analyse ancient DNA	25
1.3	Combining data from multiple chips	27
1.4	Issues with low coverage	27
1.4.1	Gains to be made with haplotype information	28
2	ChromoPainter and ancient DNA	29
2.1	Introduction	29
2.2	Methods	30
2.2.1	Description of the ChromoPainter algorithm	30
2.2.2	Generation of downsampled genomes	33
2.2.3	Generation of reference ancient samples	34
2.2.4	Imputation and phasing - GLIMPSE	35
2.2.5	Estimating imputation sensitivity and specificity	37

<i>Contents</i>	6
2.2.6 ChromoPainter analysis	38
2.2.7 ChromoPainter Principle Component Analysis	39
2.2.8 SOURCEFIND	40
2.3 Results	42
2.3.1 atlas genotype calling accuracy	42
2.3.2 Imputation accuracy	42
2.3.3 Phasing accuracy	45
2.3.4 Validating posterior probability calibration	45
2.3.5 ChromoPainter analysis	47
2.3.6 SOURCEFIND	55
2.4 Issues and possible solutions for low coverage ancient DNA . . .	58
2.4.1 PCA imputation test	58
2.4.2 Direct imputation test	59
2.5 Solutions	65
2.5.1 Accounting for allele likelihoods	65
2.5.2 Filtering SNPs	65
2.5.3 Upweighting densely genotype regions of high coverage .	67
2.5.4 Incorporating the sample size vector into SOURCEFIND	76
 3 Investigating the sub-continental ancestry of ethnic minorities within the UK Biobank from sparse genotype data	 77

3.1	Introduction	77
3.2	Methods	78
3.2.1	Data access	78
3.2.2	ADMIXTURE analysis	78
3.2.3	Data preparation - imputed data	78
3.2.4	Data preparation - non imputed data	79
3.2.5	Imputation bias test	80
3.2.6	Chromopainter	81
3.2.7	SOURCEFIND	81
3.3	Results	81
3.3.1	ADMIXTURE	81
3.3.2	Chromopainter	83
3.3.3	Verifying painting accuracy	85
3.3.4	Imputation bias	87
4	Bavaria ancient DNA	90
4.1	Introduction	90
4.2	Methods	92
4.2.1	Data generation	92
4.2.2	Stuff that Jens did (e.g. read aligning)	94

<i>Contents</i>	8
4.2.3 Genotype imputation and phasing using GLIMPSE	94
4.2.4 Estimation sample-heterozygosity	95
4.2.5 plink PCA	95
4.2.6 Chromopainter analysis	96
4.2.7 SOURCEFIND	98
4.2.8 MOSAIC admixture analysis	100
4.2.9 Allele-frequency based tests	101
4.3 Results	102
4.3.1 Broad overview of genetic ancestry	102
4.3.2 Early Neolithic	105
4.4 Hunter-gather ancestry in Neolithic farmers	109
4.4.1 Late Neolithic	113
4.4.2 Bronze Age	117
4.4.3 Iron Age	117
4.4.4 Modern day legacy of the Altheim and Molzbichl samples	118
4.4.5 Sample heterozygosity and homozygosity	120
4.4.6 Discussion	120
5 The genomics of the Slavic migration period, Early Middle Ages and their links to the present day	123
5.1 Introduction	123

5.2 Methods	127
5.2.1 Description of samples	127
5.2.2 Ancient DNA processing	128
5.2.3 present-day DNA processing	129
5.2.4 plink PCA	130
5.2.5 Sample heterozygosity and ROH	130
5.2.6 Allele-frequency based tests	131
5.2.7 ChromoPainter and fineSTRUCTURE analysis	131
5.2.8 SOURCEFIND ancestry proportion analysis	132
5.2.9 MOSAIC admixture analysis	134
5.3 fastGLOBETROTTER admixture analysis	134
5.4 Results	136
5.4.1 Mixed ancestry of migration period Slavs	136
5.4.2 Early Middle Age Slavs	141
5.4.3 Do the samples cluster together - TVD permutation test	142
5.4.4 Interactions between the two groups	144
5.4.5 Legacy of Slavic migrations in present-day individuals . .	146
5.4.6 Continuity with present-day day Slavs	150
5.4.7 Genetic structure and admixture events of present-day Slavic people	150

<i>Contents</i>	10
5.5 Discussion	153
6 General Conclusions	157
Appendices	158
A Datasets used	158
A.1 Antonio et al 2019	158
A.2 Margaryan et al 2020	158
A.3 Rivollat et al 2020	159
A.4 Brunel et al 2018	159
A.5 Allentoft et al 2015	159
A.6 Broushaki et al 2016	160
A.7 Cassidy et al 2016	160
A.8 de Barros Damgaard et al 2018a	160
A.9 de Barros Damgaard et al 2018b	161
A.10 Gamba et al 2014	161
A.11 Gunther et al 2015	161
A.12 Hofmanová et al 2016	162
A.13 Jones et al 2015	162
A.14 Marchi et al 2020	162
A.15 Olalde et al 2014	163

A.16 Sánchez-Quinto et al 2019	163
A.17 Seguin-Orlando et al 2014	163
A.18 30x 1000 genomes dataset	164
A.19 Human Origins dataset	164
A.20 MS POBI HellBus dataset	165
B Another Appendix About Things	166
C Colophon	167
Bibliography	168

List of Figures

2.1 Sensitivity of genotype calling at different coverages for different ancient individuals. calculated using rtg-tools. Calculated relative to the full coverage genome.	43
2.2 Precision of genotype calling at different coverages for different ancient individuals. calculated using rtg-tools. Calculated relative to the full coverage genome.	44
2.3 Percentage of phased genotypes which agree with the reference for each individual and each level of downsampling. Genotypes with phase deemed unresolvable by rtg-tools were excluded from the calculations. Note that these numbers are given as incorrect / (incorrect + correct - unresolved) and so values are in part driven by the relative heterozygosity of each sample.	46
2.4 Relationship between genotype likelihood and probability of genotype call being correct for Yamnaya downsampled to 0.1x coverage. Genome binned by maximum posterior genotype likelihood and mean maximum posterior genotype likelihood (x-axis) and proportion of correct calls per bin (y-axis). Rugs on each margin show the distribution of x and y values. Black line is $y = x$	48

2.5 For five different samples (columns), the proportion of DNA that each downsampled (y-axis) or full coverage (x-axis) genome matches to each of 125 ancient individuals (dots). Results are shown for 0.1x (top row) and 0.5x (bottom row) downsampled genomes.	49
2.6 TVD (metric of copyvector dissimilarity between two individuals) between each downsampled ancient individual and a flat copyvector. Flat copyvector equivalent to a vector of length N where each element = $1/N$	51
2.7 For five different samples (columns), the proportion of DNA that each downsampled (y-axis) or full coverage (x-axis) genome matches to individuals from each of 26 present-day populations (dots). Red line is $y = x$	52
2.8 Principle component analysis (PCA) of downsampled, full coverage and reference ancient individuals generated from the linked chunklengths matrix. Full coverage and downsampled genomes of the same individual are coloured the same. Reference individuals are grouped into populations plotted as the mean principle components for all individuals within the population[NEXT TO EACH LABEL, CAN YOU THEN PUT THE NUMBER OF INDS IN THAT POPULATION (JUST FOR CASES WITH > 1 INDIVIDUAL?)].	54
2.9 Each panel gives information for a different downsampled genome. Bars represent proportion of ancestry, coloured by different surrogates. Different coverages for the same individual are given within each panel. Three surrogates were used.	56

- 2.10 Each panel gives information for a different downsampled genome. Bars represent proportion of ancestry, coloured by different surrogates. Different coverages for the same individual are given within each panel. All 39 ancient surrogates were used. [ONE OPTION MIGHT BE TO COLOR ONLY {Ana_Neo,WHG,Yamnaya} AS IN FIG 2.9, THOUGH SF12 WILL BE ODD. CAN YOU SOMEHOW CATEGORISE THE SURROGATES INTO HOW THEY FALL INTO THOSE THREE FIG 2.9 CATEGORIES?]. 57
- 2.11 Principle Component Analysis on pre-imputed genotypes of all downsampled and full coverage ancient samples projected onto a set of modern populations. White labels correspond to the midpoint of all samples from that population, grey points correspond to modern individuals. 60
- 2.12 Principle Component Analysis on post-imputed genotypes of all downsampled and full coverage ancient samples projected onto a set of modern populations. White labels correspond to the midpoint of all samples from that population, grey points correspond to modern individuals. 61
- 2.13 Principle Component Analysis on post-imputed ChromoPainter output of all downsampled and full coverage ancient samples projected onto a set of modern populations. White labels correspond to the midpoint of all samples from that population, grey points correspond to modern individuals. 62

2.14 Principle Component Analysis on post-imputed ChromoPainter output of all downsampled and full coverage ancient samples projected onto a set of modern populations. White labels correspond to the midpoint of all samples from that population, grey points correspond to modern individuals.	63
2.15 Comparison of mean chunk size (cM) when using imputed and non-imputed SNPs. Each point is an individual.	64
2.16	66
2.17 R-squared between downsampled and full coverage copyvectors when filtering out sites with $0.1 < RAF > 0.9$ at 0.1x coverage (top row?L) and 0.5 coverage (R). [PERHAPS BETTER TO SHOW THIS – AND FIG 2.14 – AS A TABLE OF r^2 VALUES, SHOWING THE PREVIOUS CASE AND AFTER REDUCING LOW-FREQUENCY VARIANTS]	67
2.18 R-squared between downsampled and full coverage copyvectors when filtering out sites with $\max(GP) \geq 0.990$ at 0.1x coverage (L) and 0.5 coverage (R).	68
2.19 Relationship between copyvectors using reduced (y-axis) and full (x-axis) set of SNPs. Panels indicate different levels of reduced SNPs ($0.002 = 0.002 * \text{full number of SNPs}$). Copyvectors were estimated by averaging across all individuals within each population (black points). Also shown in red are the sample sizes of each donor population.	70

- 2.20 Relationship between copyvectors using reduced (y-axis) and full (x-axis) set of SNPs. Panels indicate different levels of SNP density. Copyvectors were estimated by averaging across all individuals within each population (black points). Also shown in red are the sample sizes of each donor population.**[AGAIN IS IT POSSIBLE TO INCORPORATE UNLINKED FOR COMPARISON – PRESUMABLY 'SPARSE' SHOULD BE THE SAME AS UNLINKED?]** 72

- 2.21 R-squared between the copyvectors estimated from 'dense' and full SNP sets (y-axis) using different sample sizes (x-axis). 'Dense' SNP set corresponds to the SNPs located on chromosome 22 at 0.9 density. Copyvectors were estimated by aggregating n randomly selected individuals within the population, corresponding to the x axis-value. Green line is local polynomial regression line.
[TO BE CLEAR – FOR EACH X-AXIS VALUE, YOU ARE USING THE SAME INDIVIDUALS WHEN CALCULATING THE 'DENSE' AND FULL-COVERAGE COPY-VECTORS? ALSO SHOULD NOTE THIS IS FOR CORNWALL.] 74

3.5 Correspondence of true birth country with estimated birth country. Each bar corresponds to a true birth country, with the length of the bar corresponding to the total number of people in our dataset born in that country. The green section corresponds to the total number of individuals where the birth country was correctly guessed and the red section to those who were incorrectly guessed. Percentage labels give percentage correct for that country.	87
3.6 The top 10 Human Origins populations which donate more haplotypes under when data is imputed compared to non-imputed. Each point corresponds to the difference between the amount an individual from that donor population donated using imputed and non-imputed data, with positive values corresponding to more copying when the is imputed.	89
4.1 Map of newly sequenced ancient individuals, positioned according to where they were excavated. Colour on label corresponds to archaeological culture which they were found.	92
4.2 Estimated radiocarbon dates for each newly sequenced ancient individual, grouped by archaeological period.	93
4.3 Principle component analysis of genotype matrix using plink2. Grey points indicate principle component coordinates for each sample. Black text indicated mean principle component coordinates for all individuals within that group. Coloured labels represent newly sequenced ancient samples.	104

- 4.4 Principle component plot of newly sequenced ancient samples and reference modern individuals performed using the finestructure library. Green labels correspond to Migration Era samples, red labels correspond to Early Middle Age samples and white labels correspond to reference populations. The position of each reference label is the mean PC coordinates of all individuals within that population. Transparent coloured points correspond to present-day individuals. 105
- 4.5 Principle component plot of newly sequenced ancient samples and reference ancient individuals performed using the finestructure library. Filled labels correspond to newly sequenced individuals and white labels correspond to reference populations. The position of each reference label is the mean PC coordinates of all individuals within that population 108
- 4.6 SOURCEFIND ancestry proportion estimates for all newly sequenced target samples (vertical columns). Target samples are grouped by archaeological age. Surrogate populations are represented as horizontal rows and also grouped into archaeological culture. Each target was modeled as a mixture of only populations which are dated to being older or contemporaneous as the the target. Numbers within each cell correspond to the ancestry proportion estimate. 110
- 4.7 Copying matrix plot for sources in 2-way admixture event for Erg1. Each panel represents one of the 2 mixing sources. Labels above each panel gives the proportion that mixing source contributed to the Early Middle Age samples. Length of the bars within each panel represent the amount that mixing source copied from a particular population. 112

4.8 qpAdm ancestry proportion estimates for a selection of European Neolithic individuals. All individuals were modeled as a 2-way mixture between Anatolian Neolithic farmers and Western-Hunter Gatherers (WHG). Outgroups given in methods 4.2.9. . .	114
4.9 SOURCEFIND ancestry proportion estimates for all newly sequenced target samples (vertical columns). Target samples are grouped by archaeological age. Surrogate populations are represented as horizontal rows and also grouped into archaeological culture. Each target was modeled as a mixture of only populations which are dated to being older or contemporaneous as the target. Numbers within each cell correspond to the ancestry proportion estimate.	115
4.10 Differences in haplotype-donation to	121
4.11	122
5.1 Principle component plot of newly sequenced ancient samples and reference ancient individuals performed using the plink2. Green labels correspond to Migration Era samples, red labels to Early Middle Age samples and black as reference populations. The position of each reference label is the mean PC coordinates of all individuals within that population	137
5.2 Principle component plot of newly sequenced ancient samples and reference ancient individuals performed using fineSTRUCTURE. Green labels correspond to Migration Era samples, red labels to Early Middle Age samples and black as reference populations. . .	139

5.3 Copying matrix plot for sources in 3-way admixture event for Early Middle Age ancient Slavic samples. Each panel represents one of the 3 putative mixing sources. Labels above each panel gives the proportion that mixing source contributed to the Early Middle Age samples. Length of the bars within each panel represent the amount that putative mixing source copied from a particular population.	143
5.4 Inferred Coancestry Curves obtained from modeling Early Middle Age samples as a 3-way mixture of present-day individuals. Black lines are empirical coancestry curves across all target individuals, light grey are per individual, green is the fitted single-event coancestry curve. Note to self - need to figure out what the numbers mean but doesn't say in the manual anywhere.	144
5.5 Distribution of East-Asian minor ancestry component in Early Middle Age samples.	145
5.6 Principle component plot of newly sequenced ancient samples and reference modern individuals performed using the finestructure library. Green labels correspond to Migration Era samples, red labels correspond to Early Middle Age samples and white labels correspond to reference populations. The position of each reference label is the mean PC coordinates of all individuals within that population. Transparent coloured points correspond to present-day individuals.	147

5.11 MOSAIC inferred 2-way admixture dates with bootstrapped 97.5% and 2.5% CI. Vertical green lines correspond to radiocar- bon estimated dates of Migration Period samples and red lines equivalent for Early Middle Age samples.	154
5.12 $1 - F_{st}$ between 3 inferred mixing sources for present-day Be- lorussians. Each panel represent a different mixing source. Each bar gives the value $1 - F_{st}$ between that samples population and the mixing source. Higher values of $1 - F_{st}$ suggest that source is well represented by a particular population.	155

List of Tables

4.1	Name of population and number of samples used in the present-day ChromoPainter analysis	98
5.1	Name of population and number of samples used in the present-day ChromoPainter analysis	133
5.2	Name of populations and number of samples used in the present-day MOSAIC analysis	135

Chapter 1

Introduction

1.1 Chromopainter and ancient DNA

In this introduction, I will discuss i) the broad outline of methods used to determine population structure in ancient DNA, ii) the history and usage of haplotype-based methods in ancient DNA and iii) the history of imputation in ancient DNA.

1.2 Methods used to analyse ancient DNA

The first ancient DNA papers relied principally on statistical methods based upon allele-sharing or allele-frequencies. These methods, in particular f-statistics [1–3] and Principle Component Analysis [4].

The early studies of ancient DNA generally considered broad-scale questions about human history, such as the nature of human-archaic interactions or the spread of farming technology across Europe [5]. Due to the infancy of the field, sample sizes were small, as efficient methods to obtain genetic data from ancient samples, such as SNP capture arrays, had yet to be developed. These studies tended to look for genetic differences between populations which had been diverged for many generations; in such cases, powerful methods are not

required. In the case of Lazaridis et al (2014), simply plotting Loschbour and Stuttgart/LBK on a PCA of modern individual showed they had substantially divergent ancestries, with Loschbour being most similar to present-day North-East Europeans, but falling well outside the variation of present-day Europeans, and Stuttgart clustering with present-day individuals from Tuscany.

Such methods, which I will hereafter refer to as ‘unlinked’, as they assume a model of linkage equilibrium between neighbouring SNPs, are useful for ancient DNA studies. Firstly, it is relatively easy to account for missingness in the data, by using e.g. a PCA projection.

The first use of chromopainter on ancient DNA was in a seminal paper from Lazaridis et al (2014) [5]. The two samples, Loschbour and Stuttgart, were of high coverage and therefore imputation was not used.

Perhaps the first study to explicitly investigate chromopainter on ancient DNA was Martiniano et al (2017) [6]. They first tested the accuracy of imputation on ancient DNA samples

As sample sizes used in ancient DNA studies has rapidly increased to >100 , more analyseses have incorporate haplotype-based methods. Each study typically carries out a small analysis to ensure that imputation in low-coverage ancient DNA samples is accurate. Antonio et al (2019) [7] analysed 127 ancient genomes of a mean coverage of 1x. To test imputation accuracy, they downsampled a single individual (NE1) to different levels of coverage and calculated the proportion of genotypes which matched the full coverage. However, this analysis was only performed on a single sample and the effect of imputation on the chromopainter process was not evaluated.

More recently, ChromoPainter has been used to study aspects of archaic hominin ancestry in present-day humans [8,9].

1.3 Combining data from multiple chips

A related issue stems from the current practice of developing a large number of genotyping arrays. Different cohorts are genotyped on different arrays and sets of SNPs, as different SNPs have different characteristics. For example, some SNPs are known to be associated with particular phenotypes, some SNPs are known to be more variable (and therefore more informative at identifying structure) in certain populations.

1.4 Issues with low coverage

Coverage is an issue which has plagued the field of ancient DNA since its inception. Compared to DNA obtained from present-day samples, ancient DNA samples typically have a much lower proportion of endogenous DNA. This is because DNA degrades over time from environmental factors. Therefore, when the DNA fragments are sequenced, relatively few of them will align to the human reference. The coverage of a genome is therefore the mean number of reads mapped to each position in the genome.

The primary issue with low-coverage data is the increased uncertainty when calling diploid genotypes, particularly when the true genotype is heterozygous. To mitigate this issue, many studies used ‘pseudo-haploid’ genotyping, where a diploid genotype is reduced to a haploid by randomly sampling an allele from all the reads which have been aligned to that position in the genome. Whilst the use of pseudo-haploid calling eradicates the need to call heterozygous genotypes at low coverage positions, it also necessarily reduces the amount of information present at each position in the genome.

I will discuss in more detail later the effect of coverage on other methods.

1.4.1 Gains to be made with haplotype information

Here, I will define ‘haplotype-based’ method as one which explicitly models linkage between neighbouring SNPs. Although LD has been studied since the earliest days of genetics (cite), its use in population structure inference was developed in the early 2000s [10].

Accounting for recombination and LD within a model is necessarily computationally complex, as the number of combinations of alleles and their associated evolutionary histories balloons as the number of loci considered increases (does it scale quadratically?). The Li and Stephens copying model was instrumental in the development of such methods [11] and provided an elegant solution to the increased complexity when using linked loci. As such, it is now a critical model in virtually all areas of genomic methodology, from imputation, phasing etc etc.

Perhaps the first paper to formalise a haplotype-based approach was that of Hellenthal et al 2008 [12].

Later, Lawson et al (2015) [13] developed what is now one of the leading approaches to modeling linkage between markers. This study showed that ChromoPainter had an enhanced ability to separate closely related populations when plotted on a PCA. ChromoPainter was originally developed in tandem with its own clustering method fineSTRUCTURE, and has since been extended into methods to detect and date admixture, and infer ancestry proportions.

It has since become a mainstay of population genetic research

Usage of haplotype-based methods is not without drawbacks. They are typically slower by several orders of magnitude

Chapter 2

ChromoPainter and ancient DNA

2.1 Introduction

This chapter is related to the use of ChromoPainter on low coverage ancient DNA samples.

First, I will describe the existing methodology, ChromoPainterV2, and then 2 new versions, ChromoPainterUncertainty and ChromoPainterUncertaintyRemoveRegions, which are designed to attempt to mitigate bias related to sequencing coverage.

Next I will perform benchmarking tests on all the steps necessary to analyse low-coverage ancient DNA with ChromoPainter; genotype calling and genotype likelihood estimation with atlas [14], phasing and genotype imputation with GLIMPSE [15], ChromoPainter [13] analysis (copy-vector estimation and PCA) and SOURCEFIND ancestry component estimation [16]. Lastly, I will describe some of the existing issues pertaining to low coverage ancient DNA and several considered mitigation strategies.

2.2 Methods

2.2.1 Description of the ChromoPainter algorithm

ChromoPainter is a method designed to infer patterns of haplotype sharing between individuals [13]. The individuals being analysed are split into 'donor' and 'recipient' haplotypes - in diploid organisms such as humans and dogs, each individual thus consists of 2 haplotypes. It employs the widely-used Li and Stephens copying model [17] to model each recipient haplotype as a mosaic of haplotypes observed in the donor panel. Unlike the original Li and Stephens model, which uses the product of approximate conditionals (PAC likelihoods), ChromoPainter reconstructs each recipient haplotype as a mosaic of *all* other donor haplotypes. Here, the term 'copying' can be thought of as a genealogical process where haplotypes are reconstructed using the genealogically closest haplotype. The copying model is implemented in the form of a Hidden Markov Model (HMM), with the observed states being the genotype data, and the hidden states being the 'nearest-neighbor' haplotype the recipient haplotype copies from. The emission probabilities are given as the probability of a recipient haplotype copying from a particular donor haplotype, given their respective genotypes. Consider a donor d and recipient r , each with an allele x at position p . There are two possibilities - either the alleles match between the donor and recipient at p , or they do not. The probability of r copying from d is:

$$p(r_x|d_x) = [(1 - \theta) * z_{dr}] + [\theta * z_{!dr}] \quad (2.1)$$

where $z_{dr} = 1$ if d and r both carry allele x , and otherwise $z_{!dr} = 0$, and θ is some pre-specified error likelihood, usually on the order of 0.001.

The transition probabilities (i.e. the probabilities of a change in r copying from one donor haplotype to another) is guided by a recombination rate map, with higher recombination rates leading to a higher probability of transitioning.

Switches between donors are interpreted as changes in ancestral relationships because of historical recombination.

In ChromoPainterV2, the input genetic data comes in the form of genotype calls (i.e. 1/0, A/T/C/G).

ChromoPainterV2 produces several different output files. The two which are most used in this work are those appended with .chunklengths and .chunkcounts. The chunklengths matrix, cl , the entry $cl_{d,r}$ gives the total number of chunks that recipient r copies from donor d . Thus, higher values of $cl_{d,r}$ indicate that recipient r and donor d share more recent ancestry.

In this work, 'copyvector' is used to refer to the vector of chunklengths that a single recipient individual copies from all donors.

2.2.1.1 EM parameter estimation

The Li and Stephens copying model that ChromoPainter is based on has two scaling parameters that may be estimated from the data (and set the same for all individuals).

We can either take a fixed value for N_e when calculating ρ , or use the EM algorithm to find a local maximum from the dataset. Begin with an initial value of N_e , and then at each iteration of the EM, replace N_e with:

$$N_e = \frac{\sum_{l=1}^{L-1} ([\sum_{k=1}^j \hat{f}_{k,l}] [\rho_l] / [1.0 - e^{-\rho * l})]}{\sum_{l=1}^{L-1} gl} \quad (2.2)$$

Where L is the total number of SNPs, j is the total number of donor haplotypes,

Similarly, the mutation rate θ can be estimated using Watterson's estimator [18], or estimated using an iterative EM algorithm. Begin with an estimate of θ , usually Watterson's estimate, and at each iteration, replace the value of θ

with:

$$\theta^* = \frac{\sum_{l=1}^L (\sum_{i=1}^j \alpha_{il} \beta_{il} I_{[h_{*l} \neq h_{il}]}/P(D))}{L} \quad (2.3)$$

2.2.1.2 Description of ChromoPainterV2Uncertainty

ChromoPainterUncertainty works in a very similar to ChromoPainterV2, bar 2 differences. Firstly, rather than genotypes, the input data is in the form of an allele probability $0 \leq x_p \leq 1$, which is given as the probability of observing the alternate allele at that position in the genome. This value is calculated from the posterior likelihood that an allele has been imputed correctly.

Consider the following example; we have a phased genotype in the form $0|1$, corresponding to the reference allele on the first haplotype and the alternative allele at the second haplotype. I define G as the sum of the genotypes at a SNP; in this case $G = 0 + 1$

We also have a posterior genotype likelihood, in the form $GL(p_a, p_b, p_c)$, where a , b , and c are the posterior genotype probabilities. Dosage, D , is the expected total number of copies of the alternate allele given GL . We can calculate U , the uncertainty as $U = |G - U|$. Then, we can assign a probability to each allele; if the allele is 1 then the allele likelihood is simply $1 - U$ and if the allele is 0 then the allele likelihood is $0 + U$.

The second difference is the incorporation of the allele probability into the emission probability of the HMM. As before, consider a donor d and recipient r at position p .

$$\begin{aligned} p(r_x|d_x) = & (1 - \theta) * [r_{xp} * d_{xp} + (1 - r_{xp}) * (1 - d_{xp})] \\ & + \theta * [r_{xp} * (1 - d_{xp}) + (1 - r_{xp}) * d_{xp}] \end{aligned} \quad (2.4)$$

, where r_{xp} is the probability that r carries the alternate allele, and d_{xp} is the probability that the donor carries the alternate allele. Note that above (3) reduces (1) if $d_{xp} = 0/1$ and if $r_{xp} = 0/1$ (i.e. there is no uncertainty in the calls).

2.2.1.3 Description of remove regions

There is one difference between ChromoPainterV2Uncertainty and ChromoPainterV2UncertaintyExcludeRegions. The user specifies 2 additional parameters. The first of these, -c, has 2 functions. The first of these is to act as the uncertainty threshold when removing regions (see below), such that SNPs with $u > c$, where:

$$u = \min(|1 - x_p|, x_p) \quad (2.5)$$

and u is the uncertainty estimate. The second additional parameters, $-l_1$ l_2 , controls the length of regions and allowed uncertainty of regions to be excluded. l_1 specifies a region of contiguous SNPs above the threshold c , which extends until there are l_2 mismatches. If a window of SNPs does not meet the criteria specified by the user, then it is excluded from the analysis.

2.2.2 Generation of downsampled genomes

I created a set of ‘downsampled’ genomes in order to explicitly quantify the effect of coverage each stage of the ChromoPainter analysis. Downsampling involves taking a high coverage genome and removing a random subset of reads from the .bam file in order to reduce the coverage to a target level. I then performed each stage of the analysis on the full coverage and downsampled genomes and compared the results to determine how they are affected by coverage.

Five high coverage ancient genomes were downloaded in the form of aligned .bam files from the European Nucleotide Archive; Yamnaya (Yamnaya Bronze Age steppe-pastoralist) [19], UstIshim (Siberian Upper Paleolithic hunter-gatherer) [20], sf12 (Scandinavian Hunter-Gatherer) [21], LBK (early European farmer from the Linearbandkeramik culture from Stuttgart, Germany) [5] and Loschbour (an 8,000 year-old hunter-gatherer from Luxembourg) [5]. The samples were chosen due to their high original coverage and diversity of ancestries.

Each .bam file was processed using the atlas (version 1.0, commit f612f28) pipeline [14] (<https://bitbucket.org/wegmannlab/atlas/wiki/Home>). First, each file was validated using ValidateSamFile command from PicardTools [22].

I downsampled each individual using the `downsample` task, resulting in a .bam file with coverages 0.1x, 0.5x, 0.8x, 1x, 2x, 3.5x, 5x, 10x and 20x per individual.

For each full coverage and downsampled .bam file, I estimated post-mortem damage (PMD) patterns using atlas `estimatePMD` task. Recalibration parameters were then estimated using atlas `recal` task. Finally, both the recalibration and PMD parameters were given to the `callNEW` task which produces genotype calls and genotype likelihood estimates for each downsampled and full coverage .bam. For this stage, I made calls at the 77,818,345 genome-wide positions present in the phase 3 thousand genomes project [23]. This was done to reduce the risk of calling false-positive non-polymorphic sites.

2.2.3 Generation of reference ancient samples

I also generated a set of reference ancient samples to use as donors in the ChromoPainter analysis (see section x).

This reference set consists of 918 other ancient samples from the literature. These 918 consist of all samples from appendices A1, A2, A3, A4, and they

were processed according to the stages outlined in appendix B.X, resulting in genotype and genotype likelihood information at the same 77,818,345 genome-wide positions. Each reference sample was processed in an identical way to the downsampled target individuals.

2.2.4 Imputation and phasing - GLIMPSE

Genotype refinement/imputation and phasing are two important steps for processing low-coverage ancient DNA. Low coverage (<1x) samples typically lack enough read information to make accurate genotype calls at most positions in the genome, or may not contain any information at some sites at all. Therefore, it can be helpful to use external information from a reference panel in order to improve the accuracy of genotype calls and reduce the impact of errors on downstream analyses. Given ChromoPainter uses haplotype rather than genotype data, it is also necessary to phase the genotypes. Phasing refers to the process of determining which alleles were inherited together on the same chromosome. Imputation and phasing must be performed on all full coverage, downsampled and reference ancient individuals.

Three different characteristics are desirable for an imputation algorithm to be useful in this context. Firstly, to allow an input in the form of genotype likelihoods (or phred-Scale genotype likelihoods). This is because genotype likelihoods they allow for flexible representation of the possible genotypes at a particular position, particularly when there may not be enough coverage to make a hard genotype call. Secondly, to emit posterior genotype-probabilities which, when accurately calibrated, give the probability that a particular genotype call is correct. This is crucial for our previous step 2.2.1.2 for including these genotype probabilities into the painting process. Thirdly, the algorithm must be able to complete in a reasonable running time when using a large number of samples and high number of SNPs. Using a large number of densely positioned SNPs (e.g. such as the approximately 77 million identified in the 1000 genomes

project) increases the useful linkage-disequilibrium information between each SNP, and it is well-known that increasing the number of individuals used in imputation/phasing reference panels improves accuracy [15, 24–26].

Two programs, Beagle 4.0 [27] and GLIMPSE [15] fulfill the first and second criteria above, but only GLIMPSE runs quickly enough to analyse SNPs with sequence-level density. GLIMPSE offers up to 1000x reduction in running time compared to Beagle 4.0 [15], so I chose to use this algorithm for the imputation and phasing steps.

Phasing and imputation ideally requires a reference panel of high-coverage present-day individuals. I used the 1000 Genomes dataset (re-sequenced to 30x coverage), containing 3202 individuals from 26 worldwide populations [28]. A description of the processing of this reference dataset can be found in appendix
...

I next merged together i) the full coverage individuals, ii) downsampled individuals and iii) reference ancient individuals into a single bcf file using bcftools (version 1.11-60-g09dca3e) [29] to act as the target for GLIMPSE. Here, ‘target’ refers to the individuals being imputed/phased and ‘reference’ refers to the reference individuals.

I followed the steps laid out in the glimpse tutorial (https://odelaneau.github.io/GLIMPSE/tutorial_b38.html). First, I used `GLIMPSE_chunk` to split up each reference chromosome into chunks, keeping both `-window-size` and `-buffer-size` to 2,000,000, their default settings. Across all chromosomes, this produced 936 chunks of an average 2.99Mb long. I used the b37 genetic map supplied by GLIMPSE for the `-map` argument.

Each chunk was then imputed separately using `GLIMPSE_phase` using the same 1000 genomes dataset as a reference. Default settings and the supplied b37 genetic map were used. This stage both imputes missing genotypes and generates a set of haplotype pairs which can be sampled from in a later step to

produced phased haplotypes.

`GLIMPSE_ligate` was then used to merge the imputed chunks back to form single chromosomes using the default settings and the supplied b37 genetic map.

Haplotypes were then sampled using `GLIMPSE_sample` to produce a .vcf with phased haplotypes for each individual, again using default settings and the supplied b37 genetic map.

Consequently, the output of GLIMPSE is i) unphased genotype calls with posterior genotype likelihoods and ii) phased haplotypes.

It is important to note that GLIMPSE leverages information from individuals that have been imputed, ‘absorbing’ them into the reference panel. For example, if there were 100 target samples and 1000 reference samples, each target is phased in turn and then absorbed into the reference panel, so that there would be 1001 reference samples when the 2nd target individual is imputed. This makes it necessary to avoid including the same sample, downsampled to different coverages, in the same set of targets for one imputation run, in order to avoid the confounding effect of allowing an individual to act as the reference to itself. For example, including Loschbour at 0.1x and 10x coverage could mean it imputed itself, a situation which would never occur in reality.

2.2.5 Estimating imputation sensitivity and specificity

After imputation has been performed, it is important to know how close to the ‘truth’ genotypes each downsampled genome is and thus how accurate the imputed genotypes are.

I used rtg-tools-3.11 [30] and the `vcfeval` task to estimate the sensitivity and specificity of variant discovery in the downsampled individuals. Here, I define the ‘baseline’ to be the genotype calls in the full coverage individual

and the ‘calls’ as the genotype calls in the downsampled individual. Thus, sensitivity can be calculated as:

$$\text{sensitivity} = \frac{TP_{baseline}}{TP_{baseline} + FN} \quad (2.6)$$

$$\text{precision} = \frac{TP_{call}}{TP_{call} + FP} \quad (2.7)$$

TP , or true-positive, is the number of events where a variant position (i.e. a SNP with a genotype that is either 0/1 or 1/1) is detected in either the full coverage ($TP_{baseline}$) or downsampled ($TP_{baseline}$) sample. FN is the number of times that a variant position is called in the full coverage sample and not the downsampled sample. Conversely, FP is the number of times a variant position is called in the downsampled sample and where the same SNP in the full coverage sample is invariant (i.e. 0/0).

`rtg-tools` also calculates the number of phased heterozygous genotypes in the calls where the phase matches that in the high coverage individual.

2.2.6 ChromoPainter analysis

It is important to understand the effect of sequencing coverage on the accuracy of ChromoPainter copyvector estimation. A ‘copyvector’, cl_r , is a vector of length D , where each entry gives the total length of genome that recipient individual r most closely matches to each of the D donor individual/populations. I sometimes refer to ‘normalised’ copyvectors; this simply refers to where each entry of cl_r is divided by the sum of all entries, scaling the copyvector to sum to 1.

I painted each downsampled and full coverage individual using a set of 124 reference individuals, hereafter referred to as the ‘standard set’, selected because

they had a sequencing depth greater than 2x. I compared the copyvectors for the same individual at each level of downsampling. For example, I compared the copyvector of Yamnaya 0.1x to the copyvector of the same Yamnaya sample at full coverage. A high correspondence between the copyvectors of the full coverage and downsampled individual suggests less effect of coverage and vice versa.

To prepare the data for ChromoPainter, I merged the .vcf containing the posterior genotype likelihoods of i) downsampled, ii) full coverage and iii) reference individuals together, and did the same for the .vcfs containing the phased haplotypes. I combined the posterior genotype likelihoods with the phased alleles to generate allele likelihoods (described in section 2.2.1.2) in ChromoPainter-uncertainty format, in addition to per-position recombination rate files. This was performed for each chromosome in turn using my own script (https://github.com/sahwa/vcf_to_ChromoPainter).

I next used ChromoPainterUncertainty to perform the painting. I assigned all reference individuals as donors and all downsampled, full coverage and reference individuals as recipients.

This produces a chunklengths matrix for each chromosome which were merged using chromocombine-0.0.4 (<https://people.maths.bris.ac.uk/~madjl/finestructure-old/chromocombine.html>). The resulting chunklengths matrix thus gives the total length of genome in centimorgans that a recipient most closely matches to each donor individual.

Unless otherwise specified, I compared copyvectors by calculating the r-squared between the full coverage copyvectors.

2.2.7 ChromoPainter Principle Component Analysis

Principle Component Analysis (PCA) can be used to reduce the underlying structure in the chunklengths coancestry matrix to 2 dimensions and thus

allows it to be visualised.

Principle component analysis was performed on the chunklengths matrix using the IRLBA R library [31].

Including the same sample, downsampled to different levels, would confound the structure on the PCA (maybe explain a bit more what this means). Therefore, it is necessary to perform a slightly altered routine of plotting principle components.

1. Subset the coancestry matrix to only reference ancients and calculate principle component coordinates
2. For each downsampled or full coverage ancient in turn, subset the coancestry matrix to just that ancient plus all reference ancients and calculate principle components
3. Combine eigenvectors from (1) and (2) and plot together

2.2.8 SOURCEFIND

The chunklengths coancestry matrix produced by ChromoPainter contains information about the estimated length of genome a recipient most closely matches a given donor individual or population. However, incomplete lineage sorting, where alleles segregate in a way that is discordant to the ‘true’ population phylogeny, means that there are regions in the genome where a recipient individual most closely matches a reference individual that is not its genealogically closest neighbor in the dataset. This manifests itself as ‘noise’ in the co-ancestry matrix, where, for example, an individual from France copies non-zero amounts from African donors, despite not having any recent African ancestry. Furthermore, unequal donor population sizes may bias the aggregated amount copied to a given population. Accordingly, the values in the lengths coancestry matrix do not correspond to true ancestry proportions, which can

be defined as..... Therefore, in order to account for differences in donor group size and to improve resolution in directly estimating ancestry proportions, it is necessary to run an additional step, SOURCEFIND [16].

SOURCEFIND takes as input i) the chunklengths matrix described in section 2.2.6 and a parameter specification file. This input file allows for the definition of ‘surrogate’ individuals/populations. SOURCEFIND models each target copyvector as a linear mixture of copyvectors from the surrogate groups, inferring the proportion of ancestry that each surrogate group contributes to the target individual. The parameter space of surrogate ancestry proportions is explored using a Markov chain Monte Carlo algorithm, where the ancestry proportions are updated using a Metropolis-Hastings step. The output of SOURCEFIND for each target individual is therefore an $n * p$ matrix, where n is the number of MCMC samples and p is the total number of surrogate groups. Ancestry proportions, credible intervals and chain mixing/convergence checking for each surrogate group were estimated using the CODA R library [32].

To test for the effect of coverage on the proportions estimated by SOURCEFIND, I performed 2 separate analyses, both using the downsampled and full coverage individuals as targets; one using 3 surrogate populations (Yamnaya, Western Hunter-Gatherer and Anatolia Neolithic Farmer) and one using an expanded list of 37 surrogate populations (individuals and population labels in Appendix B.x). I chose the first set of 3 surrogates as these are typically used in ancient DNA analysis to obtain a ‘broad’ overview of the ancestry of an individual, as it has been shown that central Europeans within the last 10,000 years can be well modeled as a mixture of those three groups [5, 33]. Note, this does not mean that there was not admixture from other sources, but that a majority of ancestry of ancient central Europeans can be derived from these sources. This stands to act as a relatively ‘easy’ test case, since the 3 populations are highly genetically differentiated from one another.

For all runs of SOURCEFIND, I used 2,000,000 iterations, of which 50,000

were designated as burn-ins, and then samples were taken every 50 iterations. 2,000,000 iterations were chosen because my previous tests show that is the minimum necessary to provide reasonably confidence of convergence within reasonably running time (reference to appendix?). The rest of the parameters were left as default; `self.copy.ind=0`, `num.slots=100`, `num.surrogates=8`, `exp.num.surrogates=4`. Ancestry proportions were estimated by taking the mean proportion across all iterations.

2.3 Results

2.3.1 atlas genotype calling accuracy

NB: Add in section here comparing the genotype calls of the downsampled individuals to those of the full coverage individuals, but before imputation. Will show us how accurate atlas is and how much improvement we get from imputing genotypes.

2.3.2 Imputation accuracy

I estimated the sensitivity (Fig. 2.1) and precision (Fig. 2.2) of genotype imputation using rtg-tools [30]. This consists of comparing the genotype calls at each position in each downsampled individual after imputation to the same individual at full coverage without imputation.

As expected, both the overall sensitivity and precision of imputation fell with coverage, with a particularly sharp drop-off in both metrics observed at between 0.5x and 0.1x coverage.

Different downsampled individuals differed in the precision and sensitivity of genotype imputation. At all coverages, Yamnaya had the both the highest sensitivity and precision. This may be because the imputation reference panel contained more individuals who are genetically closer to Yamnaya relative

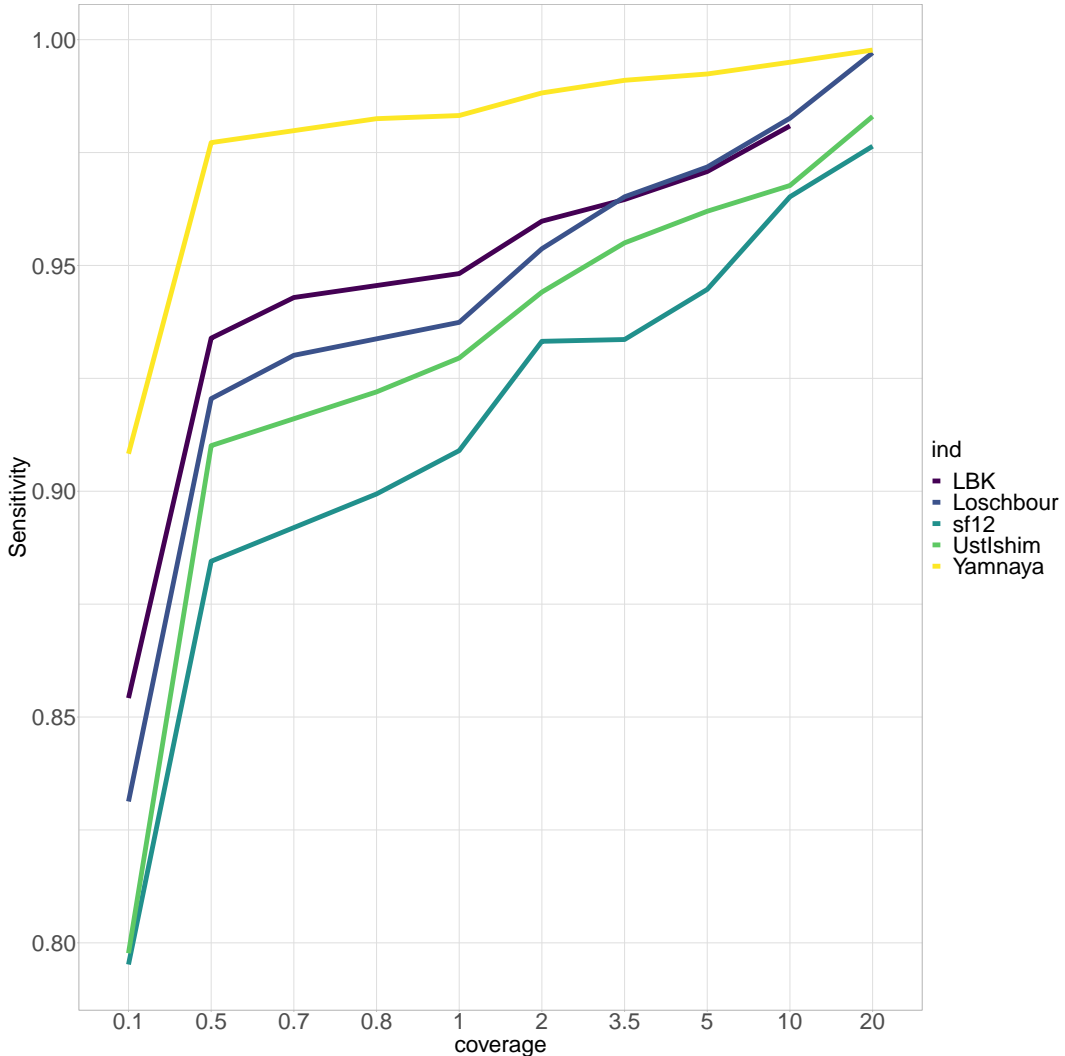


Figure 2.1: Sensitivity of genotype calling at different coverages for different ancient individuals. calculated using rtg-tools. Calculated relative to the full coverage genome.

to the other ancient individuals. This is consistent with modern Europeans containing a high proportion of Yamnaya-like ancestry, relative to e.g. Hunter Gatherer ancestry [34]. Many studies in modern individuals have shown that imputation accuracy increases when more haplotypes which are close to the target individual are found in the reference panel [24, 25]. On the other hand, the sample Ust’Ishim is known to have contributed very little genetic ancestry to modern day populations [35] and will therefore likely have fewer closely matching haplotypes in the reference panel, and correspondingly lower imputation accuracy.

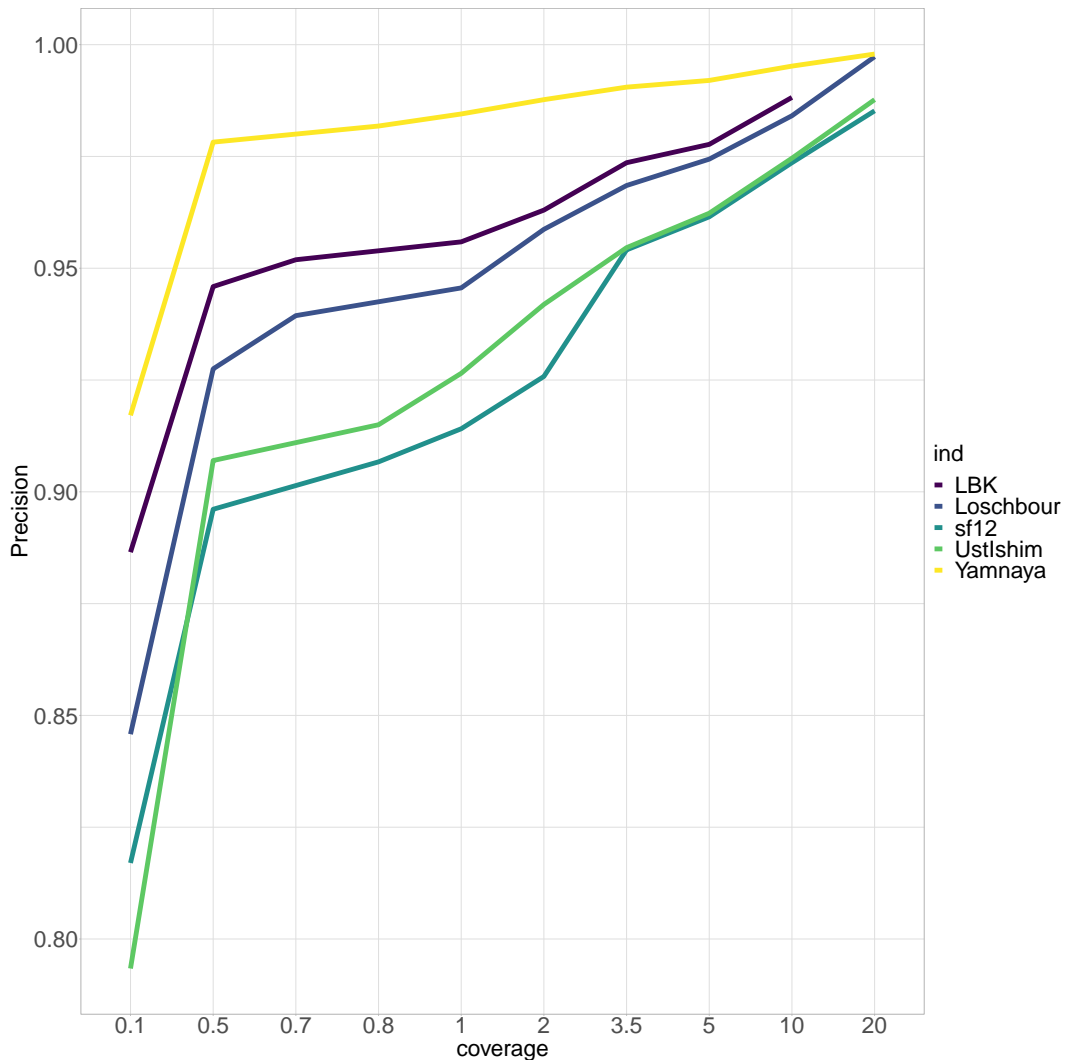


Figure 2.2: Precision of genotype calling at different coverages for different ancient individuals. calculated using rtg-tools. Calculated relative to the full coverage genome.

Imputation accuracy may also be related to demographic history. Populations which are known to have smaller effective population size, such as Western-Hunter Gatherers, also contain longer IBD tracts and fewer heterozygous positions. As imputation relies on matching long IBD tracts between individuals, imputation accuracy increases where individuals share more IBD [36]. Additionally, switch-errors during the pre-phasing step of imputation may harm imputation accuracy, so a reduced density of heterozygous positions can improve accuracy. Put together, both of these facts suggest [DEPENDS ON WHAT YOU CONSIDER HIGH SENSITIVITY AND PRECISION? YOU

SHOULD PROVIDE SOME BASELINE, E.G. WHAT ARE LEVELS LIKE IN MODERNS?]that it is possible to impute variants accurately in e.g. WHG, despite being less well represented in the reference panel.

I used GLIMPSE concordance, a method in GLIMPSE software, which shows the relationship between imputation accuracy and allele frequency.

2.3.3 Phasing accuracy

I used rtg-tools to calculate the number of phased heterozygous genotypes where the downsampled individual has the same phasing as the full coverage individual (Fig 2.3). I note that this should not be considered to be the same as estimating the switch error rate, since we do not know that the phasing in the full-coverage individual is the true phase. However, this can be used as a rough proxy for switch errors, since it is known that phasing in lower coverage individuals is likely to be less accurate than those in the high coverage individuals [15].
[IT'S MORE HELPFUL TO PUT THIS INTO THE CONTEXT OF HOW FREQUENTLY SWITCH ERRORS OCCUR – I.E. HOW MANY CONTIGUOUS SNPS (ON AVERAGE) – AND/OR HOW LONG OF SEGMENTS – ARE CORRECTLY PHASED, AS THIS IS IMPORTANT FOR CHROMOPAINTER]

2.3.4 Validating posterior probability calibration

The posterior genotype probabilities emitted by GLIMPSE give the posterior probability that a given genotype is correctly called. Genotype probabilities are important for downstream analysis, particularly for deciding which variants to filter. However, it is important to confirm that they are well calibrated (i.e. that they accurately reflect the probability a genotype call is correct).

To validate the genotype probabilities, I took a single downsampled Yamnaya 0.1x individual, and took the maximum genotype likelihood at each of the approximately 77 million positions which were processed by GLIMPSE. A high

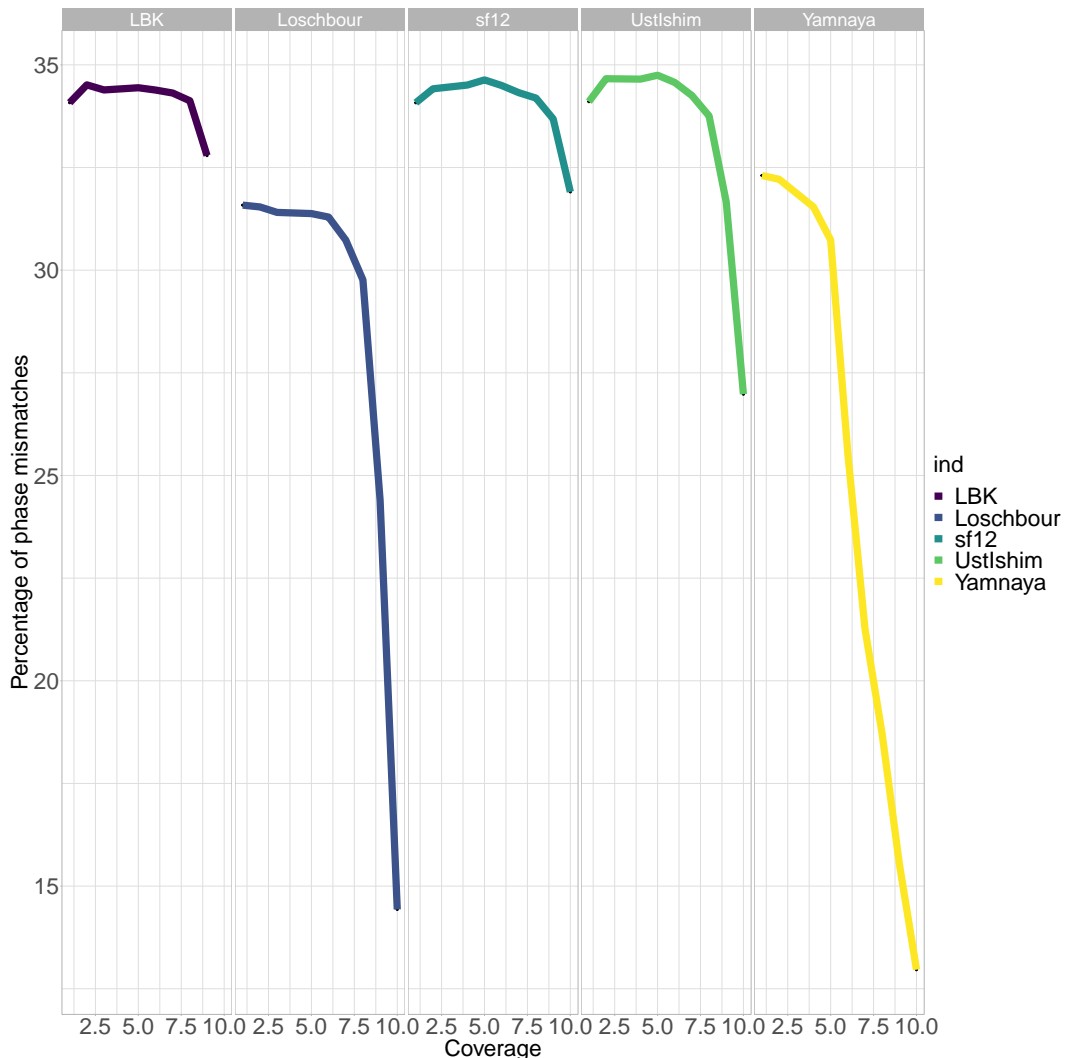


Figure 2.3: Percentage of phased genotypes which agree with the reference for each individual and each level of downsampling. Genotypes with phase deemed unresolvable by rtg-tools were excluded from the calculations. Note that these numbers are given as incorrect / (incorrect + correct - unresolved) and so values are in part driven by the relative heterozygosity of each sample.

$\max(GL)$ for a particular genotype (i.e. 0.99) corresponds to a high confidence in the genotype. Alternatively a flat $\max(GL)$ (i.e. 0.33) corresponds to no information about the genotype.

I then split the genome into 10,000 bins according to $\max(GL)$. For each bin, I calculated both the proportion of SNPs which were correctly imputed (i.e. that matched the same high coverage individual) and the mean $\max(GL)$ (Fig. 2.4). If the genotype probabilities are well calibrated, we would expect to see a clear positive linear relationship between $\max(GL)$ probability and the probability that genotype matches the full-coverage sample.

The figure confirms that the posterior genotype probabilities are well calibrated and should, in theory, be relied upon for downstream analysis. They are slightly conservative, in that a majority of the points in Fig. 2.4 are above the $y = x$ line. For example, the mean proportion of correct genotypes within all bins where $0.73 < \max(GL) < 0.76$ was 82%. I performed the same analysis using different samples at different levels of coverage and the results were qualitatively similar (result omitted).

2.3.5 ChromoPainter analysis

I merged the dataset of downsampled individuals with the ‘standard set’ of ancient reference individuals. I performed an ‘all-v-all’ painting of the merged dataset, which separately paints each individual as a recipient using all other individuals in the dataset as donors.

I was interested in how similar the proportion of genome matching to each donor individual was when comparing a downsampled individual to their corresponding full coverage individual. To do this, I estimated the r-squared between the copyvectors of the full coverage and downsampled individuals.

Fig. 2.5 displays the relationship between copyvectors for each downsampled individual the corresponding full coverage individual for both 0.1x and 0.5x

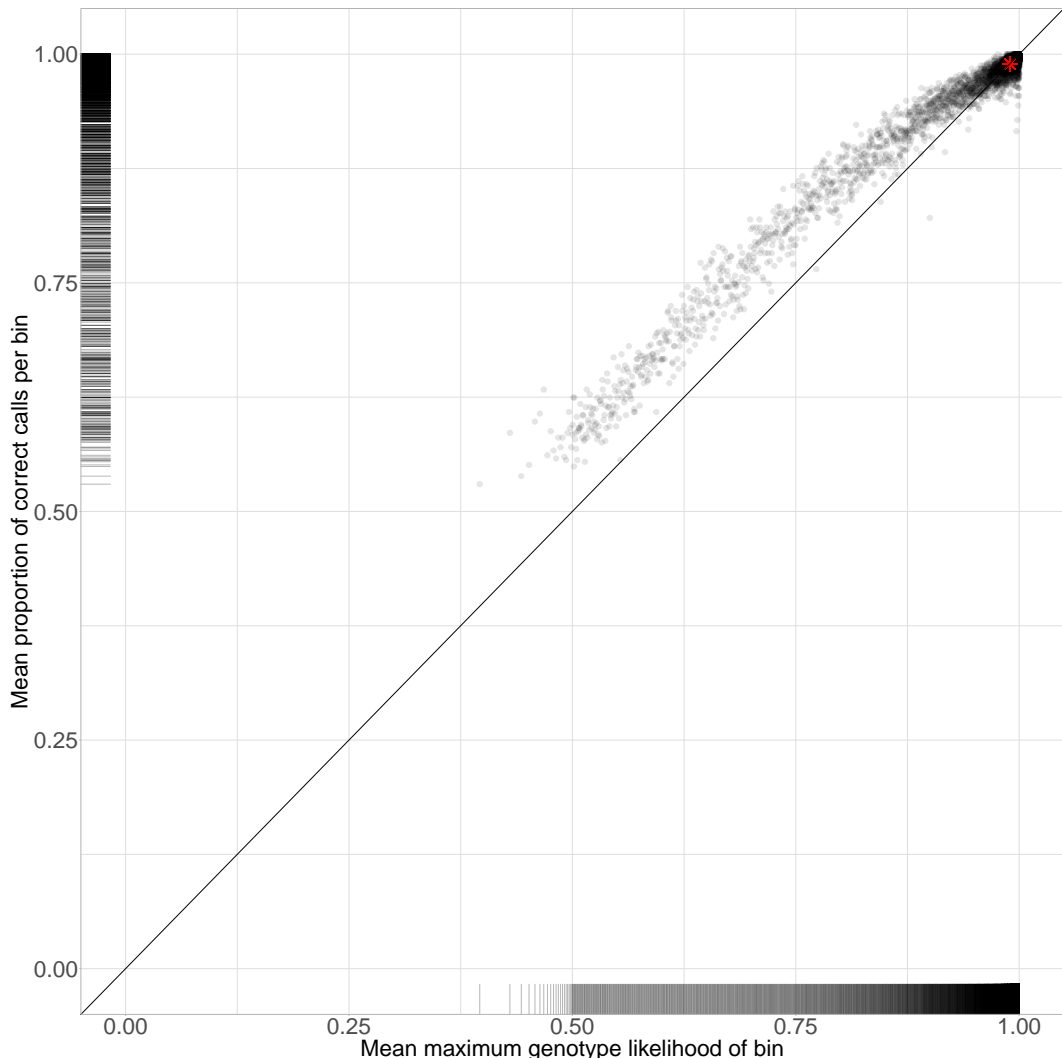


Figure 2.4: Relationship between genotype likelihood and probability of genotype call being correct for Yamnaya downsampled to 0.1x coverage. Genome binned by maximum posterior genotype likelihood and mean maximum posterior genotype likelihood (x-axis) and proportion of correct calls per bin (y-axis). Rugs on each margin show the distribution of x and y values. Black line is $y = x$.

coverage. Copyvectors were estimated using the set of high-coverage ancient samples as donors.

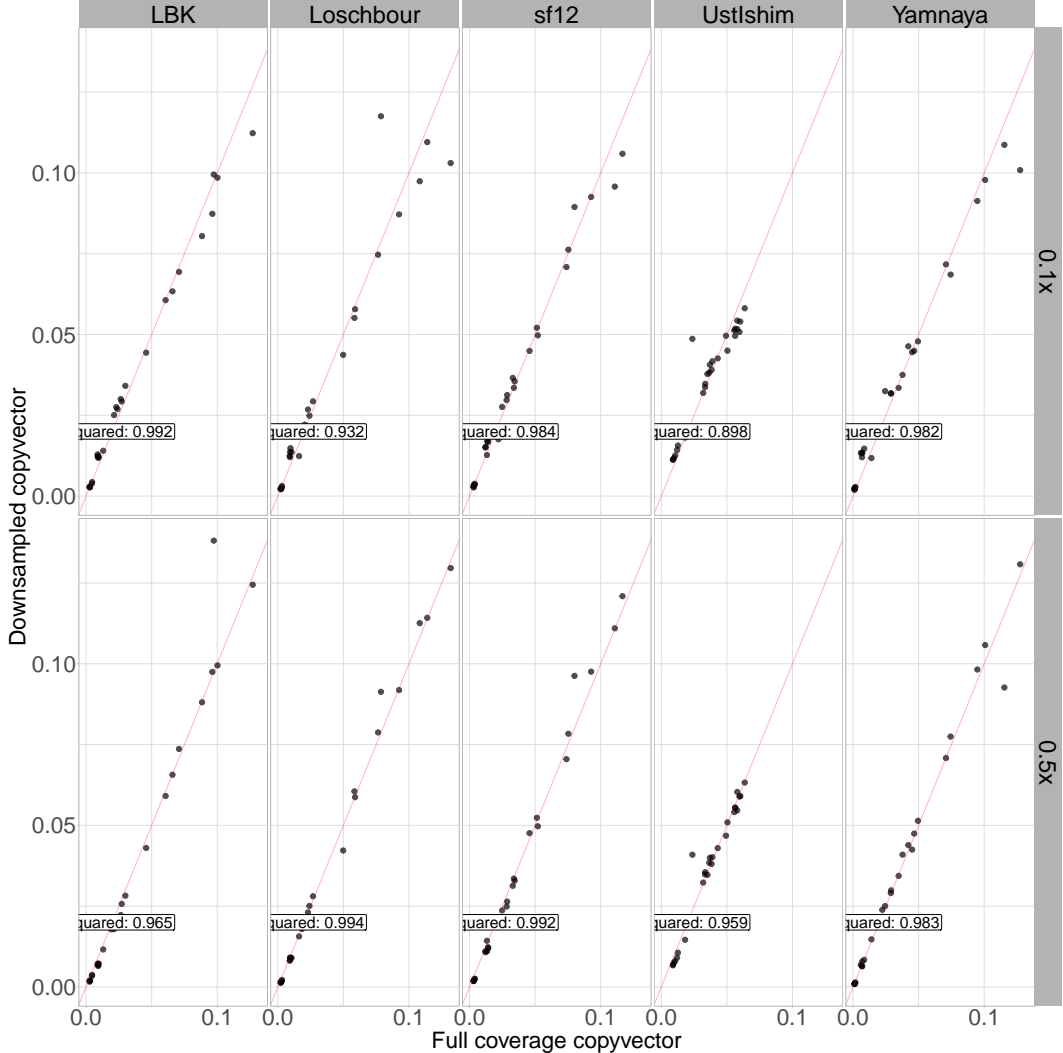


Figure 2.5: For five different samples (columns), the proportion of DNA that each downsampled (y-axis) or full coverage (x-axis) genome matches to each of 125 ancient individuals (dots). Results are shown for 0.1x (top row) and 0.5x (bottom row) downsampled genomes.

As expected, the r-squared value between the full-coverage and downsampled copyvectors increased with coverage. The 0.1x genome had a substantially reduced r-squared value, similar to the much reduced imputation accuracy. For each of the genomes downsampled to 0.1x, a particular difference to the 0.5x downsampled genomes is that, for each individual, the lowest contributing donors contribute more to the 0.1x downsampled genome than to the full

coverage genome and that the highest contributing donors contribute less to the 0.1x genome than they do the full coverage genome. Put in other words, the copyvectors at 0.1x are tending towards becoming more ‘flat’, or copying the same amount from each donor individual. This can be observed as the coefficients of the linear model lines on the figures are much less in the 0.1x than the 0.5x individuals. This can also be seen as ‘regressing to the prior’, where in this case, the prior is copying an equal amount to each donor individual. This can be visualised explicitly by calculating TVD between each downsampled genome and a flat prior, a vector of length D , where D is the total number of donor individuals and each element of D is equal to $1 / D$ (Fig. 2.6). This clearly shows the reduced TVD to the flat copyvector for the 0.1x individual relative to other coverages.**[A VITAL POINT IS TO SHOW WHETHER THERE IS BIAS CAUSED BY IMPUTATION (RATHER THAN JUST LOSS-OF-INFORMATION OR NOISE). THAT MAY BE EASIER IN LATER UKBIOBANK SECTIONS, BUT – IF SO – YOU SHOULD MENTION YOU’LL REPORT ON THIS LATER]**

I also considered the effect of coverage on the copyvectors estimated when using modern individuals as donors (Fig. 2.7). I merged the downsampled and full coverage ancient individuals with the 30x thousand genomes dataset (described in detail in appendix A.5). As was the case with the all-v-all ancients painting, the r-squared between copyvectors was lowest for the 0.1x individuals. However, the copyvectors show a strong correlation (all greater than 0.990) for 0.5x individuals.

It should be noted that utility of painting different ancient individuals with a modern reference panel depends on the ancestry and age of the ancient sample. The spread of points along the $y = x$ line in Fig. 2.7 shows how much a particular ancient recipient preferentially copies more from particular modern population over others. LBK, for example, has points which are spread evenly across $y = x$, showing that they copy much more from some populations

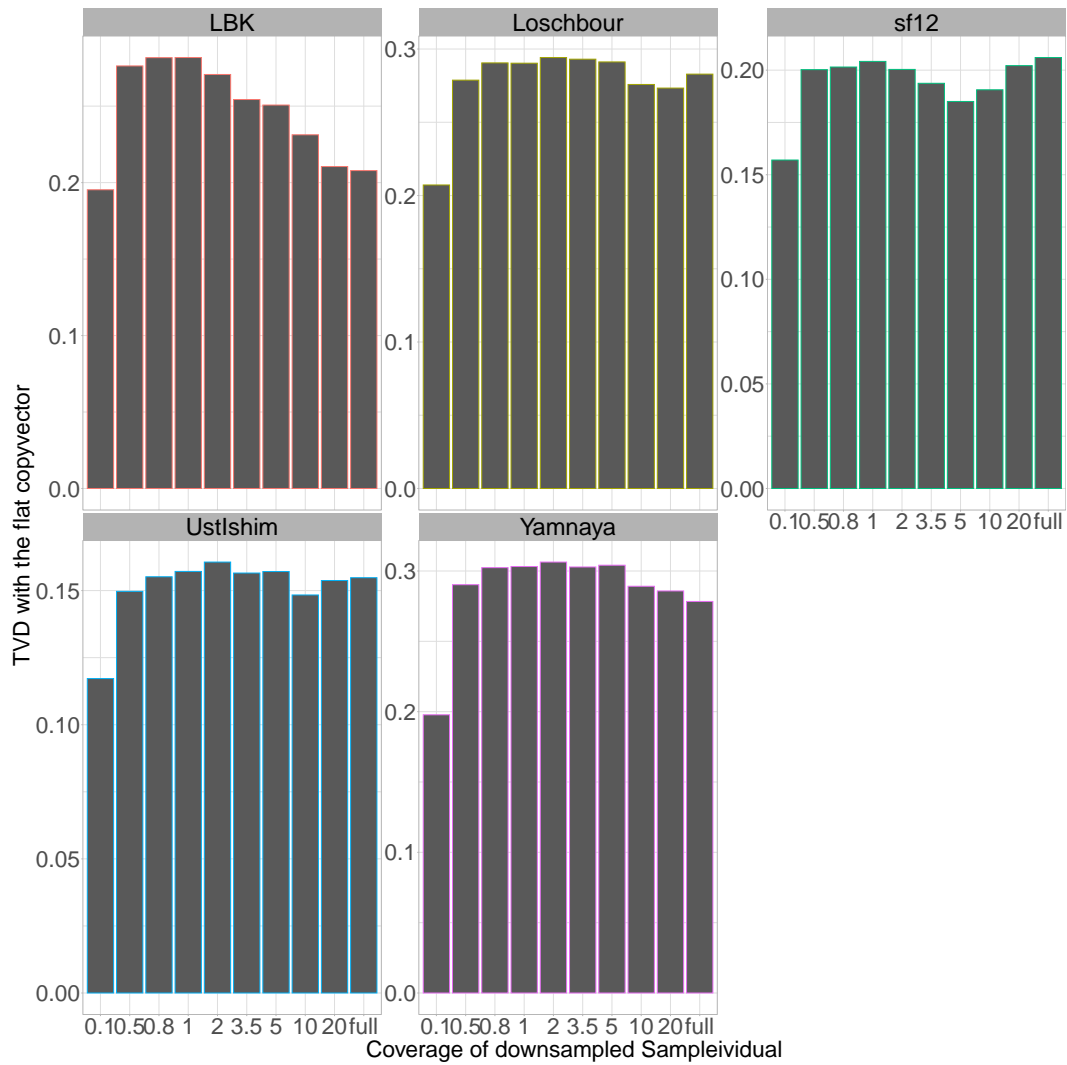


Figure 2.6: TVD (metric of copyvector dissimilarity between two individuals) between each downsampled ancient individual and a flat copyvector. Flat copyvector equivalent to a vector of length N where each element = $1/N$.

than others, suggesting modern populations are good for distinguishing this particular ancient sample. On the other hand, the points for Ust'Ishim are clumped together along lower values of $y = x$, showing that the copyvector is relatively flat and that it does not preferentially copy from some populations to the same degree that LBK does. Accordingly, relatively less useful information is obtained from painting Ust'Ishim with a modern reference panel than LBK.

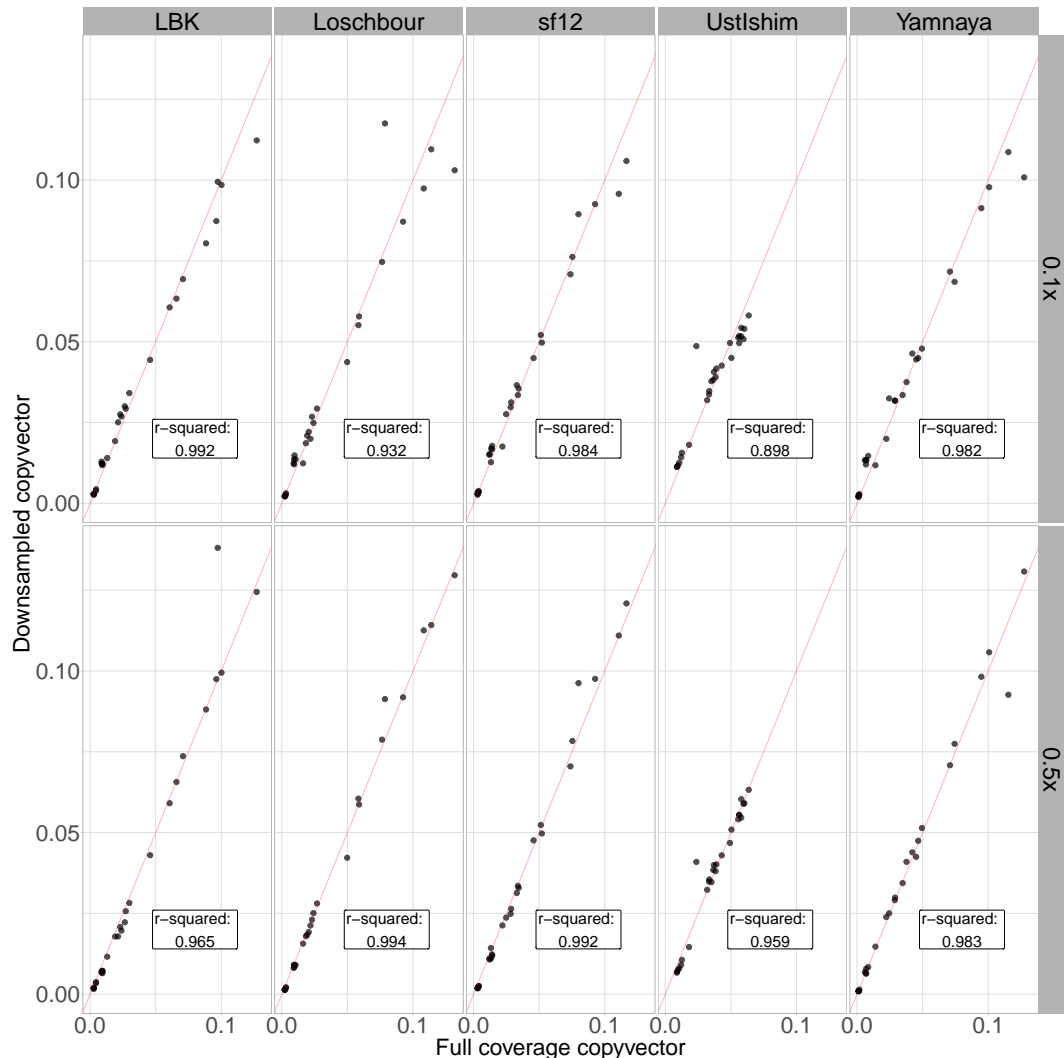


Figure 2.7: For five different samples (columns), the proportion of DNA that each downsampled (y-axis) or full coverage (x-axis) genome matches to individuals from each of 26 present-day populations (dots). Red line is $y = x$.

Principle component analysis (PCA) is a widely used technique to visualise the relative ancestry of individuals. PCA can be performed on the chunklengths

matrix in a similar way to a PCA on the genotype dosage matrix. I performed PCA on each chunklengths matrix to visualise the positions of the full coverage and downsampled genomes. PCA was performed on the chunklengths matrix containing all individuals. To avoid the confounding effect of having two almost identical individuals on a PCA (i.e. the 1x and 0.5x downsample of the same individual), I performed PCA separately for each ancient individual (see methods section x for full details).

The position of the full coverage individuals are consistent with prior knowledge about their ancestry; Loschbour is positioned alongside other Hunter Gatherers who are highly differentiated from the later Neolithic farmers and Bronze Age Europeans. sf12 clusters with the other Scandinavian Hunter Gatherers in the dataset. Yamnaya is differentiated from the group of Bronze Age individuals and situated close to individuals from the Poltavka and Srubnaya culture. LBK is located with other individuals from the early to middle Neolithic in central Europe. Consistent with sharing little ancestry with any group over another, UstIshim is positioned close to the central Bronze Age mass where most of the individuals in the PCA are located (I presume this is because UstIshim has a relatively flat copyvector and therefore is positioned near to where most of these samples are).

For all levels of downsampling other than the 0.1x, the downsampled and full coverage genomes were positioned very closely to one another on the PCA. When considering all downsampled individuals, a pattern emerges whereby the genome downsampled to 0.1x for each individual is 'pulled' towards the origin of the PCA. This may reflect a 'homogenisation' of low coverage genomes when most of the positions are imputed.[AGAIN WOULD BE HELPFUL TO KNOW IF THIS IS RANDOM NOISE OR BIAS?]

Taken together, these data suggest minimal effect of coverage down to and including 0.5x.

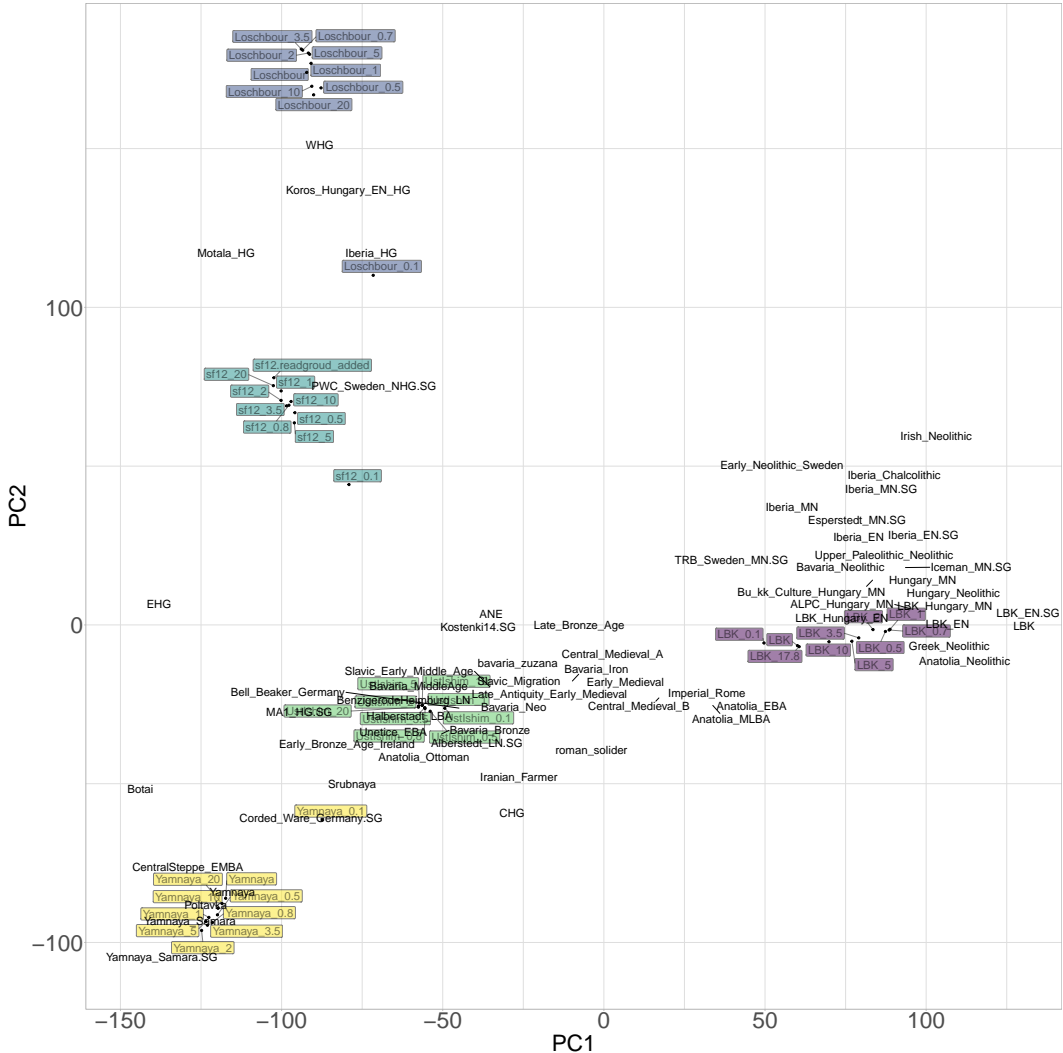


Figure 2.8: Principle component analysis (PCA) of downsampled, full coverage and reference ancient individuals generated from the linked chunklengths matrix. Full coverage and downsampled genomes of the same individual are coloured the same. Reference individuals are grouped into populations plotted as the mean principle components for all individuals within the population [NEXT TO EACH LABEL, CAN YOU THEN PUT THE NUMBER OF INDS IN THAT POPULATION (JUST FOR CASES WITH > 1 INDIVIDUAL?)].

2.3.6 SOURCEFIND

I next determined the effect of sequencing coverage on the ancestry proportions estimated by SOURCEFIND. The chunklengths matrix contains information about the total length of genome one particular individual most closely matches any other individual. However, this information is often noisy due to phenomena such as incomplete lineage sorting and variable donor group sizes. Therefore, it is often desirable to model out this noise and estimate ancestry proportions in each individual, which are cleaner and more interpretable than raw chunk lengths.

I began by considering 3 ancestral sources, or 'surrogates', fixed as Anatolia Neolithic, Western Hunter-Gatherer and Yamnaya steppe pastoralist. I compared inferred proportions for the same individual across different levels of coverage (Fig. 2.9).

The results suggest that SOURCEFIND estimates are robust to coverage effects to 0.5-0.8x coverage. At 0.1x coverage, there is an increase in ancestry components that are not present in higher coverage samples, suggesting they are artifacts caused by low coverage. For example, small components of Anatolia Neolithic and Yamnaya ancestry appear in Loschbour at 0.1x coverage, which are not present at any higher coverages. Above 0.5x coverage, the effect of coverage on estimated ancestry proportions appears to be marginal. For example, in sf12, the difference in the minor ancestry component of Anatolia Neolithic is, at most, 2.369%. [WHAT IS GOING ON WITH LBK??]

However, more than three surrogates are often used, as SOURCEFIND is meant to infer the most important contributors without a priori knowledge of the samples' ancestry. Therefore, I re-ran SOURCEFIND but with 39 surrogate populations. A strength of SOURCEFIND is that many surrogate populations can be used; unlike qpAdm or ADMIXTURE, where a reduced set must be used (reword this and get some evidence) (Fig. 2.10).

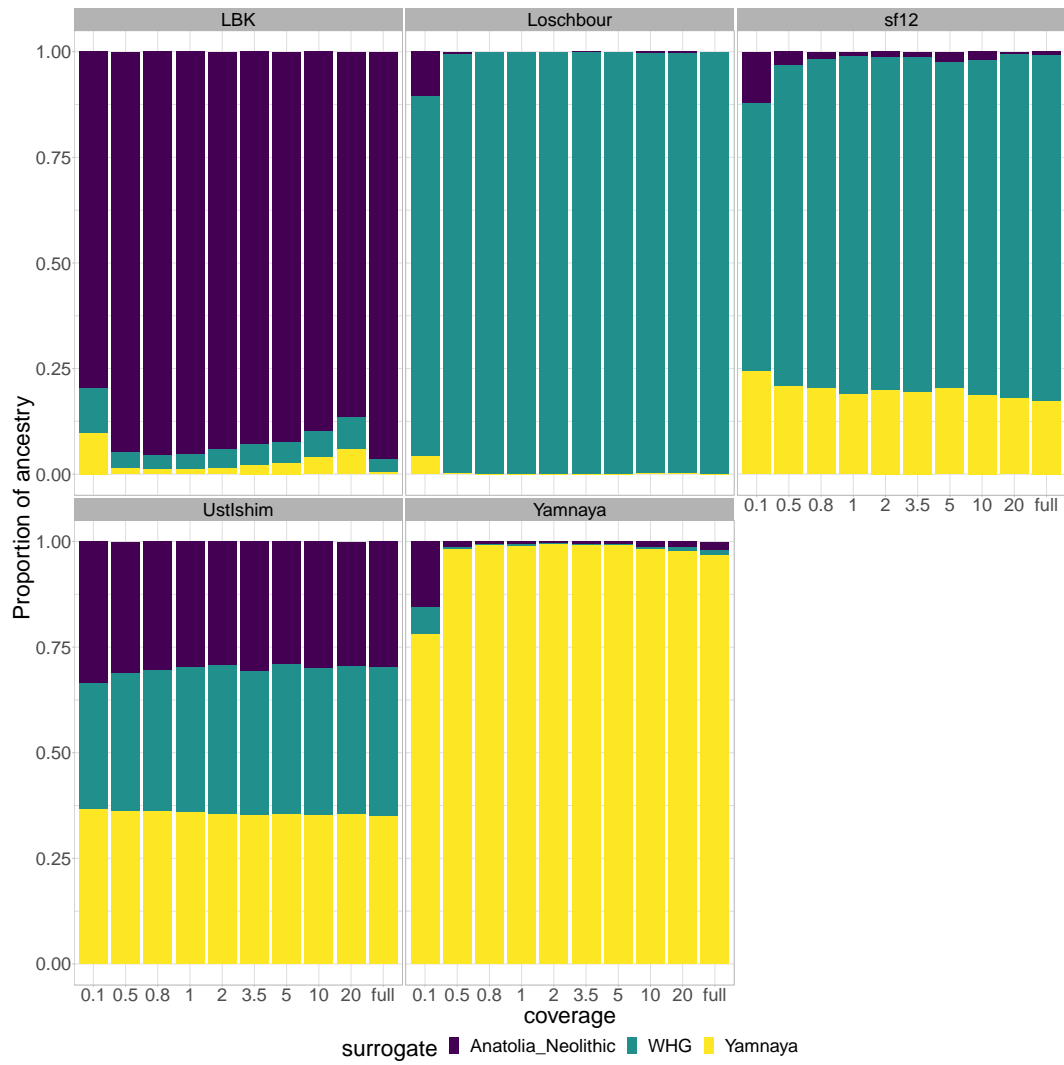


Figure 2.9: Each panel gives information for a different downsampled genome. Bars represent proportion of ancestry, coloured by different surrogates. Different coverages for the same individual are given within each panel. Three surrogates were used.

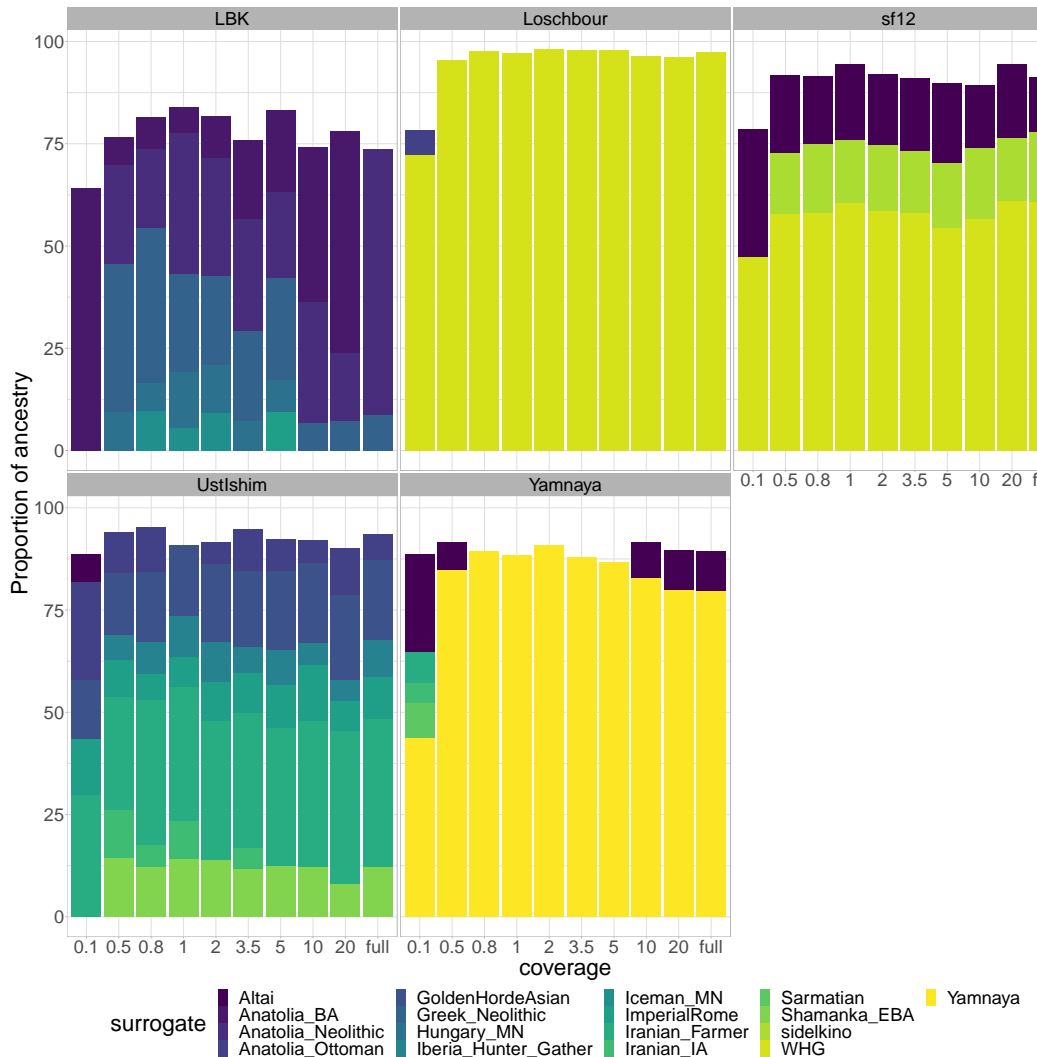


Figure 2.10: Each panel gives information for a different downsampled genome. Bars represent proportion of ancestry, coloured by different surrogates. Different coverages for the same individual are given within each panel. All 39 ancient surrogates were used. [ONE OPTION MIGHT BE TO COLOR ONLY {Ana_Neo,WHG,Yamnaya} AS IN FIG 2.9, THOUGH SF12 WILL BE ODD. CAN YOU SOMEHOW CATEGORISE THE SURROGATES INTO HOW THEY FALL INTO THOSE THREE FIG 2.9 CATEGORIES?]

Again, Loschbour seems to be the least affected by coverage, with only slight differences between the 0.5x and full coverage samples. It is known that Upper Paleolithic / Early Neolithic Hunter-Gatherer populations were small and lacked genetic diversity [5, 37, 38]. It is therefore expected that Hunter-Gatherers would share longer IBD segments than individuals from outbred populations. Accordingly, this may make estimating SOURCEFIND proportions easier.

2.4 Issues and possible solutions for low coverage ancient DNA

The previous section detailed some of the drawbacks of performing ChromoPainter analysis on low coverage (<0.5x) ancient DNA samples. In particular, reducing the sequencing coverage of ancient DNA samples has the effect of pulling each sample towards origin of a principle component analysis (PCA) relative to the same sample at higher coverage (Fig. 2.8). This is evident for the lowest coverage samples at 0.1x.

This section will therefore consider mitigation strategies. However, first it is necessary to elucidate the potential causes of this coverage related bias.

2.4.1 PCA imputation test

To explicitly test whether imputation or noise was driving the observed pattern in the low-coverage ancient genomes, I performed a series of tests.

First, to determine whether imputation was causing bias in the samples independent from ChromoPainter, I performed PCA projections of all down-sampled ancient individuals onto modern individuals using i) pre-GLIMPSE genotypes (Fig. 2.11) and ii) post GLIMPSE (imputed) genotypes Fig. 2.12).

The results show that there is no coverage-related bias in the pre-GLIMPSE

PCA, in that the 0.1x samples did not diverge substantially from the other samples. However, there is a degree of noise; for example, the LBK samples are spread over a small region on the PCA.

On the other hand, there is a clear effect of the 0.1x samples shifting to the centre of the post-GLIMPSE PCA. This suggests that coverage-related bias is being introduced in the imputation stage. On the other hand, GLIMPSE appears to have removed some of the noise in some of the downsampled individuals. For instance, the noise observed in the LBK samples in the pre-imputation PCA is substantially reduced, as all the samples fall on the same point.

I also performed a PCA, using exactly the same set of modern samples and downsampled ancient individuals as previously, but on the chunklengths matrix ChromoPainter output (Fig. 2.13). There is an increased amount of noise and evidence of coverage-related bias relative to the post-GLIMPSE genotype PCA.

Fig. 2.14 displays the PCA for the same painting, but using the unlinked chunkcounts matrix. Comparing the linked and unlinked PCAs shows the effect of including linkage (i.e. haplotype information) on the amount of bias and noise across each sample. Per-sample, there is reduced noise in the unlinked painting, suggesting discounting haplotype information may be a strategy to reduce coverage-related bias.

2.4.2 Direct imputation test

To directly test the effect of imputation on modern genomes, I performed a controlled test.

I took the POBI dataset (appendix x) which originally contained 500,000 SNPs. I removed 430,000 of those and imputed the missing SNPs using the 1000 genome as a reference.

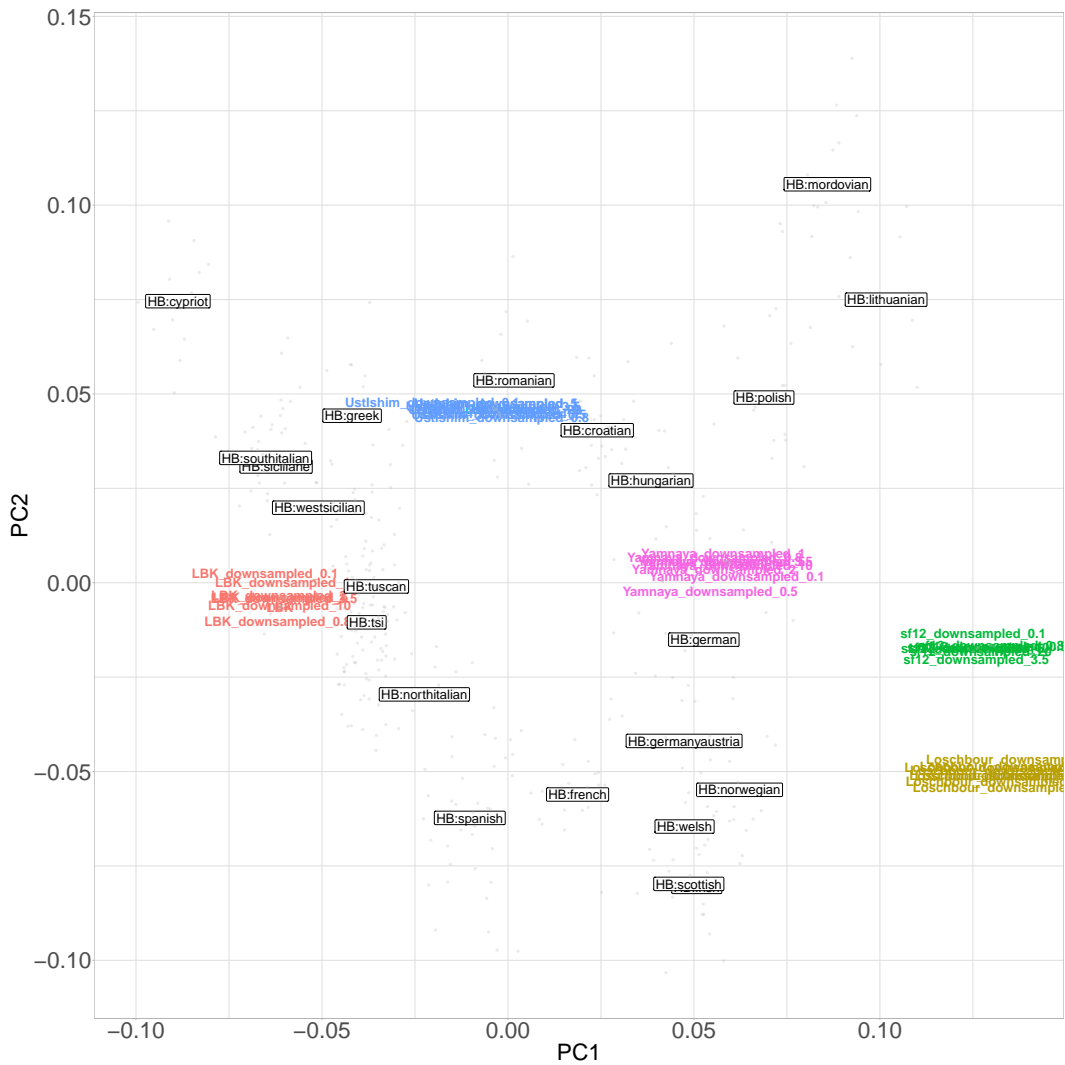


Figure 2.11: Principle Component Analysis on pre-imputed genotypes of all down-sampled and full coverage ancient samples projected onto a set of modern populations. White labels correspond to the midpoint of all samples from that population, grey points correspond to modern individuals.

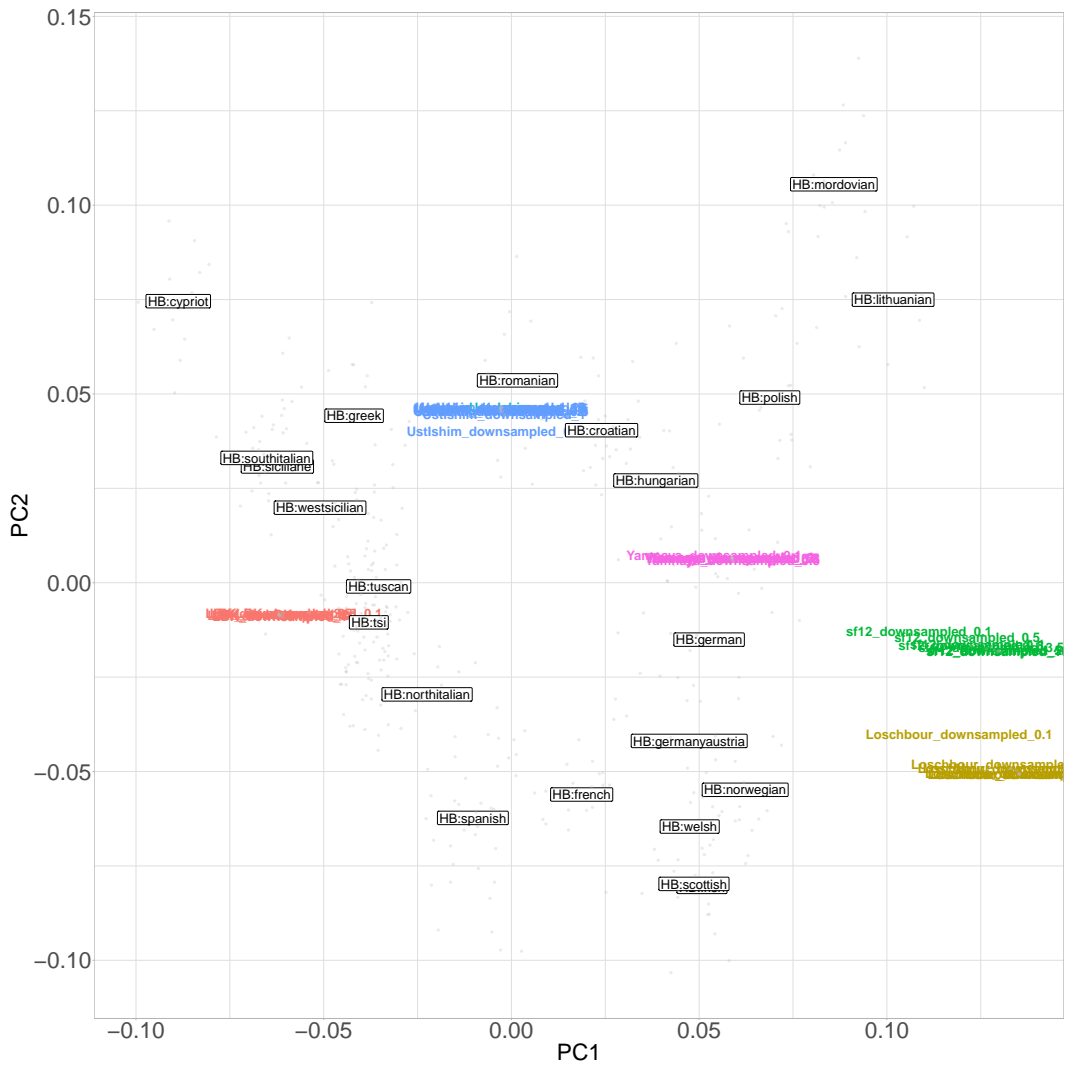


Figure 2.12: Principle Component Analysis on post-imputed genotypes of all downsampled and full coverage ancient samples projected onto a set of modern populations. White labels correspond to the midpoint of all samples from that population, grey points correspond to modern individuals.

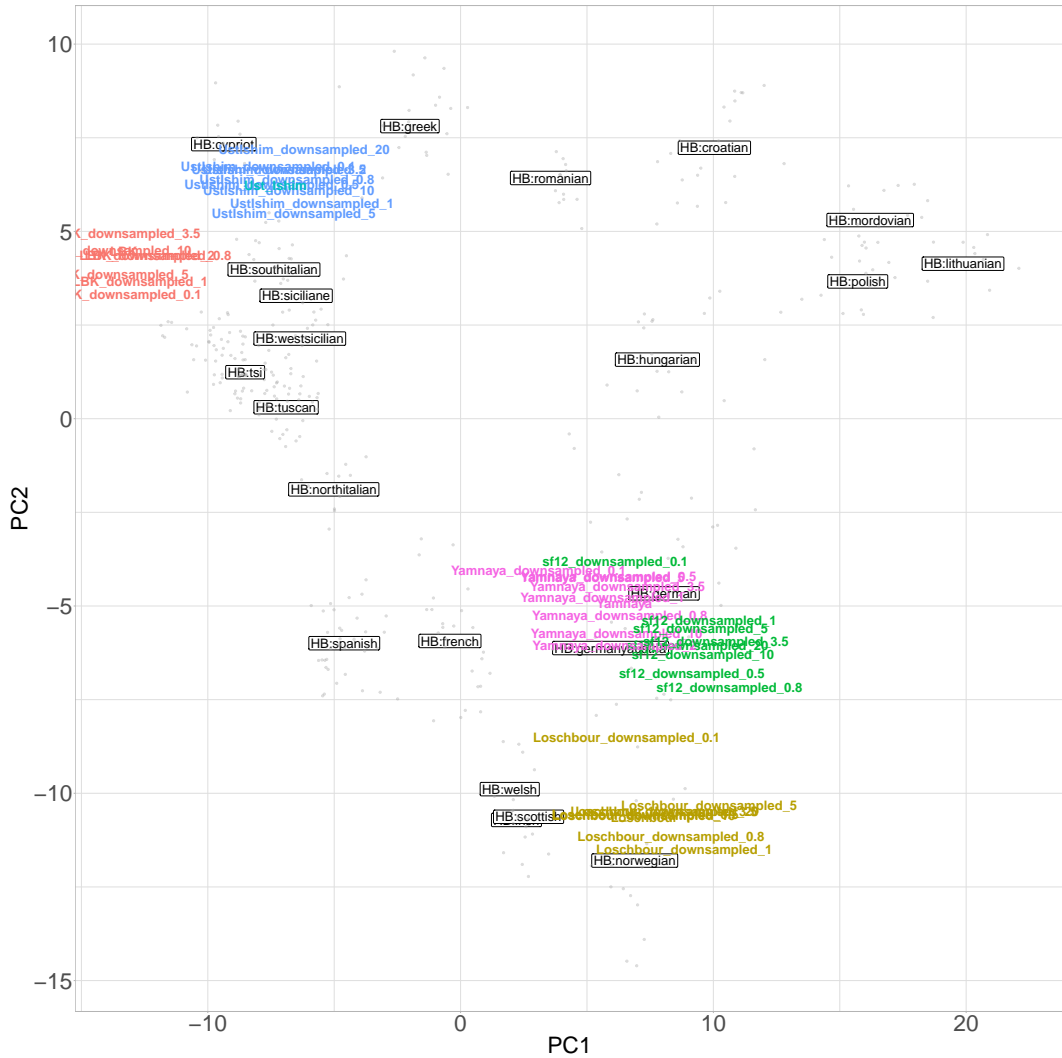


Figure 2.13: Principle Component Analysis on post-imputed ChromoPainter output of all downsampled and full coverage ancient samples projected onto a set of modern populations. White labels correspond to the midpoint of all samples from that population, grey points correspond to modern individuals.

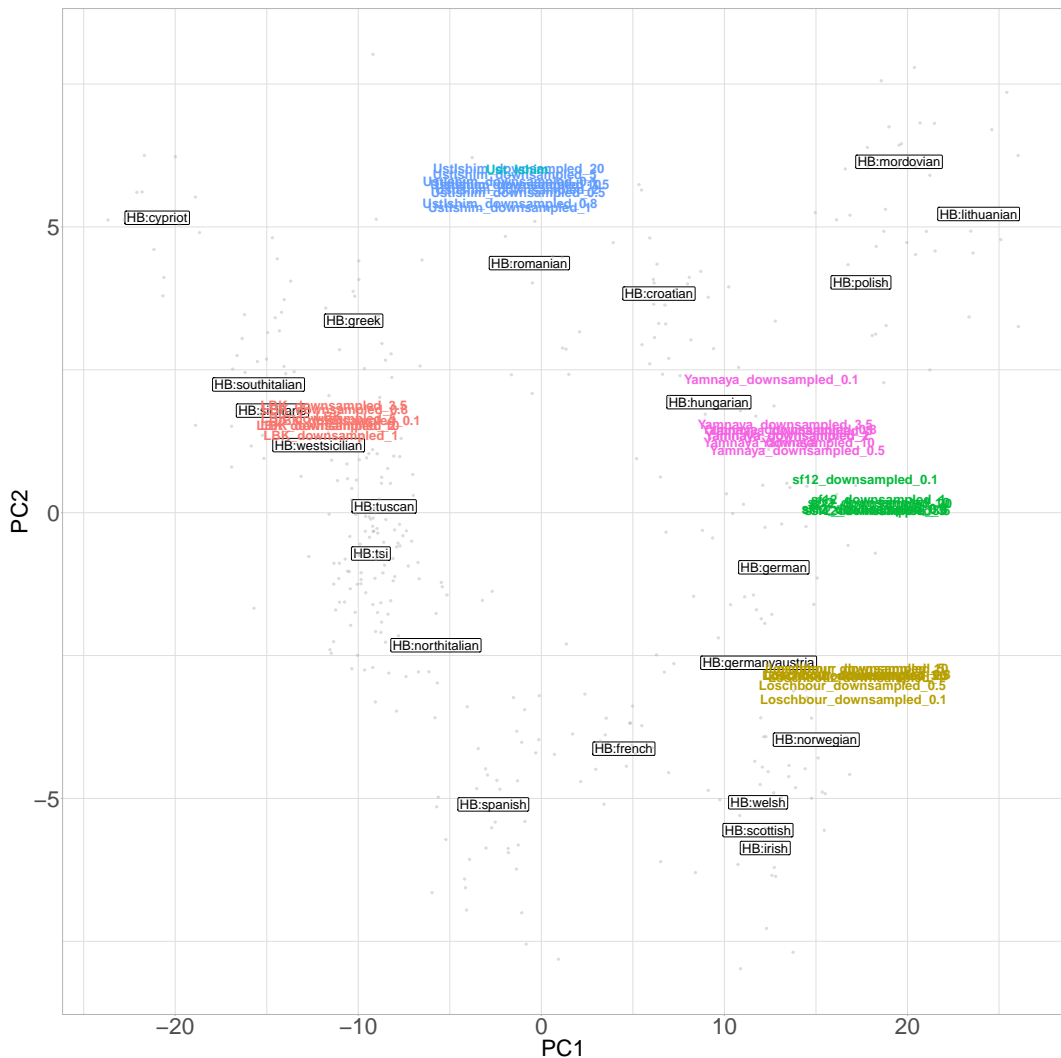


Figure 2.14: Principle Component Analysis on post-imputed ChromoPainter output of all downsampled and full coverage ancient samples projected onto a set of modern populations. White labels correspond to the midpoint of all samples from that population, grey points correspond to modern individuals.

We can make 2 predictions to determine whether it is noise or bias. First, if it is pure noise, we would expect the mean chunk size to be lower, as the chunks are being distributed randomly across donors rather than to a specific donor and vice versa. This was the case, as each individual had a longer mean chunk size using non-imputed SNPs compared to imputed SNPs.

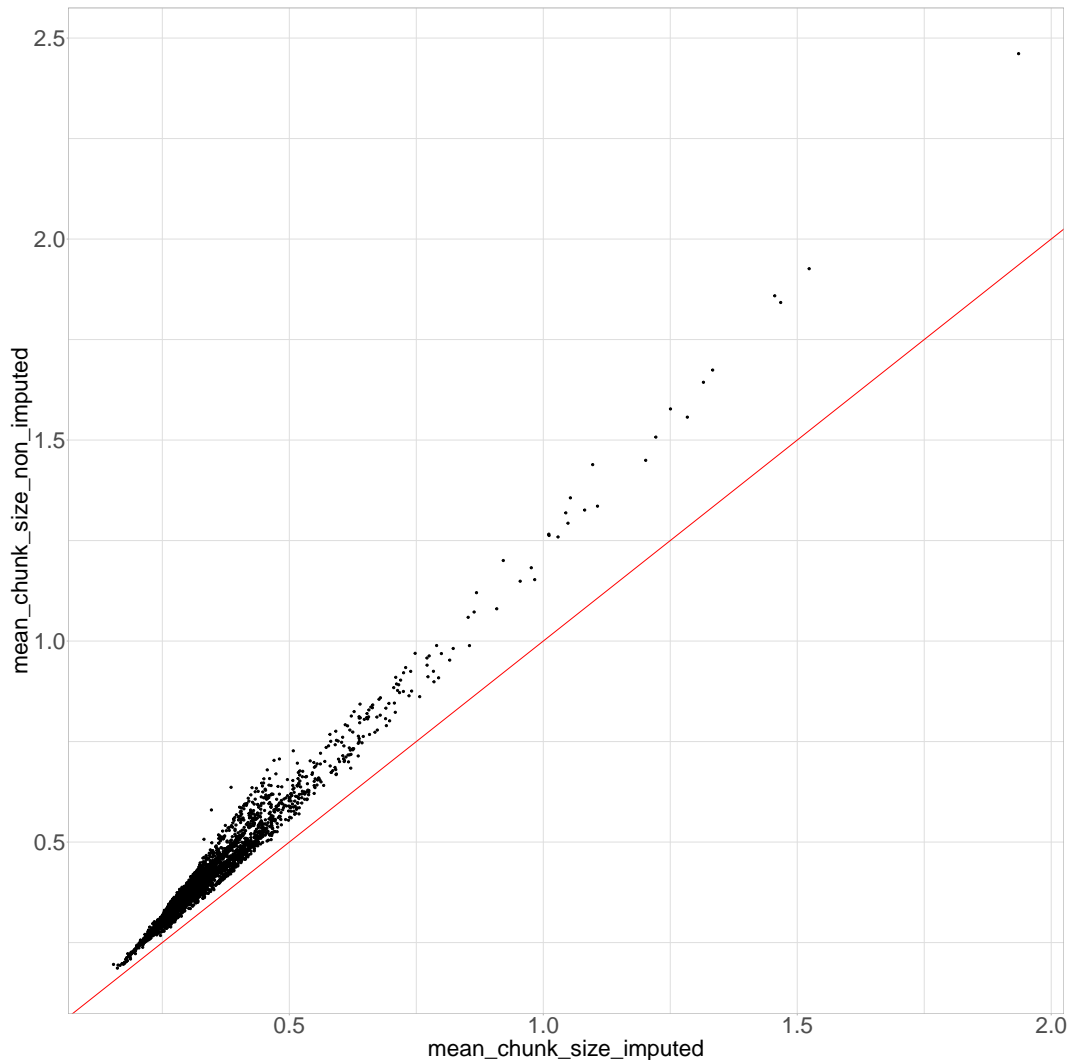


Figure 2.15: Comparison of mean chunk size (cM) when using imputed and non-imputed SNPs. Each point is an individual.

I also used this as an opportunity to test whether imputations means it is no longer possible to distinguish between Devon and Cornwall, and whether the presence of individuals from Kent in the reference panel causes a bias towards them.

2.5 Solutions

In this section I will explore several potential solutions to the issue of coverage-related bias.

2.5.1 Accounting for allele likelihoods

Section 2.2.1 describes a novel improvement to the ChromoPainter algorithm. Briefly, instead of assuming that each allele along a haplotype is correct with a probability $1 - \theta$, where θ represents a generic error probability, the posterior genotype probability from GLIMPSE is accounted for in the emission probabilities of the copying model. The motivation behind this improvement is that the uncertainty associated with genotype calls at low coverage is suitably propagated throughout the painting process, resulting in uncertain alleles contributing less towards the expected copying values than more certain ones. This is similar in spirit to that of Viera et al (2016), who account for genotype likelihoods to infer inbreeding IBD tracts from low coverage NGS data.

To test this approach, I calculated r-squared between the copyvectors of full coverage and downsampled individuals using the two different methods (Fig. 2.16) at both 0.1x and 0.5x coverage. This shows that at 0.1x, the standard ChromoPainter method clearly outperforms the new method, across all samples, whereas at 0.5x, the new method marginally outperforms the standard method.

2.5.2 Filtering SNPs

Here I will test whether filtering the set of input SNPs on different criteria reduces the effect of coverage related bias.

The frequency of a particular variant in the reference panel (RAF - reference allele frequency) used for imputation is known to affect how accurately that variant can be imputed [15, 24, 39, 40]. Specifically, we expect variants which

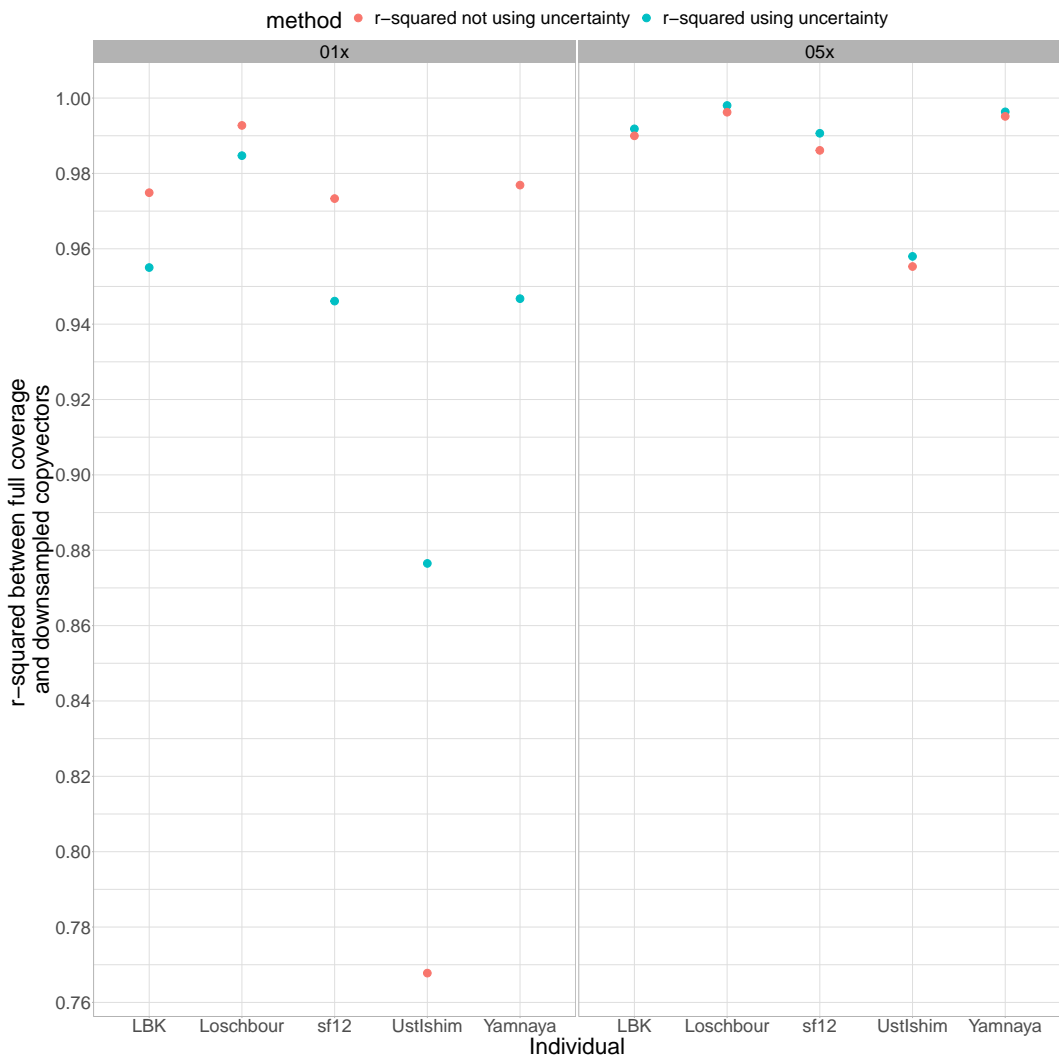


Figure 2.16

are less frequent in the reference panel to be imputed at a lower accuracy than those which are more frequent. Therefore, removing variants with a low frequency in the reference panel may mitigate the coverage related bias by removing variants which have been incorrectly imputed. In other words, we want to retain the SNPs where both alleles are relatively common within the population.

I took the 428,425 SNPs retained form the HellBus set and removed SNPs with $0.1 > RAF$ or $RAF > 0.9$, removing a total of 50,187 SNPs. I painted individuals downsampled to 0.1x and 0.5x using the standard set of 125 ancient

donor individuals.

Comparing the r-squared and visually inspecting the relationship between the copyvectors showed that this did not improve the 0.5x copyvectors (Fig. 2.17).

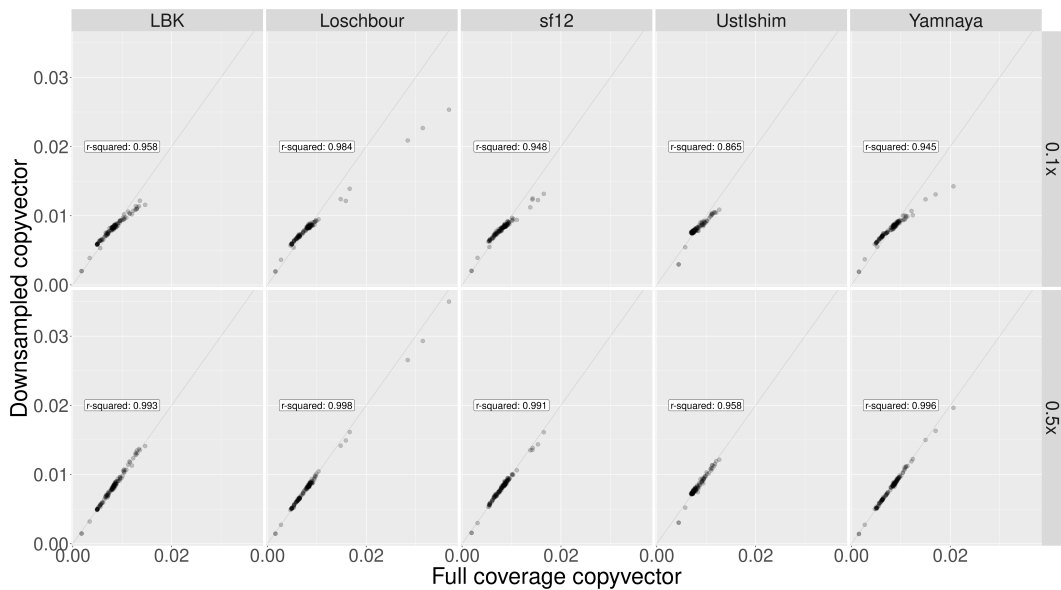


Figure 2.17: R-squared between downsampled and full coverage copyvectors when filtering out sites with $0.1 < RAF > 0.9$ at 0.1x coverage (top row L) and 0.5 coverage (R). [PERHAPS BETTER TO SHOW THIS – AND FIG 2.14 – AS A TABLE OF r^2 VALUES, SHOWING THE PREVIOUS CASE AND AFTER REDUCING LOW-FREQUENCY VARIANTS]

I then chose to filter SNPs based on $\max(GP)$ at each position. For each individual downsampled to 0.5x, I only retained positions where the $\max(GP) \geq 0.990$. This resulted in a total of 348,852 SNPs for LBK, 339,949 for Loschbour, 315,075 for sf12, 308,961 for UstIshim and 386,484 for Yamnaya. Because different SNPs were removed from different individuals, each individual was painted separately. The same standard set of 124 ancient donors was used.

Again, this did not improve the accuracy of the copyvectors (Fig. 2.18).

2.5.3 Upweighting densely genotype regions of high coverage

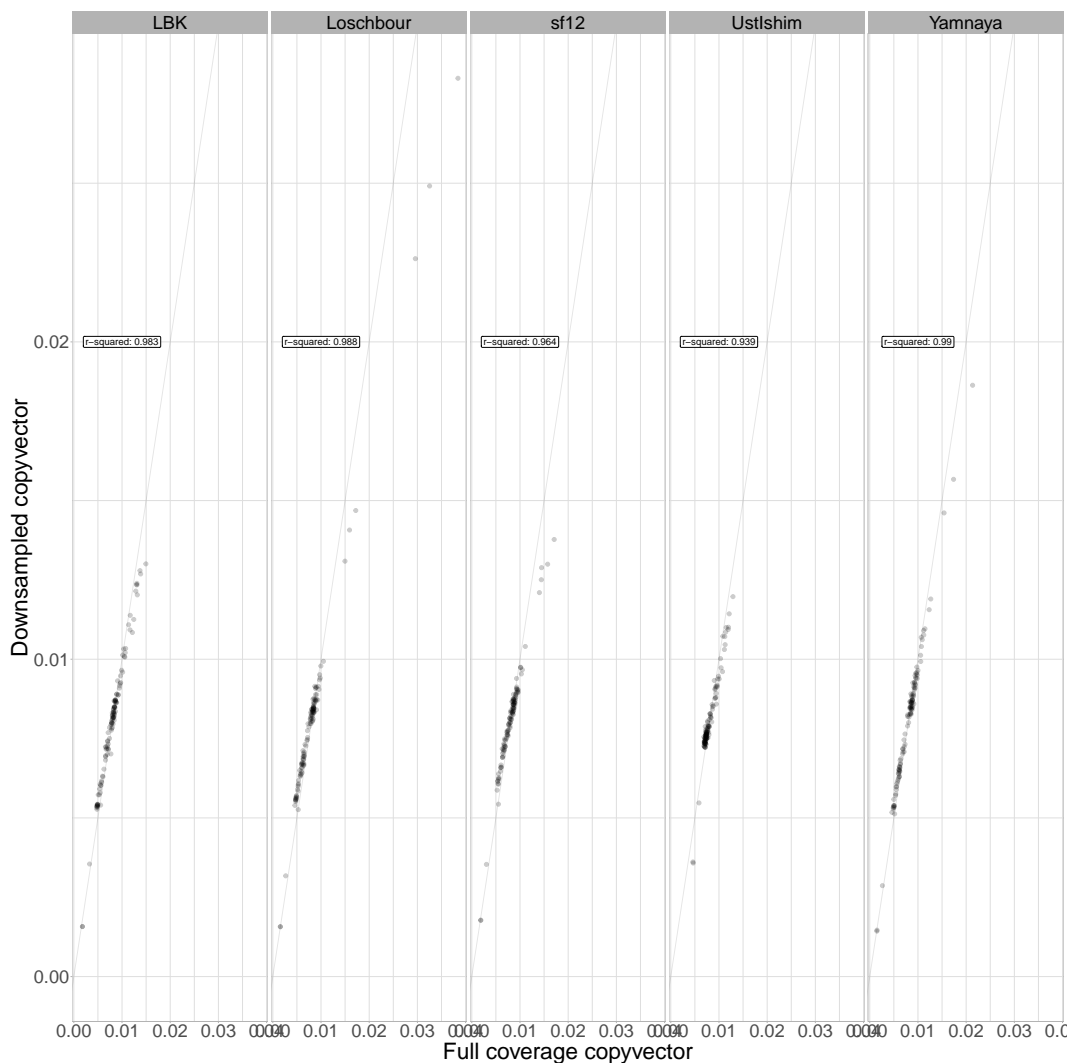


Figure 2.18: R^2 between downsampled and full coverage copyvectors when filtering out sites with $\max(GP) \geq 0.990$ at 0.1x coverage (L) and 0.5 coverage (R).

[HAVE TO COMBINE IMPUTATION HERE – E.G. WHAT IS DIFFERENCE BETWEEN USING SMALL DENSITY OF KNOWN GENOTYPES VERSUS HIGHER DENSITY OF IMPUTED GENOTYPES?] The previous section showed that imputation error was the likely cause of coverage related bias. Therefore, excluding imputed SNPs or restricting analysis to non-imputed SNPs above a certain coverage may mitigate coverage-related bias.

Excluding SNPs would result in using a set of SNPs which is necessarily
a) smaller and b) less dense than the original set of SNPs. Reducing the total

number or density of SNPs may reduce the accuracy / increase the noise of estimated copyvectors. Therefore, it is necessary to precisely determine what effect reducing the number of SNPs might have. In particular, we would like to know what the minimum number and density of SNPs is needed to retain useful haplotype information and the advantages of haplotype-based methods over unlinked methods.

One way to test this is to utilise previous results which showed it is possible to distinguish between individuals sampled from Devon and Cornwall using haplotype-based methods (e.g. ChromoPainter and the fineSTRUCTURE algorithm), but not unlinked methods (ADMIXTURE [41]) [42]. Leslie et al (2015) identified structure between individuals from Devon and Cornwall via fineSTRUCTURE groupings. The test therefore consists of attempting to replicate this result with reduced number of SNPs and lower SNP density. Repeating the fineSTRUCTURE analysis from Leslie et al is time consuming, and similar conclusions can be drawn from considering the aggregated amount individuals from Devon and Cornwall copy from their own populations.

Firstly, to test the effect of reducing the number of SNPs, I painted individuals from Cornwall with all other POBI populations as donors, using the full set of SNPs ($n=xx$) and a reduced set of SNPs

Fig. 2.19 shows the effect of reducing the number of SNPs on the estimated copyvectors of individuals from Cornwall. At the lowest level of reducing SNPs (0.002 on the figure), the black points, representing the mean amount individuals from that population copy from the particular donor population, exactly align with the red points, which is the prior expected matching to each donor group (i.e. the group's sample size). Therefore, at this number of SNPs, there is almost no information in the copyvectors, which have regressed to the prior. On the other hand, at the highest level of reducing SNPs (0.9 on the figure), the black points no longer align with the red points. **[IS THERE A WAY TO ASSESS WHAT HAPPENS AT UNLINKED?]**

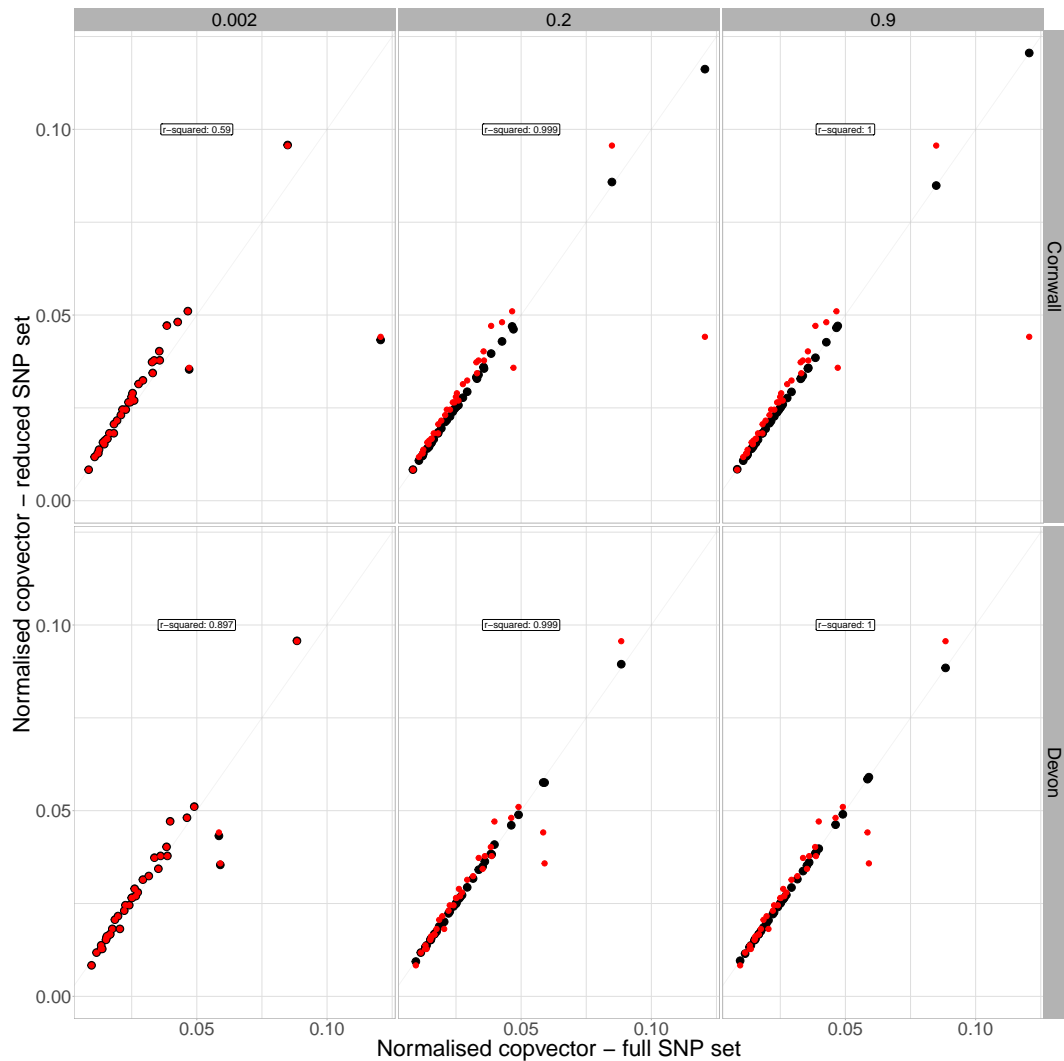


Figure 2.19: Relationship between copyvectors using reduced (y-axis) and full (x-axis) set of SNPs. Panels indicate different levels of reduced SNPs ($0.002 = 0.002 * \text{full number of SNPs}$). Copyvectors were estimated by averaging across all individuals within each population (black points). Also shown in red are the sample sizes of each donor population.

From visual inspection, 0.2 is the level of reducing SNPs in both Devon and Cornwall whereby the copyvector matches the same copyvector estimated from the full coverage of SNPs. Therefore, given populations of similar sizes in equivalent ancient individuals, we could expect to reduce the total number of SNPs to 20% of the original and still be able to distinguish between closely related populations.

Secondly, to test the effect of reducing the density of SNPs, I compared the copvectors estimated from different SNP densities, but roughly the same total number of SNPs.

In this example, using the POBI dataset, at 0.02 density there are 9,548 SNPs in total across 3000cM, giving a mean density of 1.38 SNPs/cM. On the other hand, at 0.9 density, there are 6,777 SNPs across the 144.71cM[SAME?] long chromosome 22, giving a density of 46.83 SNPs/cM. Therefore, the SNPs on chromosome 22 are substantially more dense. Henceforth I will refer to the 0.02 density set of SNPs as the 'sparse' set and the 0.9 chromosome 22 set of SNPs as the 'dense' set.

I performed three different paintings, all three using all the POBI counties as donors and individuals from Devon and Cornwall as recipients. The first painting used all chromosomes and all SNPs. The second painting used the 'sparse' SNP set. The third painting used the 'dense' SNP set. For all three paintings, the mean copyvector for Devon and Cornwall was estimated by taking the mean copyvector across all individuals within a population.

Fig. 2.20 displays the relative copyvector accuracy when using a dense and sparse set of SNPs. The r-squared value is higher using the denser set of SNPs, suggesting using denser SNPs can more accurately estimate the copy vector than the same number of more sparse SNPs. This also suggests that, if chosen well, a fraction of the original number of SNPs can recover a large amount of the original information.

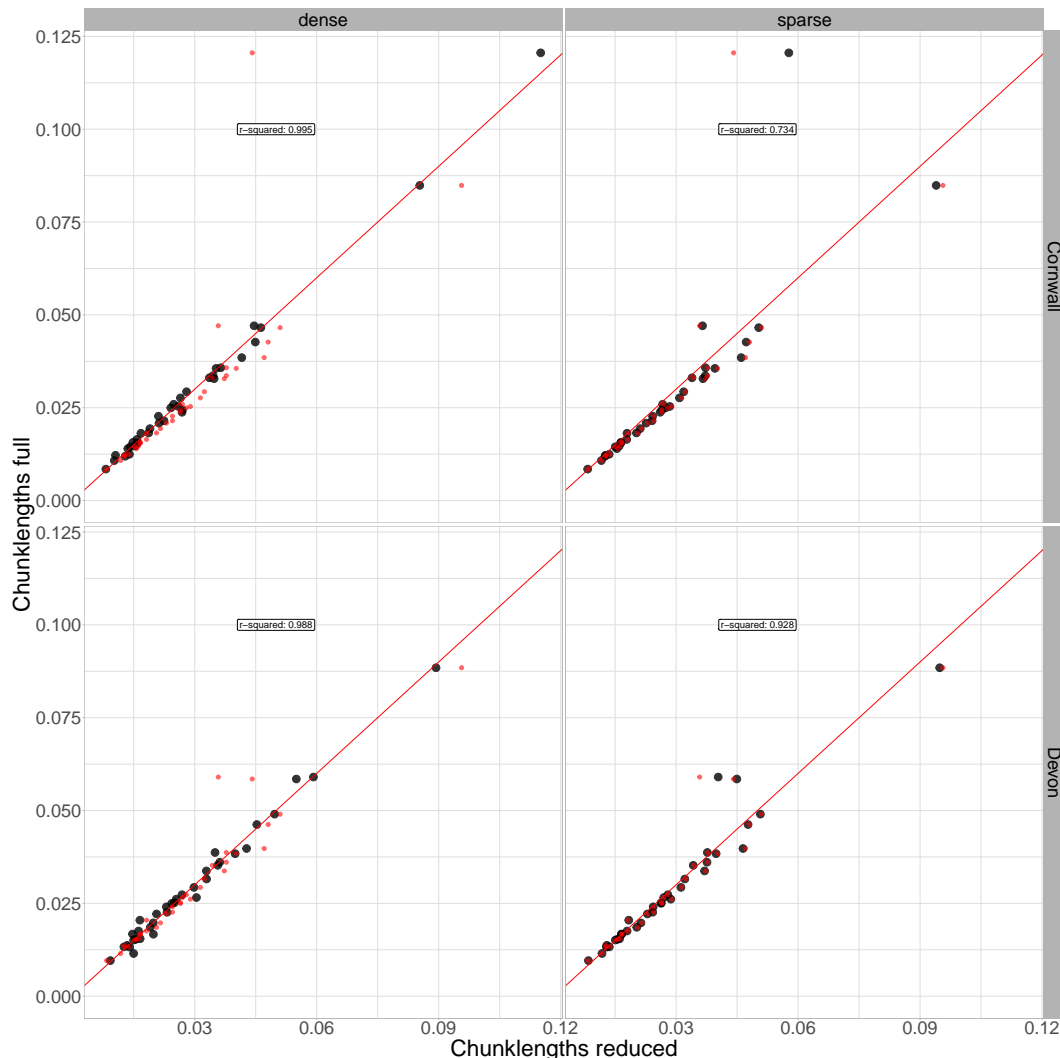


Figure 2.20: Relationship between copyvectors using reduced (y-axis) and full (x-axis) set of SNPs. Panels indicate different levels of SNP density. Copyvectors were estimated by averaging across all individuals within each population (black points). Also shown in red are the sample sizes of each donor population. [AGAIN IS IT POSSIBLE TO INCORPORATE UNLINKED FOR COMPARISON – PRESUMABLY 'SPARSE' SHOULD BE THE SAME AS UNLINKED?]

In fact, it is possible to reduce the density on the 'dense' of SNPs down to 0.3[NOT CLEAR WHAT THIS MEANS – MAYBE RELATE THIS TO SNPS PER cM AND TOTAL NUMBER OF SNPs] and still mitigate the effect of coverage.

However, the relationship between the 'dense' copyvector and full coverage copyvector is influenced by the number of individuals in the recipient population. Reducing the number of individuals within the recipient population (i.e. the number of individuals assigned to the population 'POBI:Cornwall' reduces the overall r-squared between the 'dense' and full coverage copyvectors Fig. 2.21.

With this information in mind, we can consider its use for ancient DNA. The previous section showed that imputed SNPs are the primary cause of coverage-related bias. Therefore, if we can find dense regions of non-imputed genotypes at sufficient coverage, we may be able to recover a large amount of the haplotype information from low coverage (<0.5x) samples.

The previous section informed us that 2259 SNPs spaced across chromosome 22 was enough to infer structure between individuals from Devon and Cornwall. If we can calculate i) the average size of each chunk (cM) and ii) the average number of SNPs within each chunk, iii) the total number of such chunks, then we can search the genome of a downsampled individual for such chunks.

First, to find the average number of chunks per individual, we take (`mean(rowSums(counts)) = 158`). Secondly, to find the mean number of SNPs within each chunk, we calculate (`chr22 nsnps / mean chunks per ind = 14.3`). Finally, to find the mean chunk size, we must calculate (`chr22 length cm / mean chunks per ind = 0.46cM`).

Thus, we must search the genome of a downsampled individual for windows of size 0.46cM which contain at least 14.3 'good' SNPs. Ideally, we should find at least 158 of such windows.

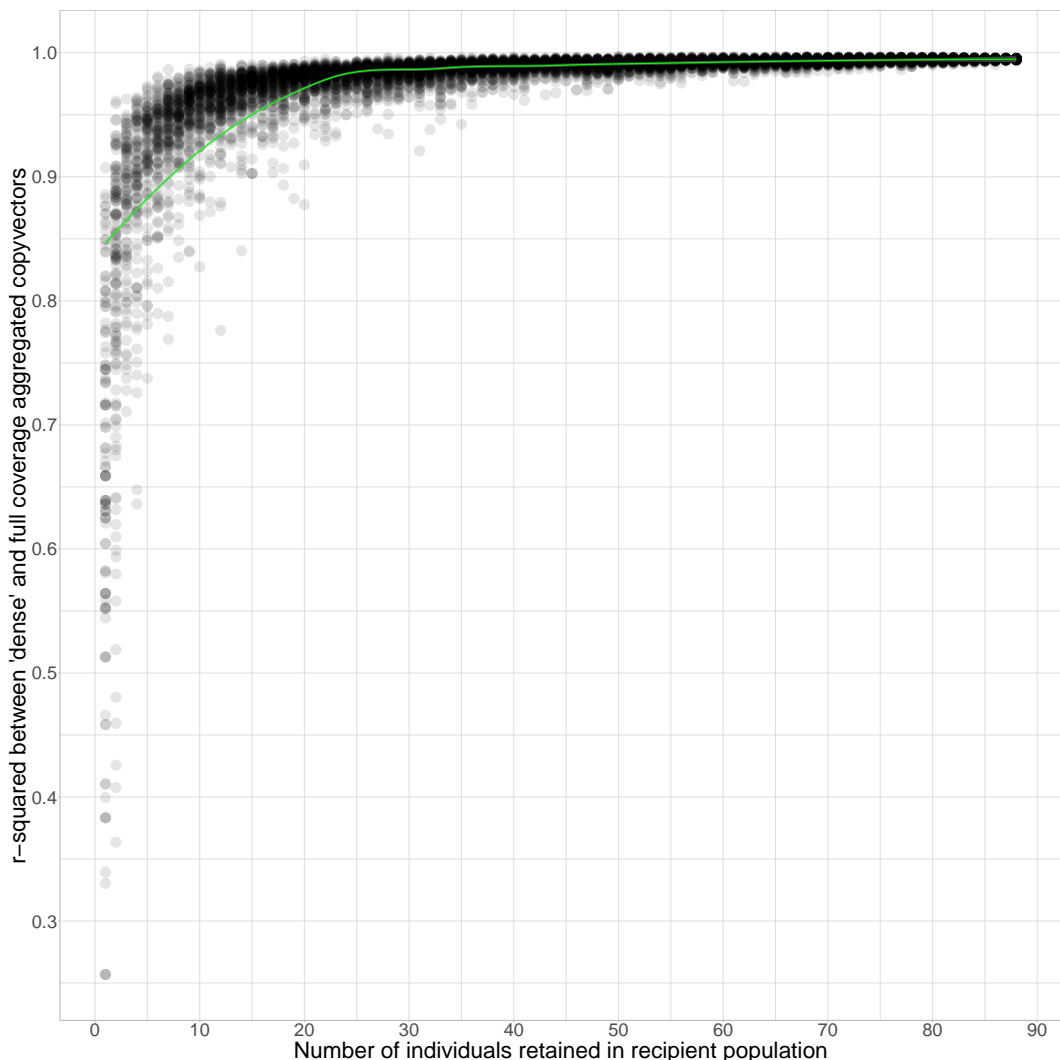


Figure 2.21: R-squared between the copyvectors estimated from 'dense' and full SNP sets (y-axis) using different sample sizes (x-axis). 'Dense' SNP set corresponds to the SNPs located on chromosome 22 at 0.9 density. Copyvectors were estimated by aggregating n randomly selected individuals within the population, corresponding to the x axis-value. Green line is local polynomial regression line. [TO BE CLEAR – FOR EACH X-AXIS VALUE, YOU ARE USING THE SAME INDIVIDUALS WHEN CALCULATING THE 'DENSE' AND FULL-COVERAGE COPY-VECTORS? ALSO SHOULD NOTE THIS IS FOR CORNWALL.]

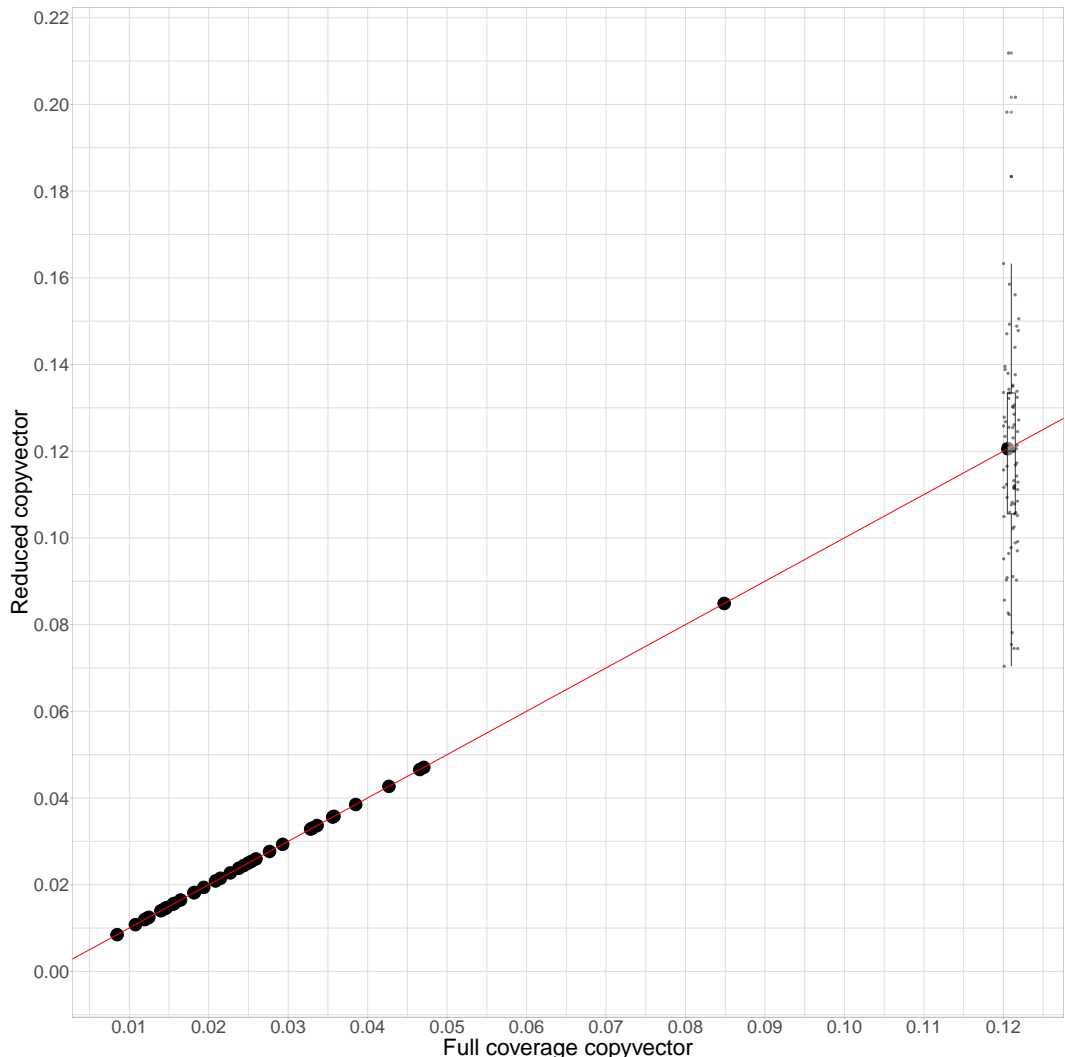


Figure 2.22: Aggregated copyvector for all individuals from Cornwall. Points correspond to the mean amount copied to different different POBI donor groups. Scattered points are the individual amounts each individual within the Cornwall group copies from the Cornwall donor group (i.e. self-copying). [AM I RIGHT THAT THIS MEANS THERE IS EFFECTIVELY no VARIABILITY IN THE AMOUNT OF MATCHING TO CORNWALL AMONG FULL-COVERAGE INDIVIDUALS? THAT IS VERY SURPRISING. OR IS THE X-AXIS JUST JITTERED? IF IT IS TRUE, THEN WE NEED TO TAKE THIS INTO ACCOUNT, BY LOOKING AT WHICH COVERAGE THE VARIABILITY IN MATCHING TO CORNWALL BECOMES VERY LARGE.]

2.5.4 Incorporating the sample size vector into SOURCEFIND

NB: Not sure if to include this if it didn't work well? [YOU CAN PROBABLY JUST NOTE THIS IN A SENTENCE SOMEWHERE, RATHER THAN GIVING IT ITS OWN SECTION]

Chapter 3

Investigating the sub-continental ancestry of ethnic minorities within the UK Biobank from sparse genotype data

3.1 Introduction

From a genetic standpoint, the native British population is one of the most highly studied in the world [?, 42].

Despite this, the roughly 8 million ethnic minorities within the U.K. remain relatively understudied. For example, all of the 27 papers were deposited between in the GWAS catalogue “UK Biobank” in the title between

We took advantage of the U.K. Biobank (UKB) resource and detailed reference panel of worldwide individuals (Human Origins) in order to investigate the ancestry of the ethnic minorities within the UKB.

3.2 Methods

3.2.1 Data access

Access was obtained to study the UK Biobank dataset via UCL genetics institute.

3.2.2 ADMIXTURE analysis

Performing chromopainter analysis on the entire UK Biobank dataset ($n=488,377$ individuals) is currently computationally infeasible. Thus, we chose to analyse only a subset of individuals; a) individuals with more than 50% non-European ancestry, b) individuals who had received a Covid-19 test.

To identify individuals who had more than 50% non-European ancestry, we split all UK Biobank individuals into 100 batches and performed supervised ADMIXTURE [41] analysis on each batch. Prior to performing ADMIXTURE, we LD pruned the SNPs using the plink [43] command `-indep-pairwise 50 10 0.02`, retaining 70,776 SNPs. The pruned UK Biobank dataset was then merged with the 1000 genomes genotypes [44].

I ran a supervised ADMIXTURE analysis on each batch by using the `-supervised` command and fixing the 4 reference populations as GBR British, Nigeria Yoruba, Han Chinese and Gujarati Indian. The rest of the arguments were left to default.

3.2.3 Data preparation - imputed data

To jointly analyse the UK Biobank the Human Origins datasets, it is necessary to merge them and retain only SNPs which have been genotyped in both datasets (i.e. contain no missing genotypes). The number of common SNPs between the UK Biobank chip and the Human Origins chip was 65,727. Using this number of SNPs in the chromosome painting analysis may reduce power

to detect fine-scale genetic differences between samples relative to using the roughly 500,000 SNPs present. One option is to therefore use the imputed UK Biobank dataset [45]. This has been imputed using the haplotype reference consortium reference panel [26].

The imputed data was downloaded and converted from .bgen to .vcf format using qctool. Strand inconsistencies between the UK Biobank and Human Origins dataset were identified using the gt-conform utility from Beagle and any inconsistent positions removed. The Human Origins and UK Biobank datasets were then merged using the bcftools merge command. The resulting merged dataset contained 493,407 individuals and 535,544 SNPs.

The merged dataset was then phased using shapeit4 [24], setting –pbwt-depth 1 to increase speed at this large sample size. The phased output was converted to chromopainter output using a custom script.

3.2.4 Data preparation - non imputed data

I also performed an analysis using only the 65,727 SNPs which overlap exactly between the UK Biobank chip and the Human Origins chip.

plink1.9 [43] was used to convert the binary plink files to bgzipped vcf format. The resulting vcf was filtered to include only those common with the Human Origins SNPs using bcftools view [46] and those individuals which had either a) at least 50% non-European ancestry or b) for which we have data on Covid-19 test, leaving 26,298 individuals. The filtered UK Biobank dataset was then merged with the Human Origins dataset using bcftools merge.

I next phased the merged UK Biobank / Human Origins dataset using shapeit4 [24]. I set –pbwt-depth 8 and left all other parameters as default. The resulting vcf of phased haplotypes was converted to chromopainter format using a custom script (appendix?).

3.2.5 Imputation bias test

When using a reference panel of individuals comprising primarily of European individuals, imputating genotypes in individuals of majority non-European ancestry can be inaccurate. Therefore, we needed to test the effect of genotype imputation on the estimated copyvectors and ancestry proportions in the African UK Biobank individuals.

To do this, we took the entire Human Origins dataset (5998 individuals and 560,420 SNPs) and submitted it to the Sanger Imputation Server, using the full Haplotype Reference Consortium (HRC) as a reference for phasing and imputation. This reference panel was chosen because it was the same one used for imputing the Biobank individuals.

I next subsetted the imputed Human Origins dataset down to SNPs present in the UK Biobank array , leaving 727,325 positions present in the imputed Human Origins dataset. I then performed an 'all-v-all' painting, forming each target haplotype as a mosaic of all other haplotypes. I also performed an identical 'all-v-all' painting of the same Human Origins dataset, but using the original set of SNPs where none had been imputed.

Therefore, we had 2 coancestry matrices of identical struture, but one was generated using a majority of imputed SNPs and the other was generated using no imputed SNPs.

I also performed SOURCEFIND analysis on both matrices. Individuals were grouped into populations and all populations were used as surrogates for each target population. Default parameters were used and each SOURCEFIND target was analysed for 2,000,000 MCMC iterations. Ancestry proportions and confidence intervals were estimated from the raw MCMC output using the Coda R library [32].

3.2.6 Chromopainter

After the decision to not use the imputed data, we performed the following painting analysis using the dataset described above in “Data preparation - non imputed data”. To maximise efficiency, we performed 2 different paintings.

Firstly, we performed an all-v-all painting of the Human Origins dataset (excluding the admixed individuals assigned to the AA Denver population). Secondly, we painted each of the retained UK Biobank individuals ($n=26,298$) as recipients and all non AA Denver individuals as donors. The resulting coancestry matrices for these 2 paintings were then combined with one another to give a combined coancestry matrix with Human Origins individuals as donors ($n=5998$) and Human Origins + retained UK Biobank individuals as recipients ($n=32,296$).

3.2.7 SOURCEFIND

3.3 Results

3.3.1 ADMIXTURE

I performed supervised ADMIXTURE on all 488,378 UK Biobank individuals in order to identify individuals with at least 50% non-European ancestry. These individuals would then be carried forward to later analyses. In total, there were 8476, 2653, 9171 individuals with at least 50% ancestry from Yoruba, Han Chinese and Gujarati reference populations respectively.

To verify the accuracy of the ADMIXTURE results, I selected all individuals who self-identified as being either “Caribbean”, “African” or “Black or Black British” ($n=7527$) and assessed the distribution of ADMIXTURE ancestry proportions, under the assumption that these individuals should contain more African than other kinds of ancestry. This was the case, with the mean

proportion of African ancestry amongst these individuals being 0.85 (Fig. [?]).

We observed substantial variation in the ancestry proportions for those self-identified as being either “Caribbean”, “African” or “Black or Black British” - proportions of Yoruban and British ancestry ranged from 0.00001 to 1, Han Chinese from 0.00001 to 0.53 and Gujarati from 0.759 to 0.00001, reflecting the diverse array of genetic ancestries that can fall under a given ethnic label.

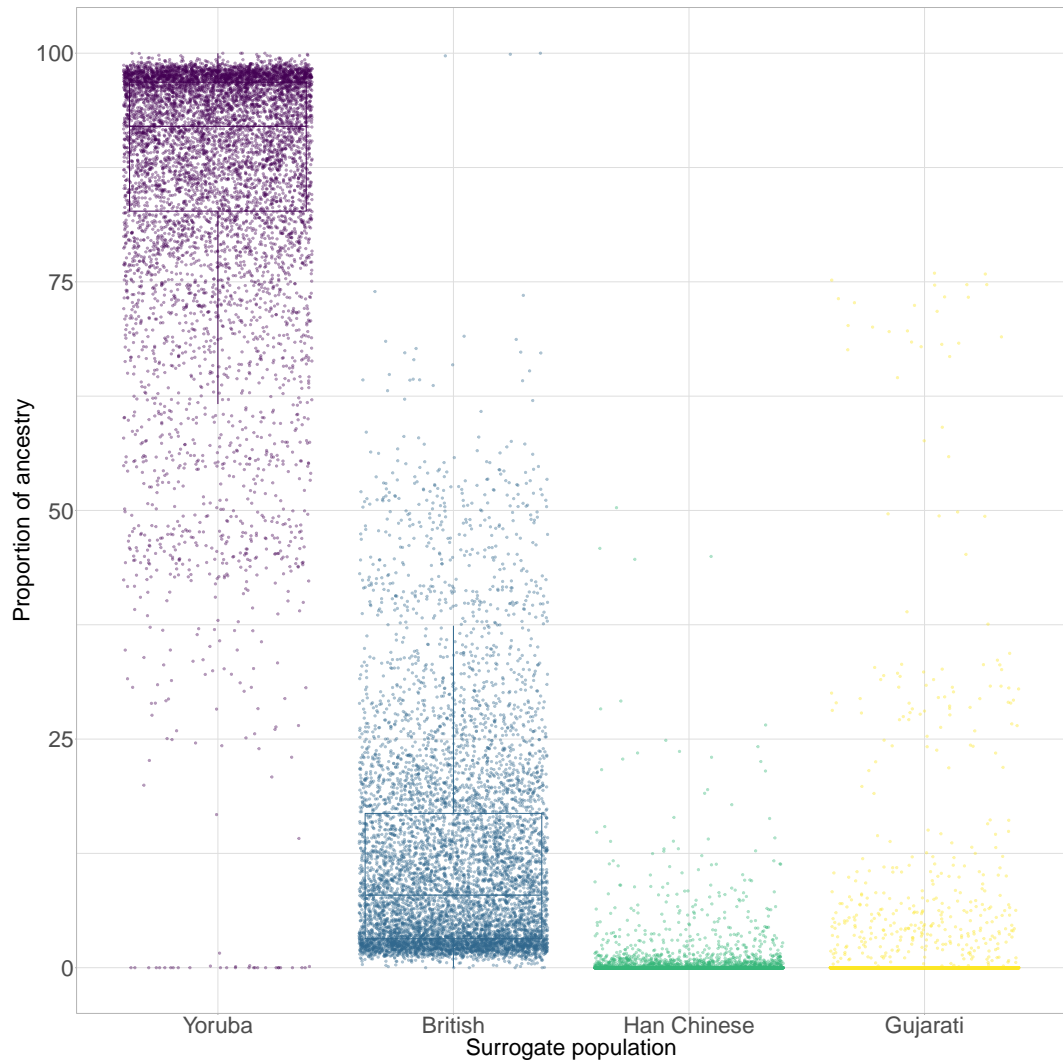


Figure 3.1: Ancestry proportions inferred from supervised Admixture run ($k=4$) for all individuals who self identified as being either “Caribbean”, “African” or “Black or Black British”.

3.3.2 Chromopainter

Our Chromopainter analysis generated a 27,529 x 5999 co-ancestry matrix. Principle component analysis on this matrix reveals the general structure of the selected individuals, alongside the reference populations (Fig. 3.2)

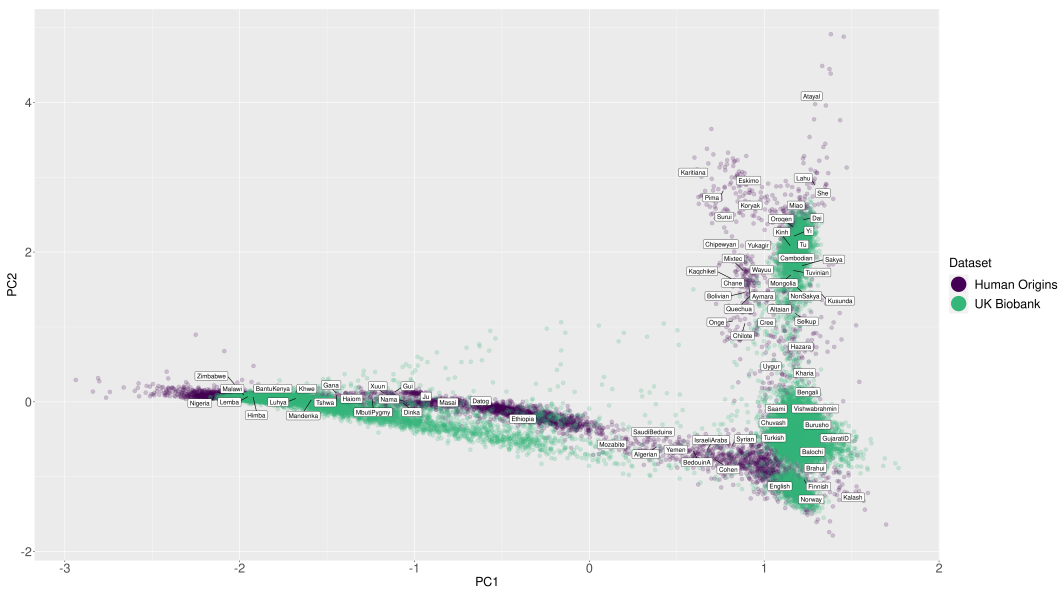


Figure 3.2: Principle component analysis of chunklengths matrix for all African UK Biobank individuals and human origins array. Individuals are coloured dependent on whether they are UK Biobank (green) or Human Origins (purple) samples. Labels indicate mean principle component coordinates for individuals in that population. A random sample of populations were chosen to have labels to prevent the figure from being too cluttered.

Aggregating the columns of the aforementioned co-ancestry matrix by reference population by mean/sum gives the total length of genome each UK Biobank individual most closely matches individuals from that reference population. This can be visualised on a map, where each point represents a reference population and the colour corresponds to the total amount that reference population contributes towards the ancestry of all retained UK Biobank individuals (Fig. 3.3).

The populations with the largest contribution to the retained UK Biobank samples are those from West Africa. This is consistent with two different

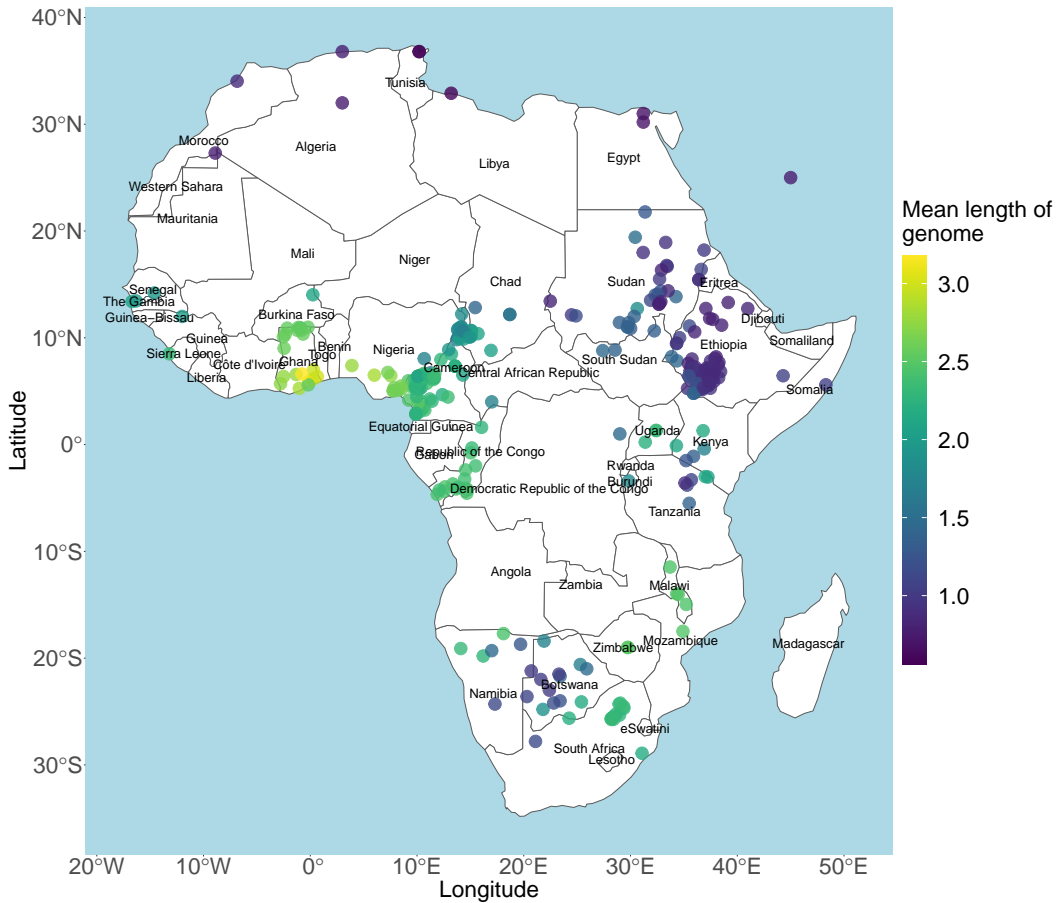


Figure 3.3: Map of haplotype donation to UK Biobank individuals. Each point represents a different African population. Colour

historical processes.

Firstly, it is known from historical and genetic studies that a majority of the individuals who were forcibly transported from Africa to the Americas during the transatlantic slave trade were from the west coast of Africa [47]. Given the UK Biobank sample contains many individuals who were either born in, or trace their ancestry from the Caribbean, we would expect there to be a large contribution of ancestry from West Africa.

Secondly and more recently, there has been a relatively large amount of

historical immigration from countries in West Africa, such as Ghana and Nigeria, to the U.K.

3.3.3 Verifying painting accuracy

Given the total number of SNPs used in the analysis ($n=65,727$) is on an order of magnitude less than is typically used in such analysis, it is important to verify the results do not simply correspond to copying the most from the reference populations with the largest sample size, as has been shown in previous analyses (refer to previous chapters). To test that the coancestry matrix contains relevant information about the ancestry of the retained UK Biobank individuals, I took advantage of the UK Biobank metadata and subsetted the coancestry matrix to contain only individuals who were born in a particular country. We would expect that individuals who were born in a particular country would copy the most from reference populations from that country. For example, we would expect individuals who were born in South Africa to copy the most from Bantu and Zulu ethnic groups from South Africa.

Fig. 3.4 shows the map of haplotype donation from reference groups to UK Biobank individuals born in South Africa. It is clear that reference populations from South Africa, in particular the Zulu ethnic group, contribute the most to these individuals. The same pattern is clear for most countries of origin.

There are several interesting cases. For example, there are N individuals who were born in the Caribbean. Visualising the haplotype donation map for these individuals shows that they are primarily of West African ancestry, consistent with historical evidence [47]. Individuals born in Brazil have ancestry from further South, again consistent with historical evidence (citation needed).

As a more formal test of the painting accuracy, I estimated SOURCEFIND ancestry proportions in each retained UK Biobank individuals. An individual was 'assigned' to a particular reference population if they had 75% or more

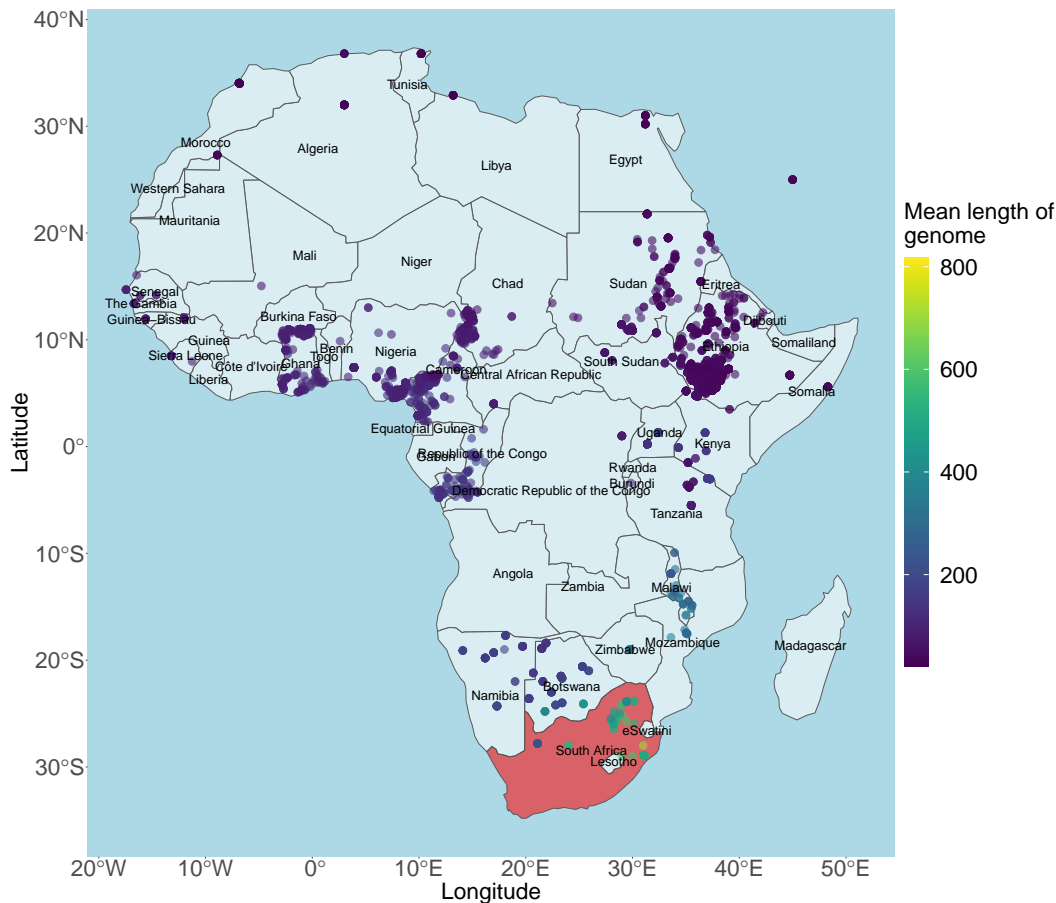


Figure 3.4: Map of haplotype donation to UK Biobank individuals born in South Africa.

ancestry from that population. If the country the assigned reference population is from matches the birth location of the individual, then I considered that a ‘success’ and a ‘fail’ otherwise. Individuals who were born in the U.K. or who had no birth country were excluded from this analysis.

The overall accuracy at predicting birth location was 81.63%, suggesting there was substantial information within the coancestry matrix. For the countries where there was a large number of reference populations, such as Ghana and Nigeria, the prediction accuracy was high. For certain countries, the prediction accuracy was much lower. For example, Tanzania was only

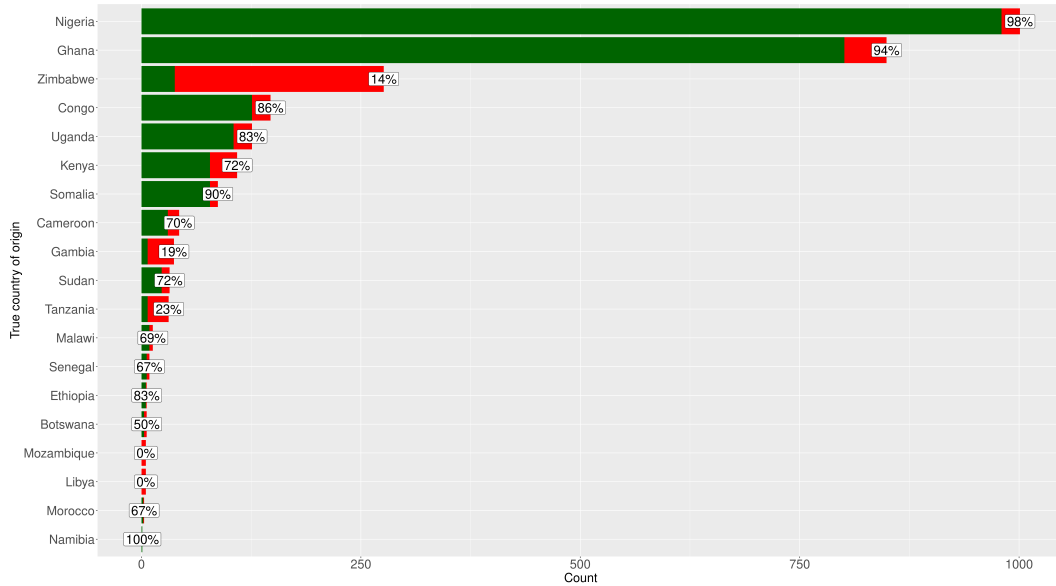


Figure 3.5: Correspondence of true birth country with estimated birth country. Each bar corresponds to a true birth country, with the length of the bar corresponding to the total number of people in our dataset born in that country. The green section corresponds to the total number of individuals where the birth country was correctly guessed and the red section to those who were incorrectly guessed. Percentage labels give percentage correct for that country.

represented by a single reference population. Zimbabwe...

3.3.4 Imputation bias

The imputed dataset consisted of 535,544 SNPs in total, 87.7% of which were imputed. Having a high percentage of imputed SNPs may bias downstream analyses.

For example, consider two UK Biobank individuals who have a large percentage of African ancestry. One of the individuals has ancestry relating to a particular Nigerian ethnic group and the other to a closely related, but different Nigerian ethnic group. We are interested in being able to determine the fine-scale differences in ancestry between these individuals. This relies on the existence of variants in each individual which are specific to that population.

Imputation relies on identifying reference haplotypes which are closest

to the target haplotypes. However, neither of the ethnic groups that the individuals derive ancestry from are present in the imputation reference panel. Therefore, we would expect that the missing variants would be imputed from the populations in the reference panel which are most closely related to our target samples. In the case of the Haplotype Reference Consortium, the closest reference population to our two target samples may be the Yoruba. If missing are preferentially imputed from Yoruban individuals, then we would expect segments of the target samples to appear to me more 'Yoruba-like' than otherwise. Correspondingly, when painted using a reference panel which includes, but is not exclusive to, those populations found in the imputation reference panel, we would expect the populations found in the imputation reference panel to donate more.

Comparing the imputed and non-imputed coancestry matrices revealed biases consistent with the above expectation. If the coancestry matrix columns are combined into populations, then the sum of each column gives the total length of genome that population contributes to all recipient individuals in the dataset. Therefore, comparing the column sums between the imputed and non-imputed matrices informs us about which populations contribute more under in the imputed dataset than the non-imputed dataset.

Of the 568 populations tested, 6 were present in the 1000 genomes reference panel.

Considering the SOURCEFIND results shows strong evidence that imputation alters the inferred ancestry proportions of the Human Origins individuals. If we take each target population and assign the surrogate with the largest ancestry proportion as the 'best surrogate', then only 30% (144/478) of the best surrogates match between the imputed and non-imputed datasets.

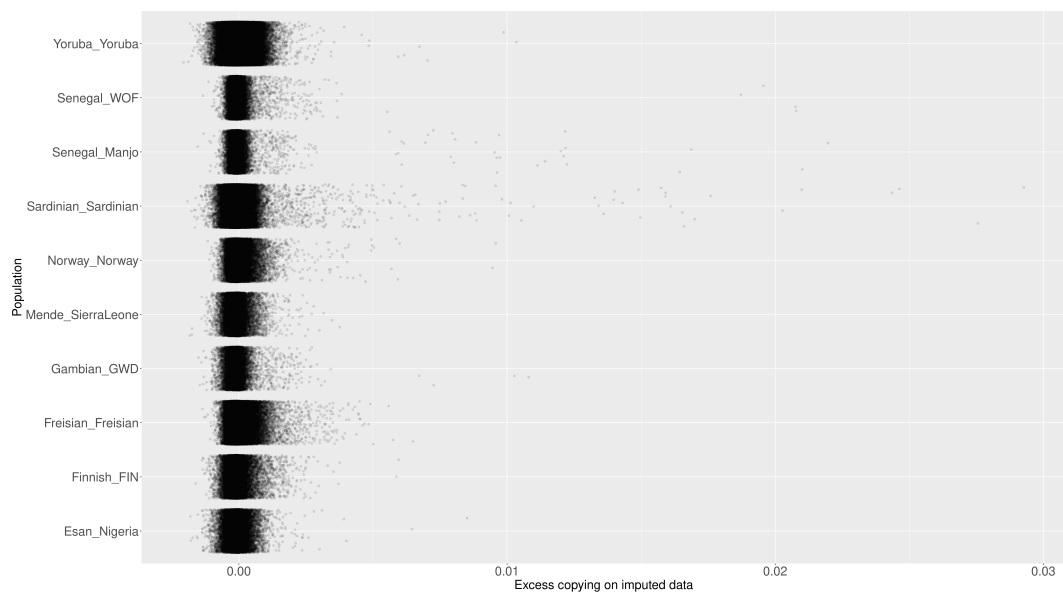


Figure 3.6: The top 10 Human Origins populations which donate more haplotypes under when data is imputed compared to non-imputed. Each point corresponds to the difference between the amount an individual from that donor population donated using imputed and non-imputed data, with positive values corresponding to more copying when the is imputed.

Chapter 4

Bavaria ancient DNA

4.1 Introduction

Throughout the Pleistocene and Holocene, Germany has been the setting for many population movements and admixture events of modern humans; the Swabian Alps is home to one of the earliest symbolic art, dated to at least 32kya [48] and musical instruments dated to 40kya [49], both assigned to the Aurignacian tradition. Later, the region was also home to one of the first Neolithic traditions in the *Linearbandkeramik*, a key culture in the Neolithisation of Europe.

Cherry-Tree cave (Kirschbaumhöhle in German) represents a perfect opportunity to study the transect of samples from the Neolithic to the present-day. The cave represents a relatively untouched layer of stratigraphy.

Bavaria obtained a distinctive

In the present-day, Germany represents a boundary point between East and West Europe; current population structure. Questions remain as to the origin of this East-West structure; is it recent structure, or does it persist to the Middle Ages or earlier?

Here, I present novel data from 11 medium-to-high coverage samples from two sites from Southern Germany and one site from one from Southern Austria. In particular, the samples from Kirschbaumhöhle span from the Late Neolithic to the Iron Age and represent an excellent opportunity to study a time transect.

Previous studies into the genomic history of Bavaria have focused, for example, on the mixed ancestry of migrant females during the Early Middle Ages.

I was interested in addressing the following questions:

1. **Second Neolithic immigration wave.** Do we observe genetic differences between the first and second wave of farmers that brought farming to the region technology from South-East Asia to Europe during the Early Neolithic?
2. **Cherry Tree Cave.** How can we make sense of the genetic ancestry changes from the Late Neolithic through to the Iron Age in Cherry Tree Cave? Do we see evidence of genetic continuity between the ages and are they characterised by admixture from outside sources?
3. **The Iron Age.** How do the samples from the Iron Age compare to the single sample from the Bronze Age, and both to central Europeans
4. **Iron Age - Middle Age** To what extent do the ‘proto-Celtic’ samples of the Iron Age show similarity to the later early ‘Germanic’ people of the middle ages.
5. Is there a distinction between the Germanic and Slavic Middle Age samples? How do these populations compare to the preceding samples from the Bronze and Iron ages.

4.2 Methods

4.2.1 Data generation

Whole-genome sequence data was generated by collaborators at the University of Mainz, Germany. In total, 11 new samples were sequenced.

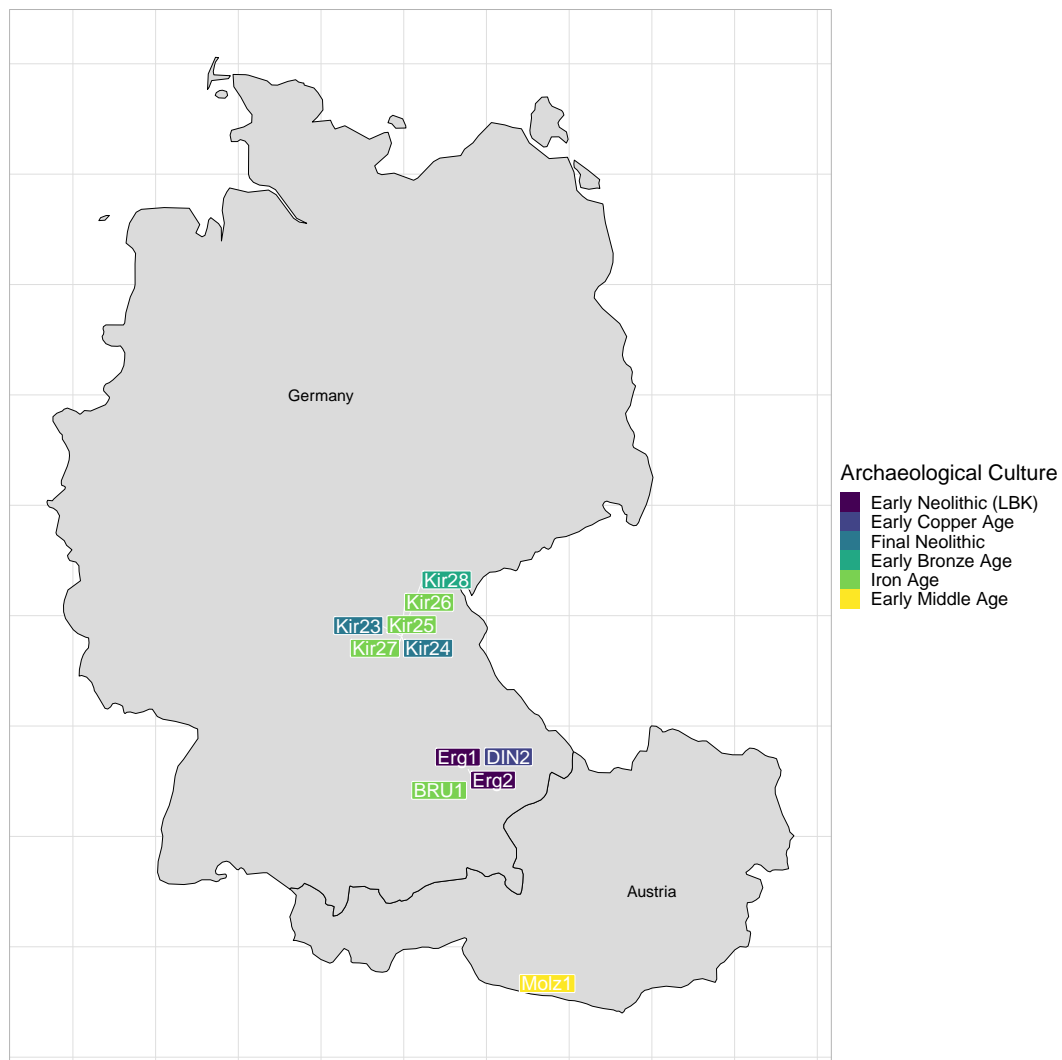


Figure 4.1: Map of newly sequenced ancient individuals, positioned according to where they were excavated. Colour on label corresponds to archaeological culture which they were found.

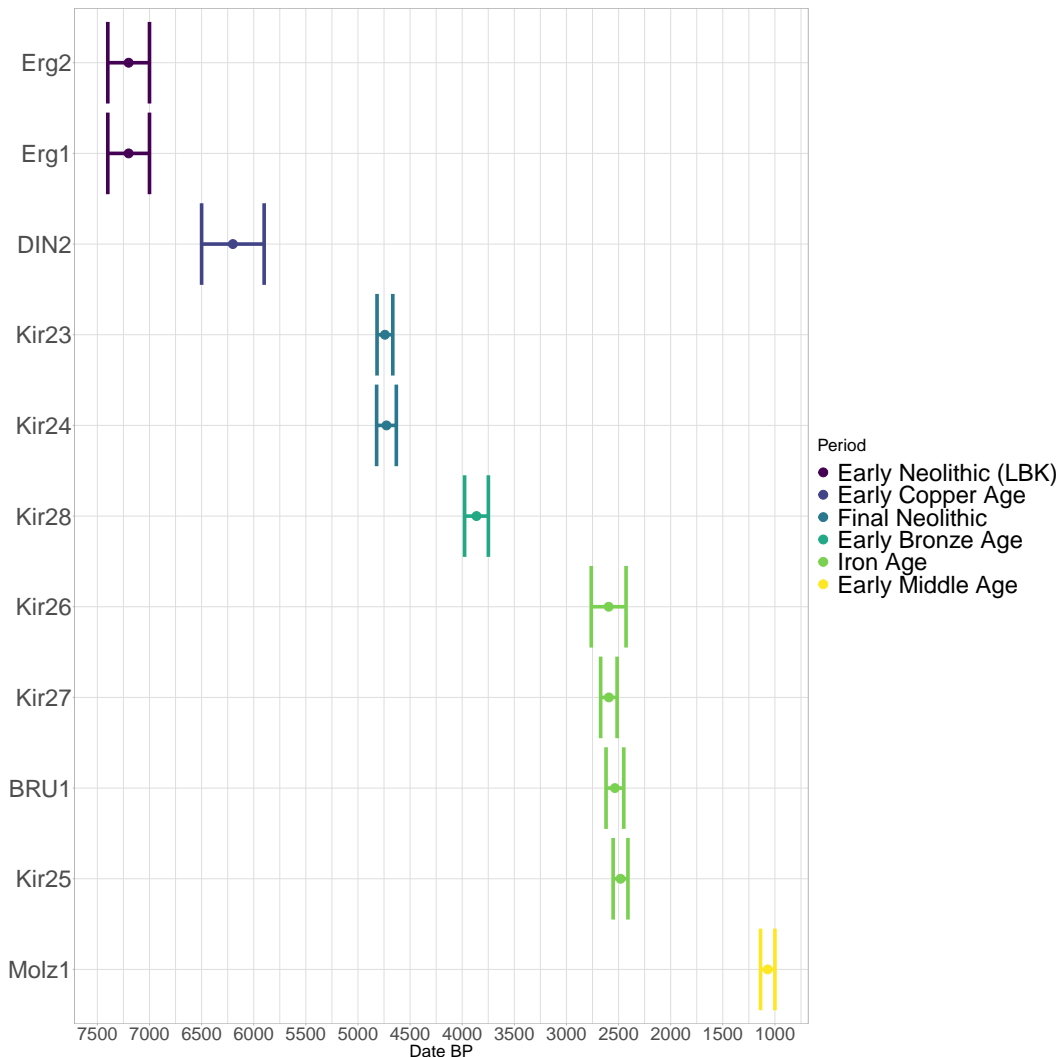


Figure 4.2: Estimated radiocarbon dates for each newly sequenced ancient individual, grouped by archaeological period.

Sample.ID	Location	Date	Period	Coverage
Erg1	Ergoldsbach-Essenbach	5200	Early Neolithic (LBK)	4.52
Erg2	Ergoldsbach-Essenbach	5200	Early Neolithic (LBK)	0.71
DIN2	Dingolfing	4200	Early Copper Age	1.71
Kir24	Cherry Tree Cave	2762	Final Neolithic	3.98
Kir23	Cherry Tree Cave	2741	Final Neolithic	17.52
Kir28	Cherry Tree Cave	1863	Early Bronze Age	17.30
Kir26	Cherry Tree Cave	595	Iron Age	4.84
Kir27	Cherry Tree Cave	593	Iron Age	16.60
BRU1	Bruckberg	535	Iron Age	11.54
Kir25	Cherry Tree Cave	481	Iron Age	4.55
Molz1	Molzbichl	1069	Early Middle Age	13.22

4.2.2 Stuff that Jens did (e.g. read aligning)

4.2.3 Genotype imputation and phasing using GLIMPSE

This section details the steps used to process the newly sequenced and reference ancient samples used in all subsequent analyses. ChromoPainter analysis requires that all samples are i) phased and ii) contain no missing genotypes (i.e. “./.”). GLIMPSE [15] is software which is designed to perform both of these steps on low-coverage sequence data with the aid of a reference panel. GLIMPSE was chosen as it is the most efficient (in terms of time and memory) probabilistic phasing / imputation software available [15]. The other possible option, Beagle4 [27], is too slow and memory inefficient to impute the large number combined number of individuals and SNPs present in this dataset.

I merged the 17 newly sequenced individuals with the reference data-sets A.1 to A.17 resulting in a total of 942 individuals in .bcf format with genotype likelihood data at 77,213,942 genome-wide SNPs. Data was then split into separate .bcf files for each chromosome and indexed using bcftools [46].

I followed the GLIMPSE [15] imputation and phasing pipeline (https://odelaneau.github.io/GLIMPSE/tutorial_b38.html) to generate genotype likelihoods and phased genotypes for each individual. For the reference panel, I used the 30x 1000 genomes dataset [28], described in appendix A.5.

GLIMPSE `chunk` was used to split the present-day reference dataset into chunks. Default settings of `-window-size 2000000` and `-buffer-size 200000` were used, generating a total of 936 regions genome wide. Splitting the genome into regions for imputation jointly maximises computational efficiency and accuracy [15]. For each region in turn, the target dataset, consisting of phred-scaled genotype likelihoods (PL), was imputed using GLIMPSE `phase` under default settings and the same reference panel. Here, ‘impute’ means filling in sporadic missing genotypes that are missing in a single individual (or

sometimes more), rather than the whole-scale imputation of non-genotyped positions. **GLIMPSE ligate** was then used to concatenate the 936 imputed regions into 22 distinct chromosomes. Finally, **GLIMPSE sample** was used to generate phased haplotypes from the output of **GLIMPSE ligate** using default settings. In total, 50,342,061 bi-allelic autosomal SNPs remained after phasing and imputation.

Previous sections (cite section) have shown that using a set of SNPs which are common yields results which are least affected by coverage related bias, likely in part because common variants can be imputed more accurately. Therefore, I chose to filter the SNPs to those 477,416 those present in the HellBus dataset (A.20). Thus these SNPs were used for all subsequent analyses.

4.2.4 Estimation sample-heterozygosity

Heterozygosity was estimated for all 942 using the **plink2 -het** command. The solved haplotypes from the previous section was used for this analysis.

4.2.5 plink PCA

To determine the overall ancestry patterns of the newly sequenced individuals in the context of 915 other ancient samples, I performed PCA on the non-imputed genotypes using **plink2**. Performing an unlinked PCA allows us to identify any data quality issues which are independent of phasing / haplotype-based analysis.

I retained only the 500,000 markers with the lowest amount of missingness and then LD-pruned the resulting SNPs using the settings **-maf 0.01** and **-indep-pairwise 50 5 0.2**. PCA was performed using default settings from **plink2** and the first two principle components plotted.

4.2.6 Chromopainter analysis

I merged the datasets of ancient individuals, described in sections 4.2.3, with the set of genotyped modern individuals described in appendix section A.20. To perform ChromoPainter analysis, the genotypes for both the ancient samples and present-day samples is required to be in ChromoPainterUncertainty format (point to section in chapter 1).

The present-day individuals were genotyped on a genotyping array and therefore could not be phased and imputed using GLIMPSE (which is designed for sequence data). As the data for present-day individuals was required to, but did not have, genotype likelihoods for each SNP, I created ‘fake’ genotype likelihoods for each individual using `bcftools -annotate`, corresponding to fully certain genotypes i.e. $\max(GL) = 1$. For each chromosome, I merged together i) the phased haplotypes for the modern and ancient datasets and ii) the genotype likelihoods for the modern and ancient dataset, both using the `bcftools -merge` command, resulting in 2 vcfs (per chromosome). I then used a custom script (https://github.com/sahwa/vcf_to_chromopainter) to convert each resulting pair of files into chromopainter uncertainty format.

I selected all ancient samples above 1.5x coverage and performed an ‘all-v-all’ painting where each haplotype was compared to all other haplotypes in turn. This retained 466 individuals for the ChromoPainter analysis. 1.5x was somewhat arbitrarily chosen as a conservative threshold to reduce coverage related bias whilst still retaining a suitable number of individuals. This allows for the characterisation of the ancestry of the newly sequenced ancient samples in the context of other ancient individuals. It is also the painting that can be used to perform fineSTRUCTURE clustering and tree building on ancient samples. Hereafter referred to as ‘ancient’ painting.

Although there were 466 individuals in the ‘ancients’ painting, not all of these were included in the chunklengths PCA. This was because many individuals

in that set were not relevant to exploring the ancestry of the individuals at hand. For instance, when plotted, samples such as those from the Xiong Nu, a 3rd century BC culture from inner Mongolia, dominate the variation in a PCA to the point where identifying structure between the samples of interest becomes impossible. Therefore, a process of ‘trial and error’ is used to decide which individuals to include in a PCA. This process is somewhat subjective, but occasionally subjective methods are required when facing heterogeneous ancient DNA datasets.

I also performed an ‘all-v-all’ painting of a selected group of present-day individuals and the newly sequenced ancient individuals. The populations retained are given in table . Hereafter referred to as ‘present-day painting’.

Both the ‘present-day’ and ‘ancient’ paintings were merged separately using chromocombine-0.0.4 (<https://people.maths.bris.ac.uk/~madjl/finestructure-old/chromocombine.html>). The ‘C’ factor, which is used for fineSTRUCTURE clustering, was also estimated for both paintings.

The fineSTRUCTURE (v0.0.5) [13] clustering and tree building algorithm was applied to the chunkcounts ChromoPainter output for the ‘ancient’ painting. This algorithm assigns individuals to genetically homogeneous clusters, estimates the ‘true’ number of clusters and builds a dendrogram of genetic similarity. This is particularly useful when combining many samples from different studies, as is the case with the ‘ancients’ painting; the population label identifiers used by different studies may not be consistent with one another. Therefore, we can use fineSTRUCTURE groupings as population labels rather than external group labels. fineSTRUCTURE was first run in MCMC mode using 1,000,000 burn-in MCMC iterations and 2,000,000 main MCMC iterations. It was then run in tree-building mode (`-m T`) using 100,000 burn-in and 100,000 main iterations.

Tree figures, co-ancestry matrix figures and principle component plots were

Population	nsamples
HB:tsi	196
HB:spanish	68
HB:bulgarian	62
HB:german	60
HB:french	56
HB:russian	50
HB:greek	40
HB:ukrainian	40
HB:croatian	38
HB:hungarian	38
HB:norwegian	36
HB:southitalian	36
HB:polish	34
HB:romanian	32
HB:mordovian	30
HB:cypriot	24
HB:northitalian	24
HB:lithuanian	20
HB:siciliane	20
HB:westsicilian	20
HB:belorussian	18
HB:tuscan	16
HB:irish	14
HB:scottish	12
HB:germanyaustralia	8
HB:welsh	8

Table 4.1: Name of population and number of samples used in the present-day ChromoPainter analysis

generated using the fineSTRUCTURE R library (<https://people.maths.bris.ac.uk/~madjl/finestructure/FinestructureRcode.zip>).

TVD is a distance metric, given as the absolute sum of the pairwise differences between two copyvectors.

4.2.7 SOURCEFIND

The chunklengths / chunkcounts matrices outputted by ChromoPainter give informative but noisy estimates of the length of the genome a given individual most closely matches to another individual. In part due to confounding effects

like variable sample size within donor populations and incomplete lineage sorting, the coancestry matrices cannot be seen to correspond to true ancestry proportions. In order to infer ancestry proportions from the data, I ran the SOURCEFIND algorithm [16] using 3 different sets of copyvector / surrogate combinations. Surrogates are populations for which we wish to estimate of in our target population. For instance, in the most simple case, we may wish to estimate the proportion of ‘African’ and ‘European’ ancestry within an admixed target individual. There, we would use 2 surrogates, perhaps a population from Yoruba and a population from France. The surrogates need not be the ‘true’ mixing sources. It is important to note that SOURCEFIND does not directly infer admixture events, in that it does not model the break down of admixture LD as does ALDER or GLOBETROTTER, but

Previous research suggests that almost all ancient Europeans (discounting particular paleolithic Hunter-Gather populations [38]) can be modeled as differing amounts of Western Hunter Gatherers (WHG), Early Neolithic farmers from present-day Anatolia and Bronze Age pastoralists from the Eurasian Steppe (best represented by individuals from the Yamnaya culture [5]). Therefore, a simple approach to identifying the broad-scale ancestry of ancient individuals is to model them as a mixture of the three aforementioned populations. Thus, I performed SOURCEFIND analysis, using these 3 populations as surrogates.

It is usually desirable to estimate more fine-scale ancestry proportions than only using the 3 aforementioned surrogates. I decided to model each newly sequenced ancient sample as a mixture of populations which are older than the target, as modeling an individual in terms of more recent populations can lead to results which are more difficult to directly interpret. I retained surrogate populations where the average age of samples within the population was older or within 100 years of the target individual. Thus, different newly sequenced ancient samples were analysed using different number of surrogate individuals.

Finally, I wanted to estimate proportions of ancestry from present-day

surrogates in ancient samples. For this analysis, I used the ‘modern’ painting and used all modern populations from the ‘HellBus’ dataset as surrogates.

For all of the three above analyses, I performed 3 independent SOURCEFIND runs. SOURCEFIND explores the parameter space of ancestry proportions using MCMC sampling. Therefore, particularly when there is a large number of surrogates, it is important to ensure that each separate MCMC run has converged to the same set of parameters and that each chain has mixed sufficiently. For each target, all 3 MCMC runs were then combined to form an MCMC list using the `coda` R library [32]. I ensured all chains had converged using the `autocorr.diag` function. I then used the `mcmc` function to jointly estimate ancestry proportions and empirical credible intervals for each target population.

4.2.8 MOSAIC admixture analysis

I inferred admixture events, dates and proportions using MOSAIC, a haplotype-based method [50]. MOSAIC was used because, unlike GLOBETROTTER [51], the ‘painting’ step and admixture inference step are combined into one, resulting in a simpler pipeline and more flexible assignment of different surrogates (i.e. the set of surrogates can be changed without repainting the samples). MOSAIC also estimates the f_{st} between the set of surrogates and the estimated ‘true’ mixing source, which is useful when a good proxy for the ‘true’ mixing source is not available.

I performed 2 different kinds of admixture modeling. Firstly, I performed an ‘ancient surrogates’ model where the high coverage ancient samples described in the previous section were used as surrogates. I used the fineSTRUCTURE groupings to assign the samples.

I then performed a ‘present-day surrogates’ analysis where a selected set of present-day populations were used to analyse both present-day Slavic popu-

lations and ancient Slavic populations. Using these samples provided cleaner results, at the cost of reduced interpretability. By this, I mean that forming, for example, a 4,000 year-old Bronze Age sample as a mixture of present Europeans may be difficult to interpret; what does it mean if it is 70% French and 30% Tuscan? As the samples become more recent (i.e. into the Middle Ages), forming them as a mixture of moderns becomes more appropriate, since there has been relatively fewer large scale population movements separating the ancient and modern samples.

Phased .vcf files, the output from GLIMPSE, were converted to .hap/.sample files using `bcftools convert -hapsample`. The resulting .hap/.sample files were then converted to MOSAIC input using the provided script (https://maths.ucd.ie/~mst/MOSAIC/convert_from_haps.R). MOSAIC was run using default settings and the following sets of populations as targets and the following sets as surrogates. I formed each target as a mixture of either 2 or 3 ancestral sources. Upper and lower quantiles for admixture dates were estimated using a bootstrap procedure when more than one sample was present.

4.2.9 Allele-frequency based tests

Many of the relevant samples in the literature were of either very low coverage (< 0.1) or genotyped on a capture array. Previous research (cite section) has shown that samples of this coverage cannot reliably be analysed using ChromoPainter. f-statistics (such as the f_3 admixture test or the f_4 branch test) are mostly robust to coverage related effects [52]. Therefore, using these methods allows for the co-analysis of a much larger number of samples. In particular, there were many low-coverage samples from LBK cultures from Rivollat et al (2020) which would not have been suitable for use with ChromoPainter [53].

I used Admixtools [2], implemented in admixtools2 R library (<https://uqrmaie1.github.io/admixtools>) to employ several different f-statistics.

I converted imputed .vcf to .ped/.map format using plink. It has been shown that using imputed markers reduced reference bias relative to using pseudo-haploid markers [6]. Convertf from the Admixtools library was then used to convert .ped/.map files into Eigenstrat format suitable for use with Admixtools.

I used the f_4 branch test to test whether 2 populations form a clade to the exclusion of 2 other populations. For example, the $f_4(french, german; yoruba, mbuti)$ would give a Z score not significantly different to zero, given we would expect *french* and *german* to form a clade to the exclusion of *yoruba* and *mbuti*. However, exchanging *french* with *yoruba* would yield $|Z| > 3$.

f_3 in the form of $f_3(A, B; C)$ was used to either i) estimate the branch length between A and B after their divergence from C , or ii) to test whether C has been formed from an admixture event between A and B , based on if C has allele-frequencies which are intermediate between A and B .

qpAdm was used to infer ancestry proportions. I followed the steps (as closely as was possible given the samples available to me) taken in Olalde et al (2018) with respect to outgroup selection, choosing the following populations/samples: *Mota*, *Kostenki14*, *papuan*, *han*, *hannchina*, *mbutipygmy*, *sannamibia*, *yakut*. These outgroups were suitable for use in investigating ancient Eurasians, since they are asymmetrically related to many ancient populations, but do not show evidence of recent gene flow with them.

4.3 Results

4.3.1 Broad overview of genetic ancestry

To obtain a broad overview of the genetic ancestry of the newly sequenced samples in the context of a large reference set of ancient individuals, I performed

a principle component analysis on the genotype matrix of selected ancient samples using plink2 (Fig. 4.3).

As expected, the samples from the Early Neolithic (approx 5200BC) and Copper Age (approx 4200BC) cluster with other samples from the European Neolithic. Previous studies have explained the pattern observed when Neolithic samples are plotted on a PCA [54]; the earliest Neolithic samples, from Anatolia and Greece, who are thought to be the source population from which all subsequent Neolithic farmers derive from [5, 55–58], are usually positioned at the end of the cluster which is farthest away from the Bronze Age samples. This likely reflects the fact they are unadmixed and perhaps more drifted with respect to the later Neolithic samples. As the Neolithic progressed, the farmers from the east mixed with local Hunter-Gatherer groups in central Europe [54], acquiring local hunter-gatherer ancestry. Accordingly, these samples are shifted away from the earlier Neolithic samples, ‘north’, towards the Bronze Age samples. I did not include Hunter-Gatherer samples in order to maximise the relevant space-efficiency of the PCA, but the later Neolithic samples would be shifted towards Hunter Gatherer populations if present (see supplementary figure x). With this in mind, the position of Erg1, shifted north away from the contemporaneous sample Erg2, is suggestive of hunter-gatherer admixture.

The 2 samples from the Late Neolithic display substantial differences; one sample, Kir24, is positioned at the extreme top-left of the PCA, close to the Yamnaya type-specimen, indicating it may share recent ancestry with the first individuals who carried ‘Steppe-related’ ancestry from central Asia to Europe. On the other hand, Kir23 clusters with samples from Neolithic Europe. The single Bronze Age sample clusters primarily with other European Bronze Age samples, whereas the 4 samples from the Iron Age are shifted substantially towards the Neolithic cluster, consistent with the placement of other samples from the European Iron Age. Finally, the 3 samples from Medieval period cluster with the Bronze Age.

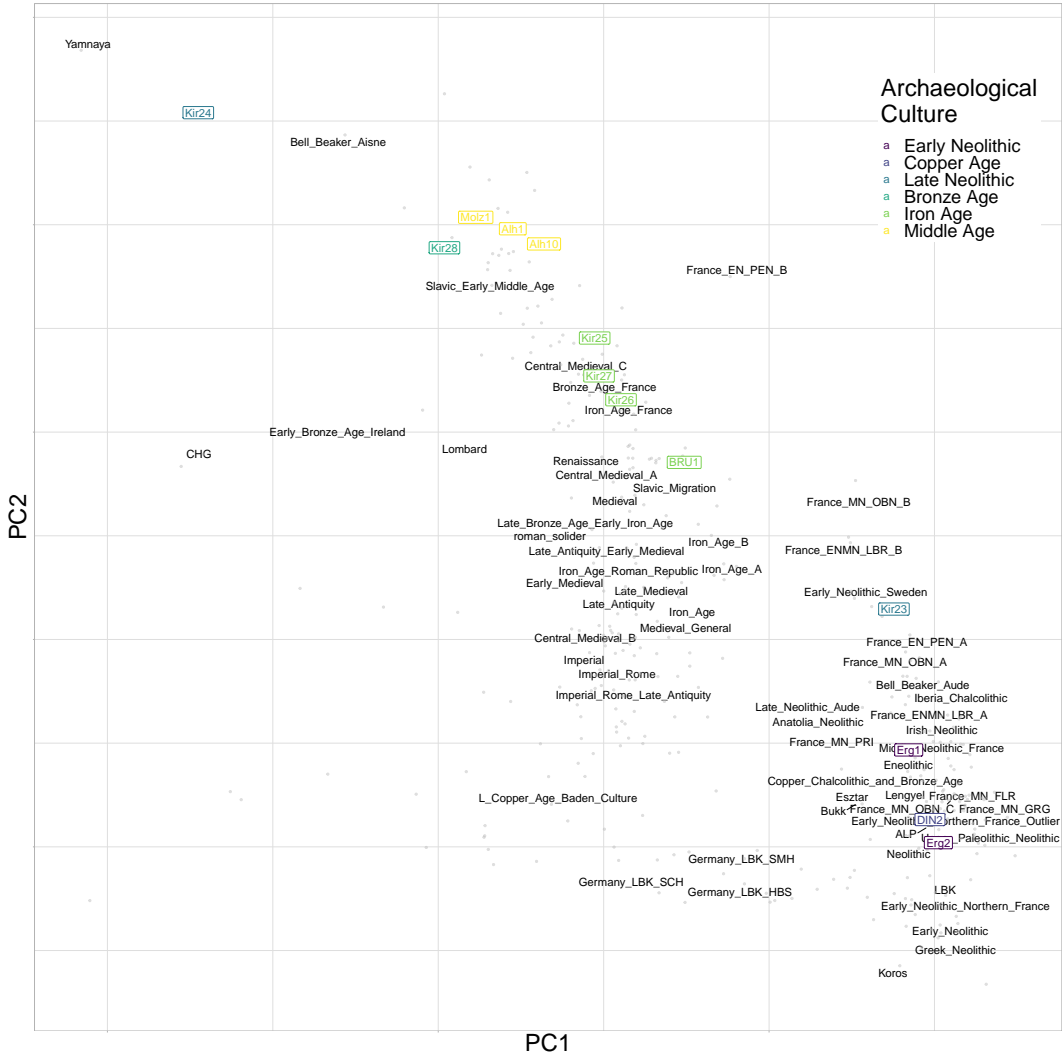


Figure 4.3: Principle component analysis of genotype matrix using plink2. Grey points indicate principle component coordinates for each sample. Black text indicated mean principle component coordinates for all individuals within that group. Coloured labels represent newly sequenced ancient samples.

4.3.2 Early Neolithic

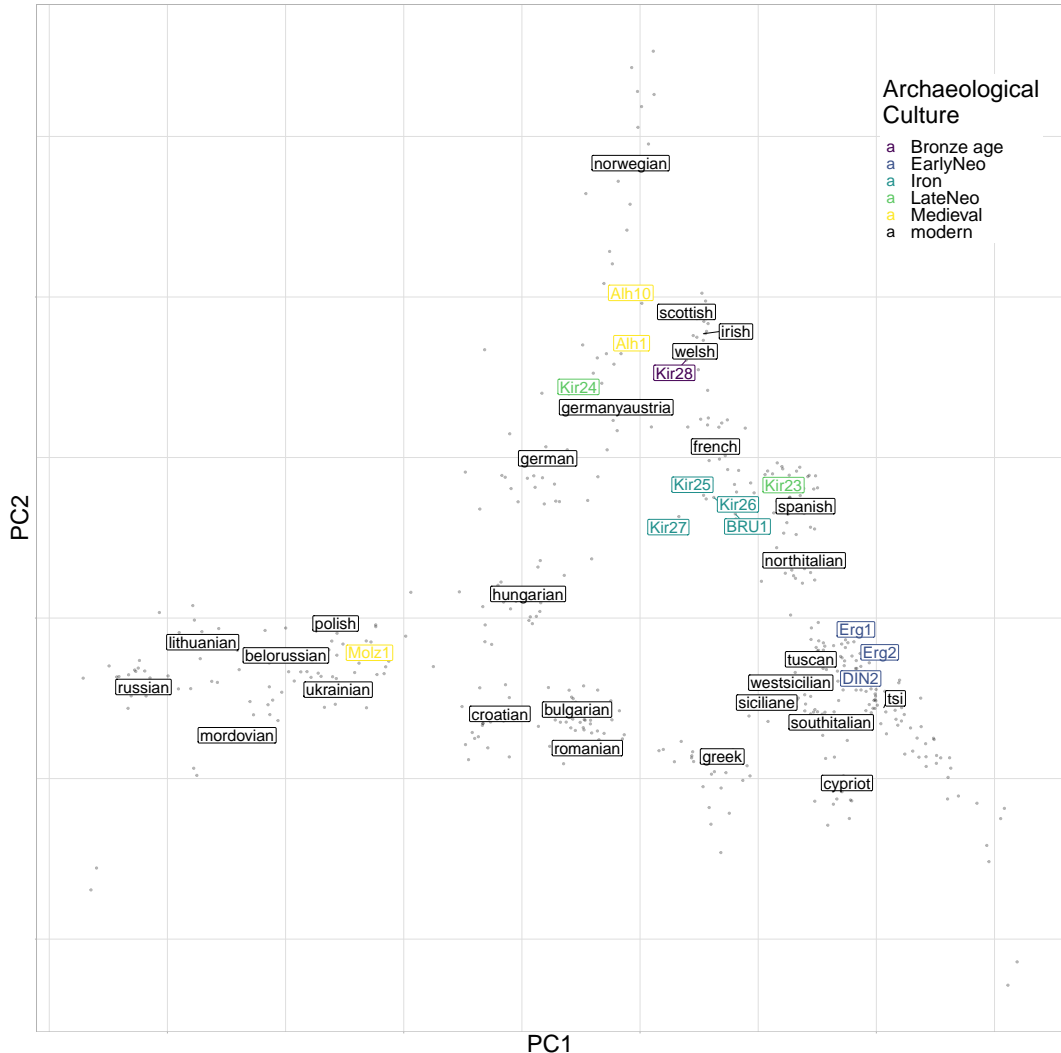


Figure 4.4: Principle component plot of newly sequenced ancient samples and reference modern individuals performed using the *finestructure* library. Green labels correspond to Migration Era samples, red labels correspond to Early Middle Age samples and white labels correspond to reference populations. The position of each reference label is the mean PC coordinates of all individuals within that population. Transparent coloured points correspond to present-day individuals.

The 3 Early-Middle Neolithic samples all display strong affinity to Anatolian farmers, consistent with the prevailing theory that near-eastern farmers were responsible for the spread of farming across Europe [5, 56–58], and that all Neolithic farmers shared recent common ancestry. *fineSTRUCTURE* analysis showed that Erg1 clusters with 2 samples from Upper Paleolithic/Neolithic

Italy and DIN2 clusters with Neolithic samples from Germany, Greece, Anatolia and Hungary. Despite their age, the variation of the Early Neolithic samples falls well within the variation of present-day individuals; when painted using modern individuals, the 3 Early Neolithic individuals cluster with present-day Italians, consistent with previous research [5, 33] (Fig. 5.6). Erg1 was assigned to mtDNA haplogroup K which has been found in Neolithic and pre-pottery sites across Europe [55, 59] and Western Asia [60, 61].

Erg1 is from the *Linearbandkeramik* (LBK) culture and is speculated to have belonged to the first wave of immigrants carrying farming technology from south-eastern Europe or Anatolia into central Europe. DIN2 is from a nearby site and around 500 years more recent, and is thought to potentially belong to a second wave of farmers who migrated along the Danube (J. Burger 2018, personal communication). It is unclear to what extent these different waves corresponded to different populations.

Considering all other recipient samples, Erg1 had the lowest *TVD* with DIN2, supporting the hypothesis that they were from the same source population. It had the second lowest *TVD* with Ess7, another LBK sample, from Essenbach, Germany. DIN2 also shares low *TVD* with Ess7, but has the lowest *TVD* with NE5 and NE7, samples assigned to Middle and Late Neolithic cultures on the Hungarian plane. DIN2 was assigned to mitochondrial haplogroup J1C, the same as the samples NE4 and NE5. Both the autosomal and mtDNA link to Neolithic Hungary supports the postulation that DIN2 migrated along the Danbian route.

To explicitly test whether Erg1 and DIN2 group together to the exclusion of other ancient samples and therefore, whether they likely originated from a similar source population, I performed f_4 tests in the form of $f_4(W = \text{Erg1}, X = \text{DIN2}; Y = \text{test}, Z = \text{Mbuti})$, where *test* is all ancient populations in my dataset. This tests whether Erg1 and DIN2 form a clade to the exclusion of *test* or not. Of the 143 comparisons, only the population labeled as WHG

had a $|Z| > 3$, ($Z = 3.057$), suggesting that Erg1 and DIN2 originate from the same local population. However, this result was surprising given we would not typically expect an individual from the LBK culture to form a clade with hunter-gatherer populations. However, this could be indicative of gene flow between a WHG-like source and Erg1. This result was robust to outgroup choice.

To determine whether Erg1 showed increased genetic similarity to local farming populations, I also performed combinations of f_3 in the form of $f_3(A = \text{Erg1}, B = \text{test}, C = \text{Mbuti})$, where *test* is all ancient populations. This tests the branch length, or the amount of genetic drift that has occurred on the branch between Erg1 and *test* since their divergence from an outgroup.² The sample/population with the highest f_3 statistic was NE7, a sample from 4,360 – 4,490 BC and the Lengyel culture (a Neolithic culture centered on the Danube River, known to be an offshoot of the LBK culture Erg1 belonged to). On the other hand, DIN2 shows a clear affinity to samples from neolithic France.

I also obtained SNP-capture data from several other local LBK populations; samples from Schwetzingen, Stuttgart-Mullhausen and Halberstadt (Rivollat samples). These samples appear to form a distinct cluster on the unlinked PCA and are shifted away from the primary cluster of Neolithic individuals and towards samples from the Anatolian Bronze Age and Baden Culture (a central European Chalcolithic culture). I wanted to know which LBK population Erg1 and DIN2 were closest to. I found strong evidence ($|Z| = 7.97$) that Erg1 shared more alleles with LBK populations from Schwetzingen than with Stuttgart-Mühlhausen, suggesting the early LBK populations showed relatively fine-scale geographic structure. Given the lack of Hunter Gatherer ancestry in the Rivollat LBK samples, this structure seems unlikely to be driven by variable amounts of Hunter-Gatherer admixture (Fig. 4.8).

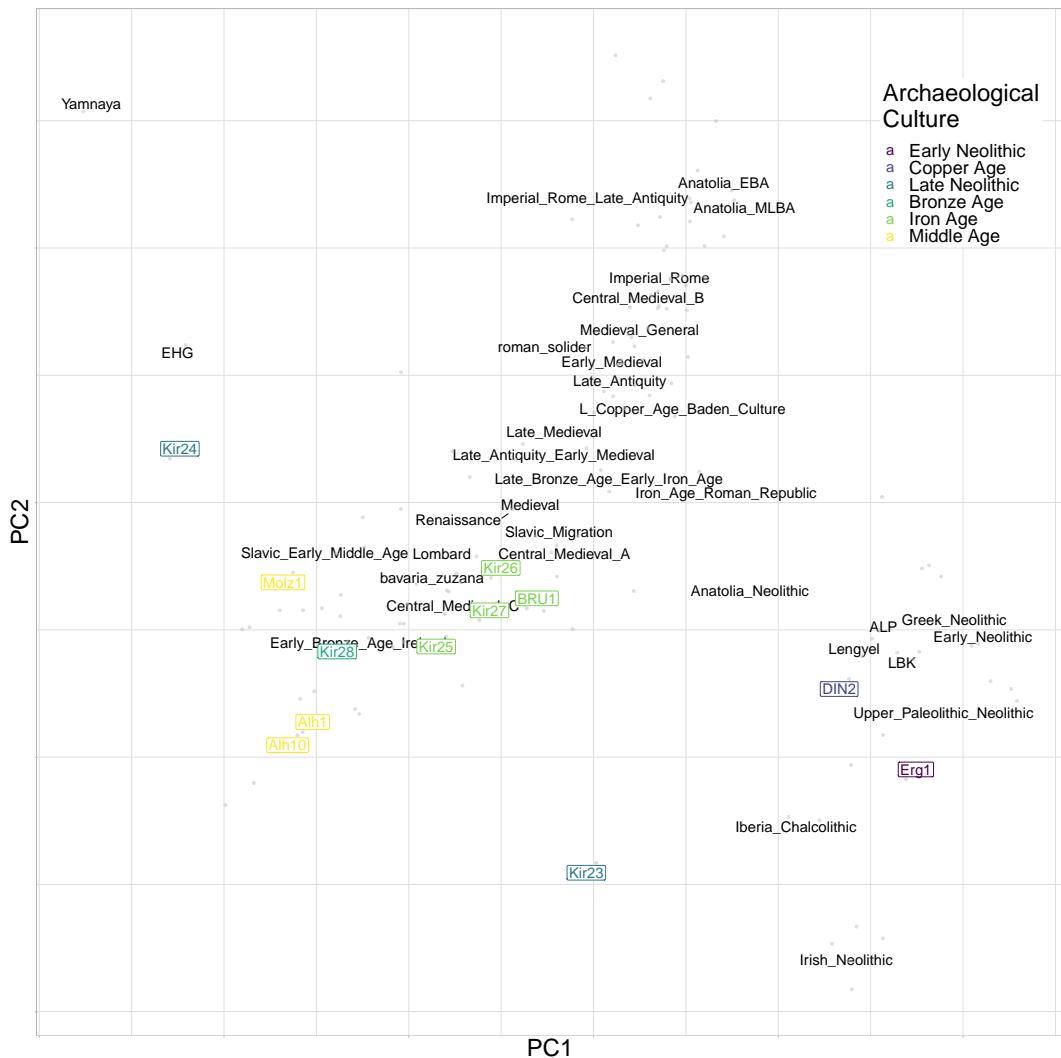


Figure 4.5: Principle component plot of newly sequenced ancient samples and reference ancient individuals performed using the finestructure library. Filled labels correspond to newly sequenced individuals and white labels correspond to reference populations. The position of each reference label is the mean PC coordinates of all individuals within that population

4.4 Hunter-gather ancestry in Neolithic farmers

Prior research has shown that admixture occurred between newly arrived farming immigrants from Anatolia and local hunter-gatherers [54, 62]. The position of Erg1 on the PCA suggests that it may have a substantial component of Hunter-Gatherer ancestry. I applied the SOURCEFIND algorithm to the ‘ancients painting’ co-ancestry matrix to infer direct ancestry proportions for all newly sequenced individuals, fixing 3 surrogate populations at WHG, Yamnaya and Anatolian Neolithic (Fig. 4.9). I inferred 26% WHG ancestry in Erg1, suggesting it may have had a relatively recent ancestor who was a Hunter-Gatherer. I inferred a smaller proportion of WHG ancestry into DIN2 (8%), perhaps suggest that they were apart of a structured local population, where different elements received varying amounts of Hunter Gatherer. qpAdm modeling broadly agreed with these estimates and showed that Erg1 can be modeled as a mixture of Anatolia Neolithic (61%, se=0.095) and WHG (0.3855%, se=0.095). Erg2 showed no evidence of Hunter-Gatherer ancestry and could be modeled directly as Anatolian Neolithic farmer.

To localise the closest source of Hunter-Gatherer admixture into Erg1, I re-performed the SOURCEFIND with 3 surrogates (Fig. 4.9) and split up the WHG surrogates into Loschbour, LaBrana, Bichon and the 2 individuals from the Iron Gates. I inferred that the two 8800-year-old Iron Gates individuals from Serbia contributed towards 33% of the ancestry of Erg1, showing that it was likely to be closest population to the mixing source in our dataset. To confirm that this was not an artefact of there being 2 Iron Gates individuals (where all of the other WHG populations had a single sample), I removed the lowest coverage Iron Gates individual from the surrogate pool and repeated the analysis. The proportion of ancestry inferred from Iron Gates was similar (31%), suggesting the sampling did not affect the inferred proportion.



Figure 4.6: SOURCEFIND ancestry proportion estimates for all newly sequenced target samples (vertical columns). Target samples are grouped by archaeological age. Surrogate populations are represented as horizontal rows and also grouped into archaeological culture. Each target was modeled as a mixture of only populations which are dated to being older or contemporaneous as the the target. Numbers within each cell correspond to the ancestry proportion estimate.

To determine the date of admixture between an Anatolian Farmer-like and WHG-like source into Erg1, I employed the software MOSAIC, which infers admixture events using a similar technique to chromosome painting. MOSAIC is able to model the ‘true’ admixing sources and determine the genetic differentiation between those and the sampled sources, in addition to the dates. When modeled as a 2-way admixture event, MOSAIC inferred highly similar WHG and Anatolia Neolithic mixing proportions to SOURCEFIND. It inferred the cluster of Italian Hunter Gatherers to be the closest population to the true mixing source (Fig. 4.7). MOSAIC is able to infer the Fst between the ‘true’ mixing groups and the sampled populations. I inferred very low Fst between the true and source populations, suggesting we had sampled a good proxy for the ‘true’ mixing sources. I inferred an admixture date of 5.3 generations before the Erg1 was alive. I caution that the admixture date may be unreliable due to only targeting a single individual and given MOSAIC bootstraps over individuals (rather than over Chromosomes as in GLOBETROTTER or LD blocks as in qpAdm), it was not possible to obtain confidence intervals around admixture date.

To confirm this admixture event, I performed an f_3 admixture test, which, when significantly negative, provides unambiguous evidence of an admixture event [2]. I performed the test $f_3(A = \text{Castelnovian_Mesolithic}, B = \text{Anatolia_Neolithic}, C = \text{Erg1})$, selecting the A and B populations as those were inferred by MOSAIC to be closest to the admixture sources. This did not yield a significant result ($Z = 1.96$). However, exchanging Anatolia_Neolithic for LBK, a source temporally and geographically more proximate to Erg1 yielded a significant result ($Z = 4.25$).

I also obtained SNP-capture data from several other local LBK populations; samples from Schwetzingen, Stuttgart-Mullhausen and Halberstadt (Rivollat samples). These samples appear to form a distinct cluster on the unlinked PCA and are shifted away from the primary cluster of Neolithic individuals

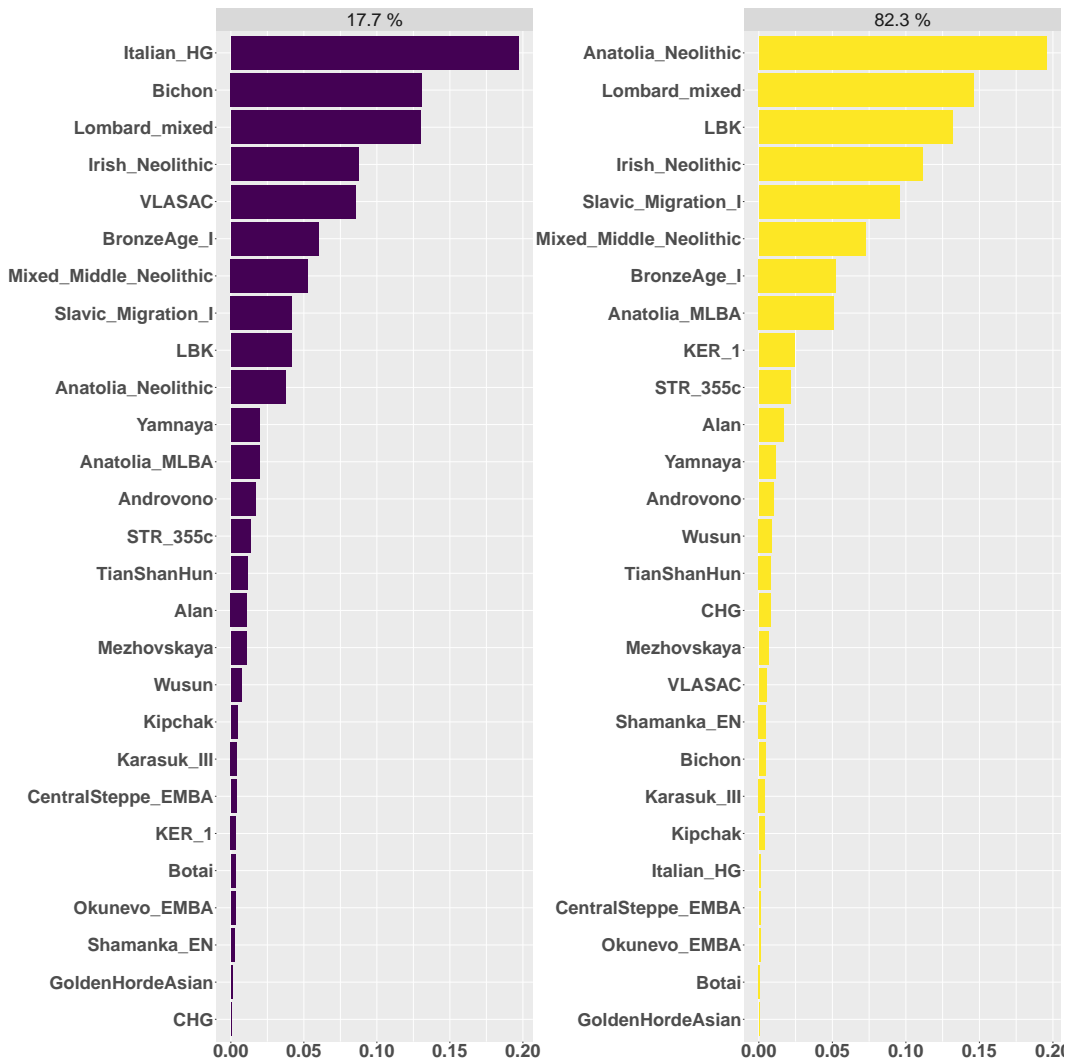


Figure 4.7: Copying matrix plot for sources in 2-way admixture event for Erg1. Each panel represents one of the 2 mixing sources. Labels above each panel give the proportion that mixing source contributed to the Early Middle Age samples. Length of the bars within each panel represent the amount that mixing source copied from a particular population.

and towards samples from the Anatolian Bronze Age and Baden Culture (a central European Chalcolithic culture) (Fig. 4.3). I wanted to contextualise the amount of Hunter-Gatherer in the newly sequenced samples, compared to different French and German farmer groups. As expected, and shown by previous studies [63], Early Neolithic populations show little sign of Hunter-Gatherer ancestry, which appears more into the Middle Neolithic and further west from Greece and Anatolia. Populations from France, in particular early samples, show the highest amount of HG ancestry. However, contemporaneous populations from Germany display much reduced levels of HG ancestry and can fit a model of purely Anatolia Neolithic ancestry well. Our sample Erg1 appears to be an exception, displaying high levels of HG ancestry comparable to the samples found in France (Fig. 4.8). On the other hand, Erg2, a sample which is contemporaneous and local to Erg1, showed no evidence of Hunter Gatherer admixture

4.4.1 Late Neolithic

This dataset included 2 individuals found in the same stratigraphical layer of Cherry-Tree cave; Kir23 and Kir24 were both dated to the Late Neolithic (approx 4700 BP). Despite their temporal and spatial closeness, they show highly different ancestry profiles (Fig. 4.9).

On both the plink and ChromoPainter PCA and fineSTRUCTURE clustering, Kir24 clusters with individuals from the Bronze Age Steppe, such as those from the Yamnaya and Afanasievo cultures, known to be responsible for the spread of Indo-European languages [33]. These results support the findings of Allentoft (2015), who concluded that the Afanasievo Culture were ‘genetically indistinguishable’ from the Yamnaya Culture. That the Yamnaya and Afanasievo samples were sampled in Russia suggests that Kir24 may have been a recent migrant from the Eurasian Steppe. This is supported by IBD analysis; of all the ancient samples in the dataset Kir24 shares the most IBD

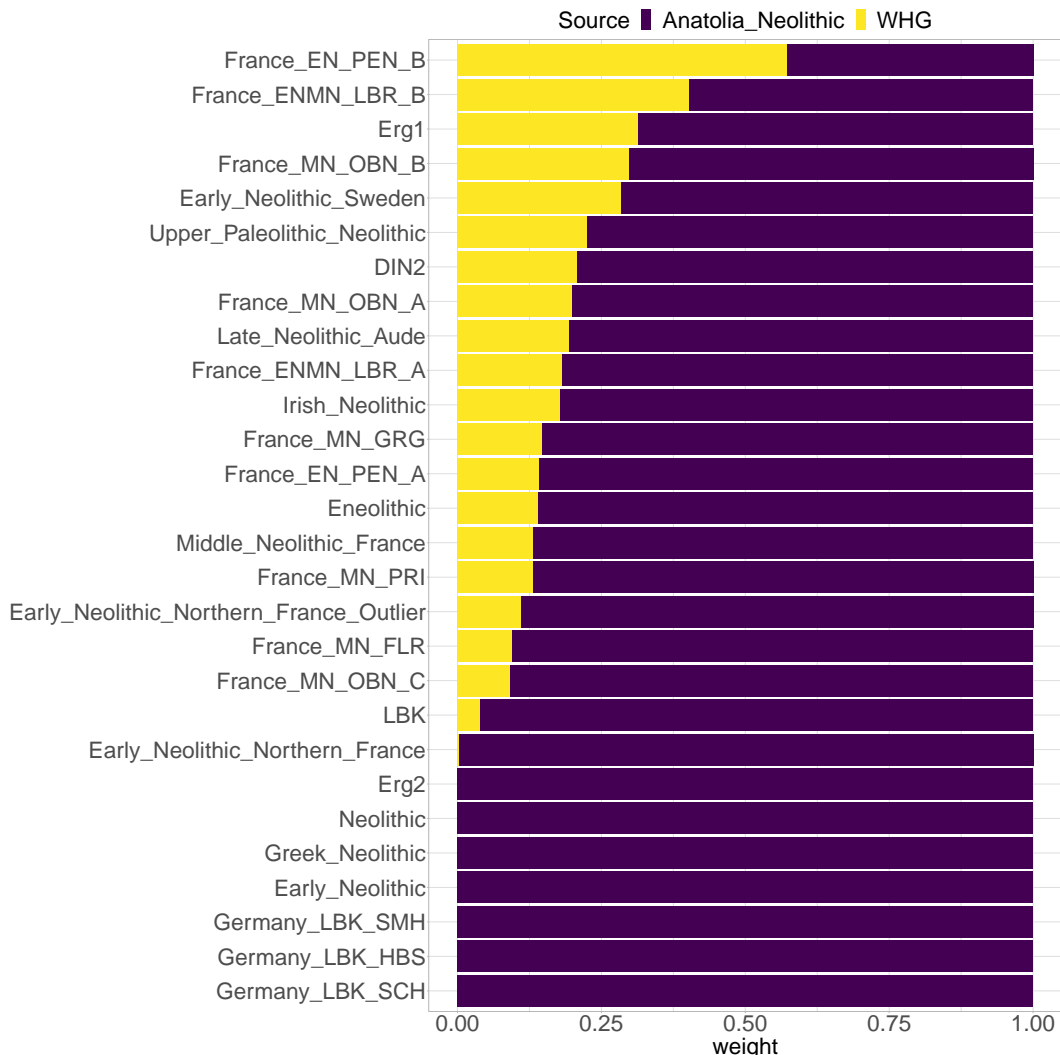


Figure 4.8: qpAdm ancestry proportion estimates for a selection of European Neolithic individuals. All individuals were modeled as a 2-way mixture between Anatolian Neolithic farmers and Western-Hunter Gatherers (WHD). Outgroups given in methods 4.2.9.

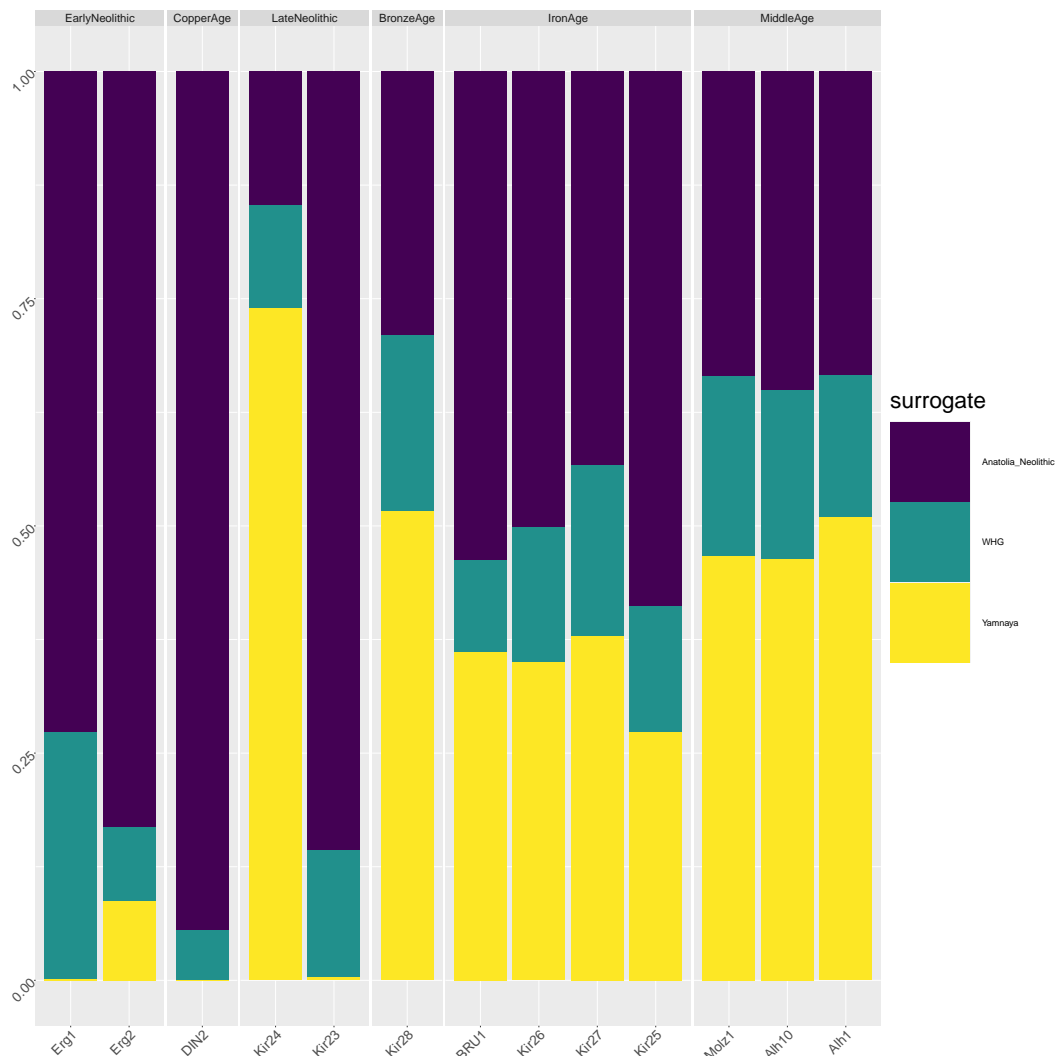


Figure 4.9: SOURCEFIND ancestry proportion estimates for all newly sequenced target samples (vertical columns). Target samples are grouped by archaeological age. Surrogate populations are represented as horizontal rows and also grouped into archaeological culture. Each target was modeled as a mixture of only populations which are dated to being older or contemporaneous as the the target. Numbers within each cell correspond to the ancestry proportion estimate.

(31.12cM) with Yamnaya and the lowest *TVD* with 2 other members of the Yamnaya population. This timing (Kir24 is dated to approximately 4700 BP) corresponds to some of the earliest appearance of Yamnaya-like ancestry in central Europe [64]. Kir24 could be modeled as a mixture of Yamnaya (93%, se=12%) and WHG (6%, se=8%) without any Neolithic ancestry.

Kir24 can be assigned to mtDNA haplogroup T1a1, which has been found in Yamna samples from the Middle Volga region and Bulgaria [65]. Additionally, they found the frequency of T1a1 to be higher in the Yamna peoples than in any other ancient or modern population.

On the other hand, Kir23 is found in a fineSTRUCTURE cluster with Ballynahatty, an Irish Neolithic sample from 3343-3020BC, and is positioned on the PCA with other late Neolithic samples. It is found in adjacent fineSTRUCTURE groups to samples from Neolithic Spain and Ireland. As is the case with other Neolithic samples of this era, Kir23 has a component of Hunter-Gatherer ancestry; it is known that Middle Neolithic individuals are characterised by admixture with the existing Hunter-Gatherer populations. qpAdm modeling showed that Kir23 could be formed from a mixture of Neolithic Anatolia (96%, se=14) and Hunter Gatherer (6.25, se=0.91) without the need for additional Steppe ancestry.

To test whether the source of Neolithic ancestry in Kir23 was from local groups, I performed f_4 tests in the form $f_4(W = \text{Kir23}, X = \text{mbutipygy}; Y = \text{test}, Z = \text{Erg2})$, which tests whether Kir23 forms a clade with Erg2, a local farmer individual, or *test*, where *test* was one of several different farmer populations. Erg2 was chosen as the local group because it lacked any potentially confounding Hunter Gatherer ancestry. Kir23 always formed a clade with Erg2, suggesting that the source of ancestry into Kir23 was local and that there was a degree of continuity within the region.

4.4.2 Bronze Age

The single Bronze Age individual, Kir28, is dated to approximately 4000BC. Kir28 is found in a fineSTRUCTURE group with other Central Europe Bronze Age samples; RISE150, a sample from the contemporaneous Bronze Age Unetice culture and Rathlin1, a sample from early Bronze Age Ireland. Thus, this sample is typical

qpAdm modeling showed that the Kir28 can be modeled as a mixture of the two previous Late Neolithic samples in roughly equal proportions, or a mixture of Bell Beakers and Irish Neolithic populations.

4.4.3 Iron Age

From both the ancient PCAs, a shift in the Iron Age samples towards the cluster of Neolithic individuals relative to the Bronze Age can be observed. The same pattern is also seen in the modern PCA, where the Iron Age samples are shifted substantially towards Spain / Northern Italy relative to the preceding Bronze Age sample which is situated among Northern / Western European populations (Germany, Wales) (Fig. 5.6). Previous studies into the Bronze-Iron Age transition in Western-Europe (France) have shown relative continuity [66]. Other studies in Eastern-Central Europe (Hungary) have shown the Bronze-Iron Age transition was accompanied by an increase in Eastern-European ancestry (albeit from a single sample) [62]. I was interested to see whether the transition in Bavaria had elements of either of these phenomena.

To first identify the possible source of ‘southern’ ancestry in the Iron Age samples, I formed each Bavarian population as a mixture of all other ancient populations using SOURCEFIND. I detected a component represented by ‘Renaissance’, a population from approximately 1500CE from Italy, which contributed towards 26% of the ancestry to Iron Age individuals, but was found in neither the preceding Bronze Age nor subsequent Middle Age. Thus,

Renaissance samples appear to be a good proxy for the mixing source. qpAdm modeling showed that the Iron Age samples can be well formed from a mixture of the preceding Bavarian Bronze age sample and those from either Renaissance Italy, Imperial Rome, Imperial Rome Late Antiquity or ‘Roman Solider’ from Veeramah et al (2018). All other possible sources included with Bronze Age resulted into poorly fitting models. This suggests a model of admixture from populations best represented by those from post Iron-Age Italy.

To determine whether this was an admixture event, I grouped the Iron Age samples together and performed MOSAIC admixture analysis. In the 2-way admixture model, the Iron Age samples could be formed of a mixture of a source closest to an Alamannic-Frankish sample (510 – 530 AD) 17.7% and a source closest to Anatolian Neolithic / LBK samples (82.3%). The estimated F_{st} between the 2 mixing sources was 0.016, approximately equivalent between present-day Germans and Palestinians [67]. Bootstrapped dates estimated the date to between 7.86 and 11.31 generations ago. This signal is supported by the fineSTRUCTURE groupings. All 4 Iron Age individuals were grouped alongside several Lombard samples and a Roman solider from 300AD.

Based on SOURCEFIND modeling with the extended older surrogates set, unlike Gamba et al (2014) [62], we found no evidence of East-Asian or East-Asian-like admixture (Fig. ??).

4.4.4 Modern day legacy of the Altheim and Molzbichl samples

Finally, our dataset included 3 samples from the Middle Age period. The two genomes from Altheim, Germany, date to around 500AD and were found in a Roman context. The single individual from Molzbichl, Austria, dates to around 300 years later, and has been assigned to a ‘Slavic’ context.

The 3 Middle Age samples appear to share common ancestry based on

the plink PCA. Some structure is apparent from the ChromoPainter PCA, with the two Altheim samples clustering more closely together to the exclusion of the Slavic sample; however, this difference appears to be subtle. f_4 in the form $f_4(mbutipygmy, Bavaria_{Iron}; Bavaria_{Slav}, Bavaria_{Germanic})$ returned a non-significant result, showing that samples from the Iron Age in Bavaria were symmetrically related to the later Middle Age sample. These results suggest that the differentiation between ‘Germanic’ and ‘Slavic’ populations arose post Iron Age. However this non-significant result could be caused by low sample sizes in the Middle Age populations.

The two Germanic samples fall into a fineSTRUCTURE cluster with a set of contemporaneous samples from Northern Europe, including 10-11th century Vikings from Estonia, Sweden and Iceland. On the other hand, Molz1 clusters with other individuals known to be from Early Slavic populations. Interestingly, the Slavic cluster also containing a sample DA29, also known as ‘GoldenHordeEuro’. This sample is from Karasuyr, Kazakhstan, and was dated to 1200-1400 CE. The Golden Horde was a Mongol khanate established in the 13th Century CE. Given this sample shows clear evidence of European ancestry and clusters alongside individuals from Early Middle Age Europe, it has been proposed that this individual was captured in Europe during the Mongol raids of the 13th Century, when they assaulted the Kievan Rus’ federation.

It is currently unknown whether, in addition to cultural and linguistic differences, genetic differentiation exists between the ‘Germanic’ peoples represented by the two Altheim samples, and the ‘Slavic’ peoples represented by the Molzbichl sample. All 3 samples are positioned close on the ancients PCA, suggesting they lack differentiation in the context of ancient samples. However, their positions on the modern PCA reveals there was strong differentiation between early Slavic and Germanic peoples (Fig. ??). Molz1 clusters with present-day Slavic speaking populations such as Poland, Ukraine and Belarus.

On the other hand, the two Germanic samples cluster with present-day individuals from Germanic-speaking countries in Western Europe, such as Scotland, Germany and Wales.

Plotting differential haplotype sharing between the Slavic and Germanic sample makes this pattern clear (Fig 4.10). There appears to be a clear division down the centre of Europe, dividing it into East and West that shows the structure in present-day Europeans has existed since at least the Early Middle Ages.

These results were recapitulated using SOURCEFIND, where we modeled each individual as a mixture of different modern-day populations. The two samples from Altheim derived a large proportion of their ancestry to modern day Germans (81.8%, se=12.8), whereas the Molzbichl sample derived a large proportion of its ancestry from modern day Polish (77.85%, se=20.3) and Croatians (11.7%, se=9.1).

4.4.5 Sample heterozygosity and homozygosity

I calculated per-sample heterozygosity and runs-of-homozygosity for all samples above 3x coverage.

4.4.6 Discussion

I found that there was structure even within samples which were extremely spatially and temporally close. For example, Erg1 and Erg2 were found in the same layer and in the same location; yet Erg1 shows evidence of recent Hunter-Gatherer ancestry, whereas Erg2 shows no evidence of admixture. This raises the possibility that admixture between farmers and Hunter-Gatherers occurred on an extremely fine geographic and temporal scale. Similarly, the two Late Neolithic samples showed differences in genetic ancestry, with one sample possibly being a recent migrant from the Eurasian Steppe, displaying ancestry

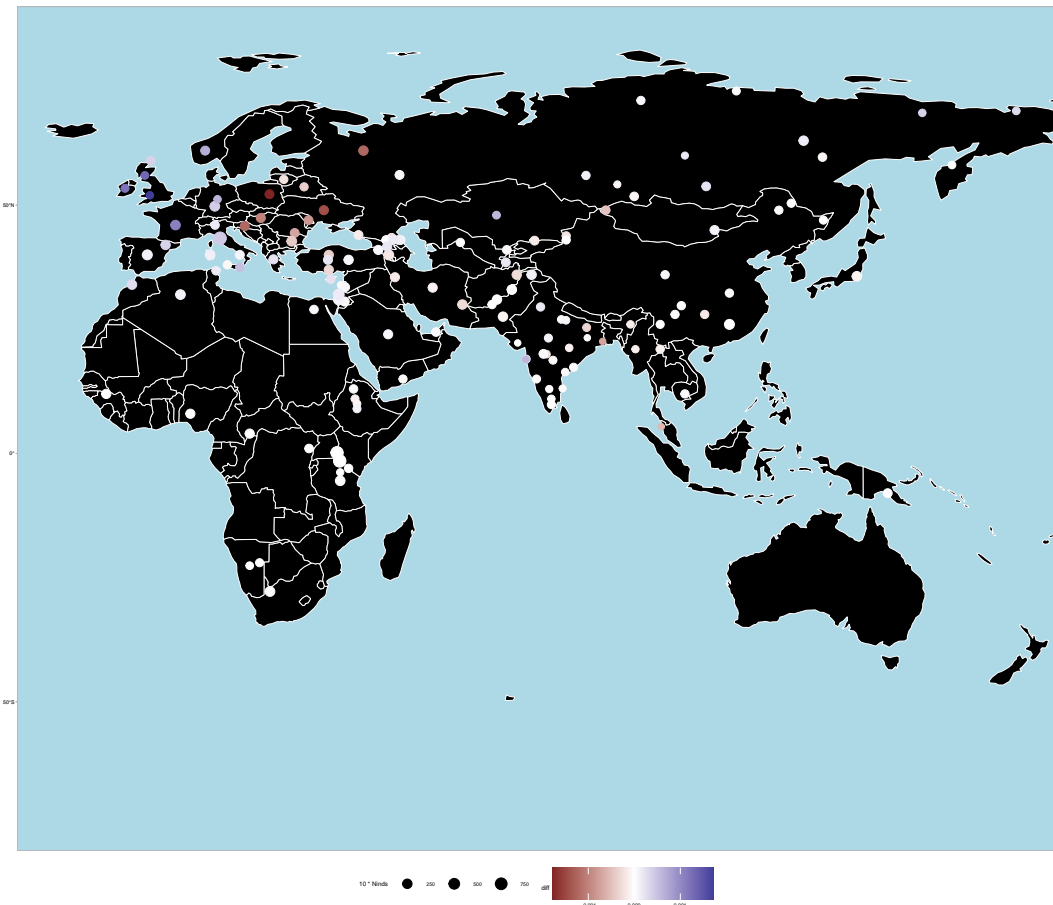


Figure 4.10: Differences in haplotype-donation to

typical of the Yamnaya steppe-pastoralists and the other being of primarily farmer ancestry. These results clearly demonstrate that individuals who were likely genetically and phenotypically distinct lived amongst one another during the Late Neolithic.

I found that across the different archaeological periods, within Cherry-Tree Cave, there was a degree of continuity, but with evidence of admixture from the outside.

Using 3 ancient genomes, I showed that the distinction between ‘Germanic’ and ‘Slavic’ peoples can be seen

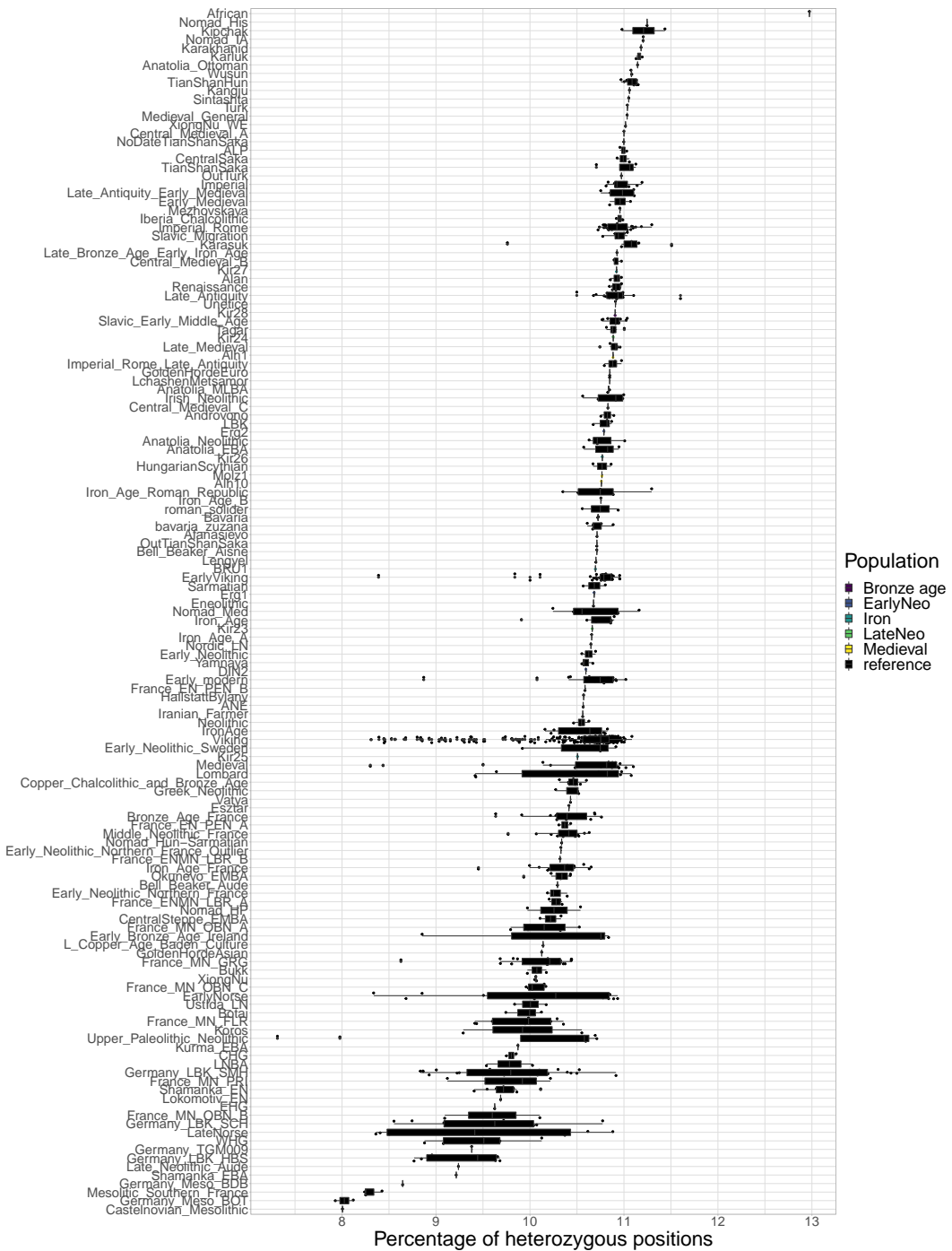


Figure 4.11

Chapter 5

The genomics of the Slavic migration period, Early Middle Ages and their links to the present day

5.1 Introduction

The Slavic peoples originated as a diverse network of tribal societies who lived in Central and Eastern Europe from the first Millennia AD [68] and whose origin, although disputed, is thought to be Polesia (a marshy forested area straddling Poland, Belarus, Russiana and Ukraine) [69]. Although various Roman and Greek sources refer to Slavs as *Veneti* and *Spori* as early as the 1st and 2nd centuries AD, the term ‘Slavs’ was first used in writing by Roman bureaucrat Jordanes at the beginning of the 6th century after their attack on the Byzantine empire [70]. This era, known by historians as The Migration Period, was a period of European history, roughly between 375-568 AD after the fall of the Roman Empire [71], characterised by the large-scale movement of various peoples. The Migration Period began with the Huns moving into

Eastern Europe at the end of the 4th Century, occupying an area including present-day Hungary and Romania. During the 5th century, various Germanic groups invaded and established a homeland across parts of the Western Roman Empire. This was followed by the expansion of Slavic populations into regions of low population density in the sixth century.

Across the next 2 centuries, these peoples had settled across large parts of Europe. In particular, the Early Slavs had expanded southwards into the Balkans and Alps [68, 72–74]. It has been proposed that these migrations were key to forming the foundations of present-day Slavic (speaking) nations [68].

By the beginning of the 12th century, Slavs constituted a large part of a number of many medieval Christian states across Europe. As from this time period, Slavs could be broadly split up in 3 groups: the Eastern Slavs as part of the Kievan Rus', Southern Slavs in the Bulgarian Empire, the Principality of Serbia, Kingdom of Croatia and the Banate of Bosnia, and Western Slavs in the Principality of Nitra, Great Moravia, the duchy of Bohemia and the Kingdom and Poland. In addition, Slavic settlement also occurred in the Eastern Alps; Slovenia, large parts of present-day Austria and Friuli.

The differentiation of Slavs into these 3 broad groups can still be seen today in the different language groups. Today 315 million people speak Slavic languages. Linguistic evidence suggests that they can be broadly split into 3 groups; Western Slavs (Poles, Czechs and Slovaks), Eastern Slavs (Ukrainians, Belarusians and Russians) and Southern Slavs (Croatians, Bulgarians, Slovenians, Bosnians, Macedonians, Montenegrins and Serbians) [75].

The history of the Slavic peoples can be artificially be split into 3 periods; Migration Period(375AD - 568AD), Early Middle Ages/High Middle Ages (600AD - 1250AD) and present-day. Although previous studies have investigated the genetics of the transitions between these periods, they have been relatively limited in their scope. Juras et al (2014) used uniparental

mtDNA markers from ancient DNA samples from Poland to show continuity between both Roman Iron Age period (200 BC – 500 AD) and Medieval Age (1000–1400AD) with present-day Poles, Czechs and Slovaks [76]. Whilst informative about sex-biased migrations, uniparental markers carry only a fraction of the information that autosomal markers do, and therefore may provide misleading or incomplete information about the relationship between present-day and ancient samples [77] (although see [78]). For example, it is known that mtDNA and nuclear DNA may have different evolutionary histories and thus display discordant phylogenetic trees [79].

Kushniarevich et al (2015) [80] combined results from mtDNA, non-recombining Y and autosomal DNA to investigate the population structure of a wide range of present-day Balto-Slavic populations in order to understand the historical processes that have formed the present-day genetic structure. They proposed that admixture of incoming Slavic speakers during the Migration Period with the pre-existing substrate of regional genetic components, which differed between South, East and West Slavs. Using this evidence, they propose that the “cultural assimilation of indigenous populations by bearers of Slavic languages as a major mechanism of the spread of Slavic languages to the Balkan Peninsula”.

More recently, Macháček et al (2021) [81] analysed ancient rune inscriptions on an animal bone from Lány, Czechia, dated to approximately 600AD. The bone is inscribed with Germanic runes. Finding Germanic runes in the context of Slavic peoples provides evidence of early interactions between Slavic and Germanic peoples. However, whether there was early genetic contact as well is yet to be determined.

Several studies into present-day Slavic populations have detected signatures of admixture from East-Asia [50, 51, 82–84]. Whether or not these signals can be observed in ancient individuals is yet to be seen and could further refine the admixture date. For example, different admixture dates in different Slavic

populations may reveal structure amongs present-day Slavs.

Finally, several studies have used haplotype-based methods to explore the structure of present-day Slavic populations. Ralph and Coop [85] compared regions of IBD matching across different European populations. They found a relatively high degree of IBD sharing among pairs of individuals from Eastern Europe, suggestive of expansion from a smaller, common source population. This expansion was tentatively estimated to between 0-1000AD. Consistent with estimates of a small population size, Hellenthal et al (2014) [51] inferred an excess of IBD-sharing among Eastern European individuals, albeit with a more constrained admixture data of 440 - 1080 CE. However, this could also be interpreted in terms of a small effective population size [86,87].

Despite these efforts, no studies have integrated autosomal DNA from ancient and present-day samples whilst applying powerful haplotype-based methods to infer population structure, ancestry proportions and admixture events. Therefore in this chapter, I will analyse 17 new medium to high coverage whole ancient genomes from Czech Republic, spanning the Migration Period and Early Middle Ages. These are, to my knowledge, the first high-coverage whole ancient-genomes from Slavic I will merge the newly sequenced sampled alongside a detailed reference datatset of other ancient individuals and a large reference set of relevant present-day European individuals in order to understand their ancestry in the context of both present-day and ancient samples. In particular, I am interested in considering the following questions:

1. Can we gain an understanding of the geographical origins of the Slavic peoples from ancient DNA
2. Do the labels “Migration Period” and “Early Middle Ages” make sense from a genetic standpoint (i.e. do samples from either period cluster with another to the exclusion of the other)
3. Was there interactions between Germanic and Slavic peoples during the

Early Migration Period.

4. If so, what genetic differences can be observed between these periods? Are they characterised by admixture from outside sources? If so, what are these sources and can the admixture events be dated?
5. What is the relationship between the ancient samples and present-day Slavic populations. Are they continuous?
6. Do the different ancient Slavic samples have different affinities to different present-day Slavic language groups?

5.2 Methods

5.2.1 Description of samples

Whole-genome sequence data was generated from 17 ancient individuals.

All newly sequenced samples are from Czechia, split across two different field sites.

The newly sequenced samples are grouped into two temporal categories; 5 samples are from the Migration Period (348 AD - 504 AD) and 12 samples are from the later Early Middle Ages (724 AD - 995 AD).

Code	Site	Date (AD)	Period
LIB5	Břeclav – Líbivá	348	Migration period
LIB4	Břeclav – Líbivá	472	Migration period
LIB12	Břeclav – Líbivá	475	Migration period
LIB2	Břeclav – Líbivá	495	Migration period
LIB3	Břeclav – Líbivá	509	Migration period
LIB11	Břeclav – Líbivá	741	Early Middle Ages
LIB7	Břeclav – Líbivá	830	Early Middle Ages
POH11	Pohansko – Lesní školka	783	Early Middle Ages
POH27	Pohansko – Jizní Předhradí	783	Early Middle Ages
POH28	Pohansko – Jizní Předhradí	822	Early Middle Ages
POH41	Pohansko – Lesní školka	875	Early Middle Ages
POH13	Pohansko – Lesní školka	879	Early Middle Ages
POH36	Pohansko – Jizní Předhradí	880	Early Middle Ages
POH40	Pohansko – Lesní školka	950	Early Middle Ages
POH3	Pohansko – Lesní hrúd	956	Early Middle Ages
POH44	Pohansko – Pohřebiště U Kostela	NA	Early Middle Ages
POH39	Pohansko – Jizní Předhradí	866	Early Middle Ages

Apart from the age of the samples, the differentiation between the Migration Period and Early Middle Age samples can be determined via pottery (Z. Hofmanova, personal communication).

Include details of processing. Read alignment, read filtering, ATLAS calling etc.

5.2.2 Ancient DNA processing

I merged the 17 newly sequenced individuals with the reference data-sets A.1 to A.17 resulting in a total of 942 individuals in .bcf format with genotype likelihood data at 77,213,942 genome-wide SNPs. Data was then split into

separate .bcf files for each chromosome and indexed using bcftools.

I followed the GLIMPSE [15] imputation and phasing pipeline (https://odelaneau.github.io/GLIMPSE/tutorial_b38.html) to generate genotype likelihoods and phased genotypes for each individual. For the reference panel, I used the 30x 1000 genomes dataset [28], described in appendix A.5.

GLIMPSE was chosen as it is the most efficient (in terms of time and memory) probabilistic phasing / imputation software available [15].

First, GLIMPSE chunk was used to split the present-day reference dataset into chunks. Default settings of –window-size 2000000 and –buffer-size 200000 were used, generating a total of 936 regions genome wide. Splitting the genome into regions for imputation jointly maximises computational efficiency and accuracy. For each region in turn, the target dataset consisting of phred-scaled genotype likelihoods (PL) was imputed using GLIMPSE phase under default settings and the same reference panel. GLIMPSE ligate was then used to concatenate the 936 imputed regions into 22 distinct chromosomes. Finally, GLIMPSE sample was used to created phased haplotypes from the output of GLIMPSE ligate using default settings.

Previous sections (cite section) have shown that using a set of SNPs which are common yields results which are least affected by coverage related bias, likely in part because common variants are easier to impute. Therefore, I chose to filter the SNPs to those 477,416 those present in the HellBus dataset (A.20). Thus these SNPs were used for all subsequent analyses.

5.2.3 present-day DNA processing

I chose the MS-POBI-HellBus dataset, described in detail in appendix A.20, because it contains a high number of relevant samples from central and Eastern Europe. I removed samples from Australia, New Zealand and USA, as these samples were not from native individuals from that country.

The modern and ancient samples were phased separately. This was because GLIMPSE, which is necessary to phase the ancient samples with, is not suitable to phase the modern samples with, for two reasons. Firstly, GLIMPSE is designed to work with sequence-level density of data, and the modern samples have been genotyped on a low-density genotyping array. Secondly GLIMPSE accepts data as genotype likelihoods; these were not available for the modern samples. Therefore, the modern samples were phased using shapeit4 [24].

Appendix A.20 describes the initial filtering that was used to generate this dataset. It was then phased using shapeit4 [24] without the use of a reference panel and setting the number of conditioning haplotypes to 8. It was then converted to ChromoPainter input format using a custom R script and merged with the dataset of ancient samples described in the previous section.

5.2.4 plink PCA

To determine the overall ancestry patterns of the newly sequenced individuals in the context of 915 other ancient samples, I performed PCA on the non-imputed genotypes using plink2. Performing an unlinked PCA allows us to identify any data quality issues which are independent of phasing / haplotype-based analysis.

I retained only the 500,000 markers with the lowest amount of missingness and then LD-pruned the resulting SNPs using the settings `-maf 0.01` and `-indep-pairwise 50 5 0.2`. PCA was performed using default settings from plink2 and the first two principle components plotted.

5.2.5 Sample heterozygosity and ROH

I used plink (v1.90p) to calculate the total length (kB) of runs of homozygosity (ROH) within each sample across all ancient and present-day individuals in the combined dataset.

5.2.6 Allele-frequency based tests

I used Admixtools [2], implemented in Admixr R library [88] to employ several different f-statistics.

I converted imputed .vcf to .ped/.map format using plink. It has been shown that using imputed markers reduced reference bias relative to using pseudo-haploid markers [6]. Convertf from the Admixtools library was then used to convert .ped/.map files into Eigenstrat format suitable for use with Admixtools.

5.2.7 ChromoPainter and fineSTRUCTURE analysis

I began with a merged dataset of present-day and ancient individuals, described in sections 5.2.2 and 5.2.3 in ChromoPainter format.

Firstly I selected all ancient samples above 2x coverage and performed an ‘all-v-all’ painting where each haplotype was compared to all other haplotypes in turn. 2x was somewhat arbitrarily chosen as a conservative threshold to reduce coverage related bias whilst still retaining a suitable number of individuals. This allows for the characterisation of the ancestry of the newly sequenced ancient samples in the context of other ancient individuals. It is also the painting that can be used to perform fineSTRUCTURE clustering and tree building on ancient samples. Hereafter referred to as ‘ancient’ painting.

I also performed an ‘all-v-all’ painting of a selected group of present-day individuals and the newly sequenced ancient individuals. The populations retained are given in table ???. Hereafter referred to as ‘present-day painting’.

Both the ‘present-day’ and ‘ancient’ paintings were merged separately using chromocombine-0.0.4 (<https://people.maths.bris.ac.uk/~madjl/finestructure-old/chromocombine.html>). The ‘C’ factor was also estimated for both paintings.

The fineSTRUCTURE [13] clustering and tree building algorithm was applied to the chunkcounts ChromoPainter output, for both the ‘present-day’ and ‘ancient’ paintings. This algorithm assigns individuals to genetically homogeneous clusters, estimates the ‘true’ number of clusters and builds a dendrogram of genetic similarity. This is particularly useful when combining many samples from different studies, as is the case with the ‘ancients’ painting; the population label identifiers used by different studies may not be consistent with one another. Therefore, we can use fineSTRUCTURE groupings as population labels rather than external group labels.

fineSTRUCTURE (v0.0.5) was applied to the resulting chunkcounts matrices for both the ancients painting and the moderns painting. It was first run in MCMC mode using 1,000,000 burn-in MCMC iterations and 2,000,000 main MCMC iterations. It was then run in tree-building mode (-m T) using 100,000 burn-in and 100,000 main iterations.

Tree figures, co-ancestry matrix figures and principle component plots were generated using the fineSTRUCTURE R library (<https://people.maths.bris.ac.uk/~madjl/finestructure/FinestructureRcode.zip>).

5.2.8 SOURCEFIND ancestry proportion analysis

The chunklengths / chunkcounts matrices outputted by ChromoPainter give informative but noisy estimates of the proportion of the genome a given individual most closely matches to another individual. However, these cannot be seen as true admixture fractions, due to phenomena such as incomplete lineage sorting. In order to infer ancestry proportions from the data, I ran the SOURCEFIND algorithm [16] on each cluster of individuals inferred from fineSTRUCTURE.

Each of the 47 clusters inferred by fineSTRUCTURE was analysed in turn, using the other 46 clusters to act as surrogates. Each cluster was run across

Population	nsamples
HB:tsi	196
HB:spanish	68
HB:bulgarian	62
HB:german	60
HB:french	56
HB:russian	50
HB:greek	40
HB:ukrainian	40
HB:croatian	38
HB:hungarian	38
HB:norwegian	36
HB:southitalian	36
HB:polish	34
HB:romanian	32
HB:mordovian	30
HB:cypriot	24
HB:northitalian	24
HB:lithuanian	20
HB:siciliane	20
HB:westsicilian	20
HB:belorussian	18
HB:tuscan	16
HB:irish	14
HB:scottish	12
HB:germanyaustralia	8
HB:welsh	8

Table 5.1: Name of population and number of samples used in the present-day ChromoPainter analysis

3 independent MCMC runs, using 50,000 burn-in iterations, 500,000 main iterations, thinned every 5 iterations.

All 3 MCMC runs were then combined to form an MCMC list using the coda R library [32]. First, I ensured all chains had converged using the autocorr.diag function. I then used the mcmc function to jointly estimate ancestry proportions and empirical credible intervals for each target population.

5.2.9 MOSAIC admixture analysis

I inferred admixture events, dates and proportions using 2 different (but similar) haplotype-based methods; MOSAIC [50] and GLOBETROTTER [51].

I performed 2 different kinds of admixture modeling. Firstly, I performed an ‘ancient surrogates’ model where the high coverage ancient samples described in the previous section were used as surrogates. I used the fineSTRUCTURE groupings to assign the samples. The results for these analysis were noisy and difficult to interpret, perhaps for several reasons, outlined in the discussion section.

I then performed a ‘present-day surrogates’ analysis where a selected set of present-day populations were used to analyse both present-day Slavic populations and ancient Slavic populations. Using these samples provided cleaner results, at the cost of reduced interpretability.

Therefore, I decided to only use the present-day surrogate set unless otherwise stated. Phased .vcf files were converted to .hap/.sample files using bcftools convert –hapsample. The resulting .hap/.sample files were then converted to MOSAIC input using the provided script (https://maths.ucd.ie/~mst/MOSAIC/convert_from_haps.R).

MOSAIC was run using default settings and the following sets of populations as targets and the following sets as surrogates. I formed each target as a mixture of either 2 or 3 ancestral sources. Upper and lower quantiles for admixture dates were estimated using a bootstrap procedure.

5.3 fastGLOBETROTTER admixture analysis

I also used fastGLOBETROTTER to estimate admixture events in ancient and modern samples. To this end, I performed 2 different paintings; the painting required to generate the samples (P1) and the painting required for

Population	nsamples
HB:han	34
HB:bulgarian	31
HB:japanese	28
HB:sardinian	28
HB:russian	25
HB:yakut	25
HB:greek	20
HB:ukrainian	20
HB:croatian	19
HB:hungarian	19
HB:mongolian	19
HB:southitalian	18
HB:chuvas	17
HB:polish	17
HB:romanian	16
HB:buryat	15
HB:mordovian	15
HB:altai	13
HB:tuva	13
HB:evenk	12
HB:northitalian	12
HB:cambodian	10
HB:dai	10
HB:hannchina	10
HB:lithuanian	10
HB:miao	10
HB:nganassan	10
HB:selkup	10
HB:siciliane	10
HB:tu	10
HB:tujia	10
HB:uygur	10
HB:westsicilian	10
HB:yi	10
HB:belorussian	9
HB:daur	9
HB:oroqen	9
HB:xibo	9
HB:hezhen	8
HB:naxi	8
HB:tuscan	8
HB:dolgan	7
HB:chukchi	5
HB:koryake	5
HB:yukagir	4
HB:myanmar	3
HB:burya	2
HB:ket	2
HB:malayan	1

Table 5.2: Name of populations and number of samples used in the present-day MOSAIC analysis

the copyvector estimation (P2).

Painting P1 consisted of painting the set of target populations in table x using the set of donor populations in table y, setting the -s samples flag to 10.

Painting P2 consisted

5.4 Results

To understand the ancestry of the newly sequenced ancient samples in the context of other ancient individuals, I performed a PCA using plink2 (Fig. 5.1). The PCA showed that Migration Period samples do not all cluster together and instead appear to fall on a cline of similarity between a broad cluster of Central European Middle Age/Iron Age samples (top-left) and Neolithic samples (bottom-right). The Early Middle Age samples are more clustered together, with all samples occupying the broad region containing European Iron Age samples. However, some samples, notably POH39 and POH3 display an elevated affinity to samples from Early Bronze Age Ireland.

5.4.1 Mixed ancestry of migration period Slavs

In order to reveal further structure in the ancient samples, I performed an all-v-all painting of 152 ancient samples with a coverage greater than 2x. I then applied the fineSTRUCTURE clustering algorithm to the samples in order to assign them to genetically homogeneous groups.

The migration period consisted of whole-genomes from 5 individuals from Břeclav (Líbivá), Czech Republic, from 5 different burial sites, who had radiocarbon dates corresponding to the Migration Period (348 - 509AD). It is apparent from both the unlinked (Fig. 5.1) and linked PCAs (Fig. 5.2) that the Migration Period samples represent a heterogeneous group of individuals who do not originate from the same source population. LIB2 (495AD) is located

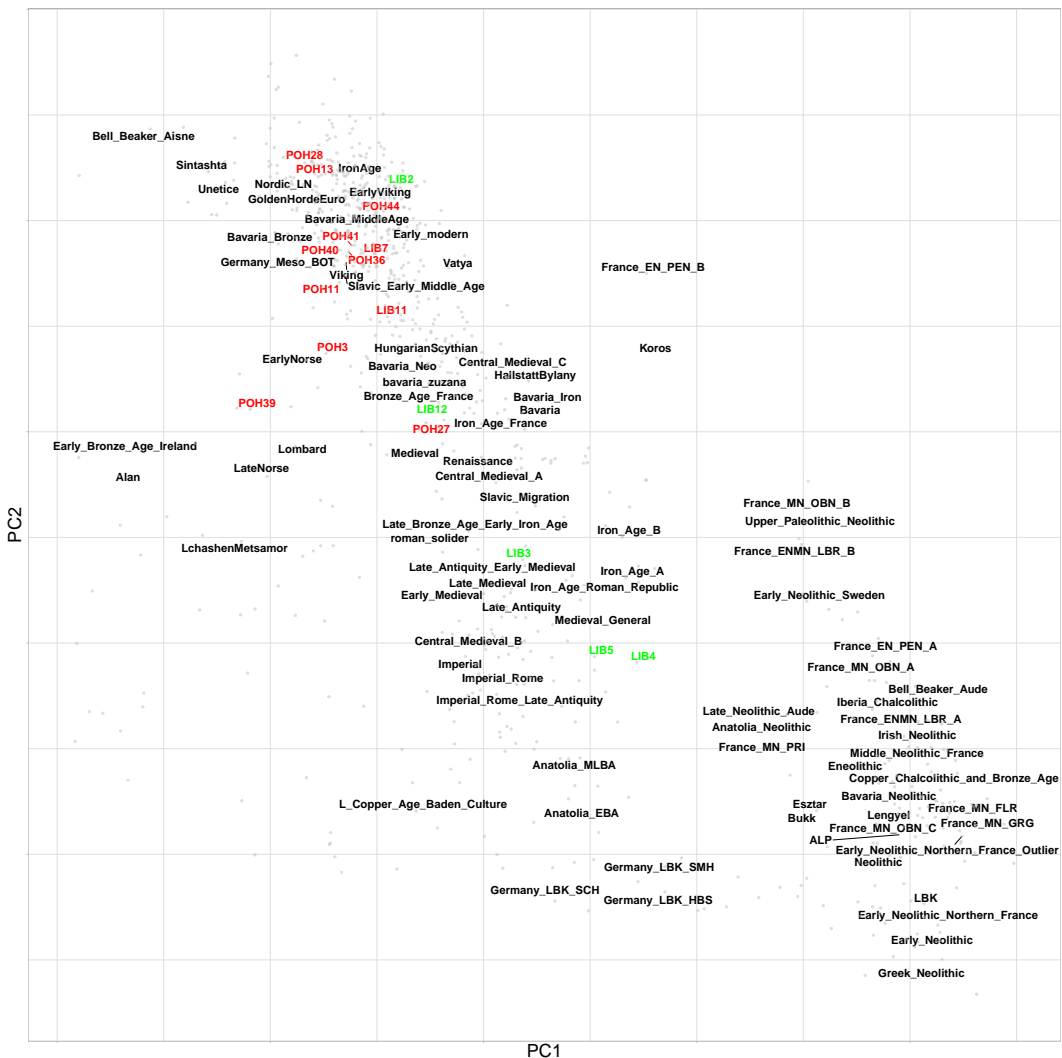


Figure 5.1: Principle component plot of newly sequenced ancient samples and reference ancient individuals performed using the plink2. Green labels correspond to Migration Era samples, red labels to Early Middle Age samples and black as reference populations. The position of each reference label is the mean PC coordinates of all individuals within that population

in the centre of a large cluster of contemporaneous individuals from Iron Age Central and Northern Europe. This individual shares the most haplotypes with Viking individuals from Denmark, Estonia and the UK from roughly the same time period. fineSTRUCTURE analysis grouped LIB2 primarily with Viking era individuals from Sweden, Denmark, Iceland, Estonia and Norway from 300-1100AD. When painted using a present-day set of reference samples, LIB2 matches the most haplotypes and clusters with present-day Norwegians (Fig. 5.7). Put together, these data suggests LIB2 may be a recent migrant from Viking regions.

There are many sources which detail the links between the Viking and Slavic peoples towards the end of the first millennium [89, 90]. However, most evidence suggests these links occurred later than the date of these samples. For example, it is known that the Scandinavian colonists settled in present-day Russia as early as 750. Therefore, we could suggest that this is evidence of an earlier link than previously known. In their large-scale study of ancient DNA of Viking samples from across Europe, Margaryan et al (2020) present Viking samples and ancestry in Estonia, but not until the beginning of the 8th Century, some 200 years after the estimated date of LIB2.

On the other hand, LIB4 and LIB5, show an affinity the European Neolithic, indicated by their position on the linked and unlinked PCA. Interestingly, they share the most haplotypes with several Italian Neolithic samples, despite being separated by approximately 6000 years (not a clue why this is). Despite sharing the most haplotypes with these samples, LIB4 and LIB5 are found in fineSTRUCTURE clusters with more recent samples from Italy (Early Iron Age / Renaissance), suggesting the link to Neolithic Italy may have been transmitted by more recent populations (need to expand more on this). Both LIB4 and LIB5 share the most haplotypes with one another; this and their consistent positions on PCA and fineSTRUCTURE groupings suggest they are closely related and could be from the same local population.

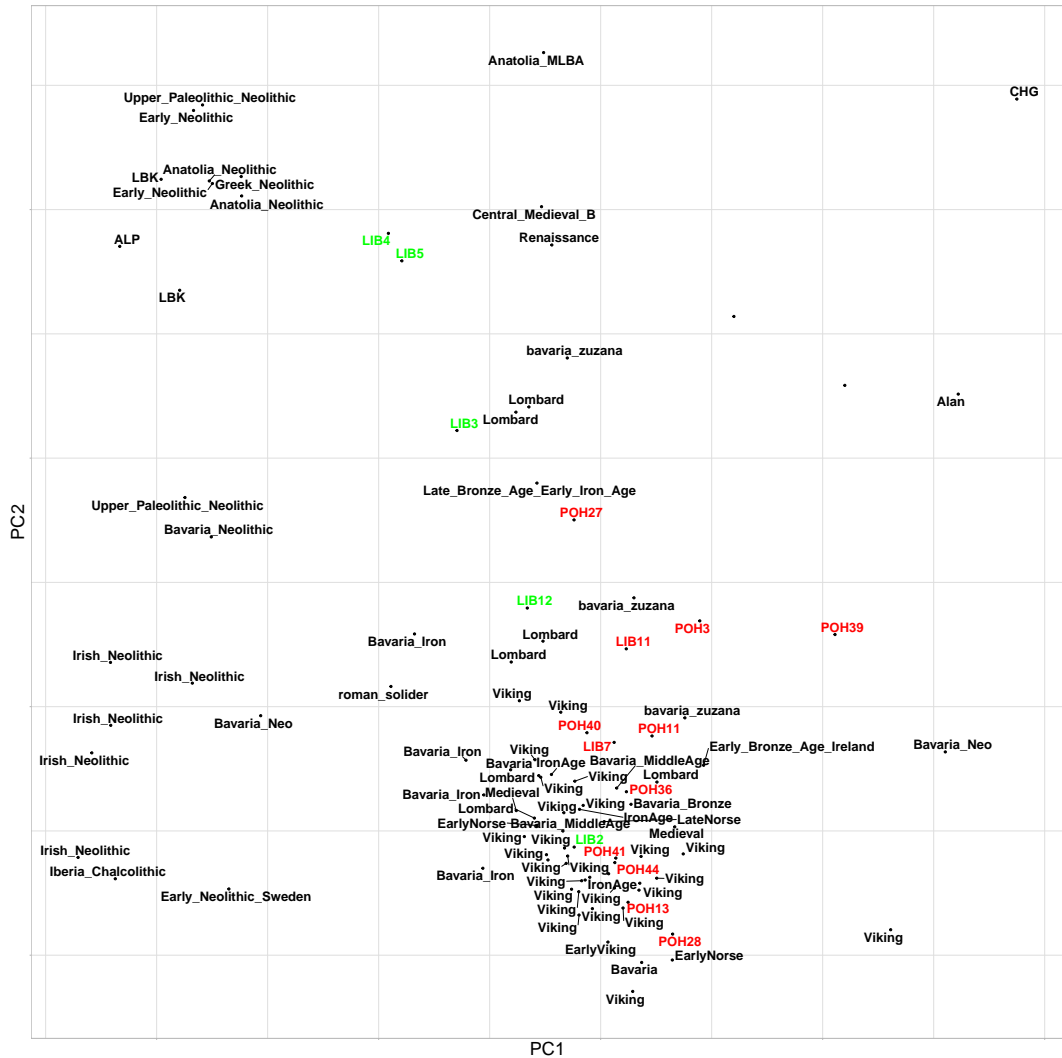


Figure 5.2: Principle component plot of newly sequenced ancient samples and reference ancient individuals performed using fineSTRUCTURE. Green labels correspond to Migration Era samples, red labels to Early Middle Age samples and black as reference populations.

The appearance of Neolithic-like ancestry deep into the first millennium is similar to a signal found in a study exploring the ancestry of individuals with elongated skulls in medieval Bavaria (approximately 500AD) [91], where it was discovered particular individuals harbour substantial ‘southern’ ancestry from outside of Bavaria, closest to individuals from present-day Greece and Turkey. There are at least two possible explanations for the presence of this ancestry in the Migration Era samples. Firstly, LIB3, LIB4 and LIB5 may be similar migrants to the region. This is consistent with the fact that (at least LIB3, need to check others) is female; Veeramah et al (2018) showed that there was a tendency for females to migrate from southern regions, perhaps related to the formation of strategic alliances. Alternatively, it is possible these individuals are a leftover from a historically described Lombard migration that moved from Northern Germany (nobody really knows where it started according to Zuzana) through Czechia, Slovakia, Hungary and ended up in Lombardia. Accordingly, this could appear as genetic similarity to present-day populations from Northern Italy. This hypothesis is supported by the clustering of LIB3, LIB4 and LIB5 with present-day Italian samples in the ‘present-day’ fineSTRUCTURE analysis (Fig 5.10).

Ancestry proportion estimation using SOURCEFIND showed that the cluster containing these samples shares 25% of their ancestry most recently with people from Anatolia, 16% from LBK (Linearbandkeramik) and 12% from a cluster containing Lombard individuals.

I performed MOSAIC admixture modeling using present-day samples as surrogates and the clusters of newly sequenced ancient samples as targets. I did not detect an admixture even when targeting LIB3, LIB4 and LIB5. This could be due to low power or a low number of samples, or that the samples are unadmixed with respect to the surrogate populations.

On the fineSTRUCTURE PCA, LIB3 clusters with Lombard samples from Northern Italy. Historical evidence cites alliances between Slavs and Lombards

in the 5th century [92]. In the ‘present-day’ painting, LIB3 clusters with and shares the most haplotypes with present-day Tuscans.

Finally, LIB12 displays ancestry which is more typical of the preceding Central European Bronze Age. It copies the most haplotypes from samples from Bronze Age Ireland (Rathlin) and Bavaria and is found in a cluster with several other Bronze Age samples. This suggests it may represent a ‘leftover’ from a local Bronze Age population which was unaffected by the Antiquity / Iron Age migrations to the region.

5.4.2 Early Middle Age Slavs

In comparison to the 5 Migration Period ancient Slavs, the 12 Early Middle Age Slavs (741-956 AD) represent a more homogeneous set of samples. All 12 samples were clustered into the same fineSTRUCTURE group (named Slavic Early Middle Age II), alongside Viking/Medieval samples from Ukraine, Poland and Sweden. SOURCEFIND analysis showed that this cluster derives roughly equal parts of ancestry from the clusters Viking 10C Scan I, BronzeAge I and Lombard mixed cluster. Interestingly, these are 3 ancestry sources which are similar to those found in the Migration Period samples. We could tentatively therefore suggest that the Early Middle Age Slavs were formed from the mixture of ‘Northern’ (represented by Viking) and ‘Southern’ represented by Lombard onto a substrate of local Bronze Age populations. Note that I suggest that these are the most representative populations and not necessarily the ‘true’ populations that mixed.

MOSAIC admixture modeling using ancient surrogates proved inconclusive. However, using present-day individuals as surrogates provided cleaner results. The best fitting model was a 3-way admixture event involving sources closest to present-day North-Central Slavs (76.6%), Southern-Eastern Slavs (21.9%) and East Asians, best represented by Mongolians (1.5%) (Fig. 5.3). This admixture even was estimated to have occurred 9.4 (2.5% 5.7gens - 97.5%

17.9gens) generations before the samples (Fig. 5.5).

This admixture event is consistent with a signal found in both present-day day Eastern European individuals [50, 51]. In previous studies, this admixture event was dated to approximately 1200CE (MOSAIC) and 438CE (GLOBE-TROTTER). Despite the differing dates, the proportion of ancestry is consistent across studies (approximately 2%), suggesting the signal is genuine. To further support the event, the proportion of ancestry from this source is consistent across 2-way and 3-way MOSAIC admixture models.

5.4.3 Do the samples cluster together - TVD permutation test

fineSTRUCTURE analysis suggested that the Migration Era and Early Middle Age samples did not originate from the same source population. To formally establish whether the Early Middle Age and Migration Period samples cluster within their respective populations, following Leslie et al 2015 [42], I performed a TVD permutation test. TVD is a distance metric which can be calculated from the chunklengths matrix and is equivalent to finding the absolute distance between two copyvectors, with larger values meaning two samples have more different ancestry profiles.

Using the ancients chunklengths matrix, I grouped the samples into Migration Period and Early Middle Age and calculated the average copyvectors C_{mp} and C_{ema} across samples within each groups. Then, I calculated the empirical TVD between the two groups as $TVD_{mp,ema} = \sum |C_{mp} - C_{ema}|$. For 10,000 iterations, I then randomly permuted the population labels among the samples and then calculated a ‘random’ TVD, $TVD_{mp,ema}^{rand}$ between the samples with randomly permuted populations. We can then calculate the p-value that we can reject the null model of no significant differences between the groups (not sure if this is the right way of wording it) as the number of randomly permuted

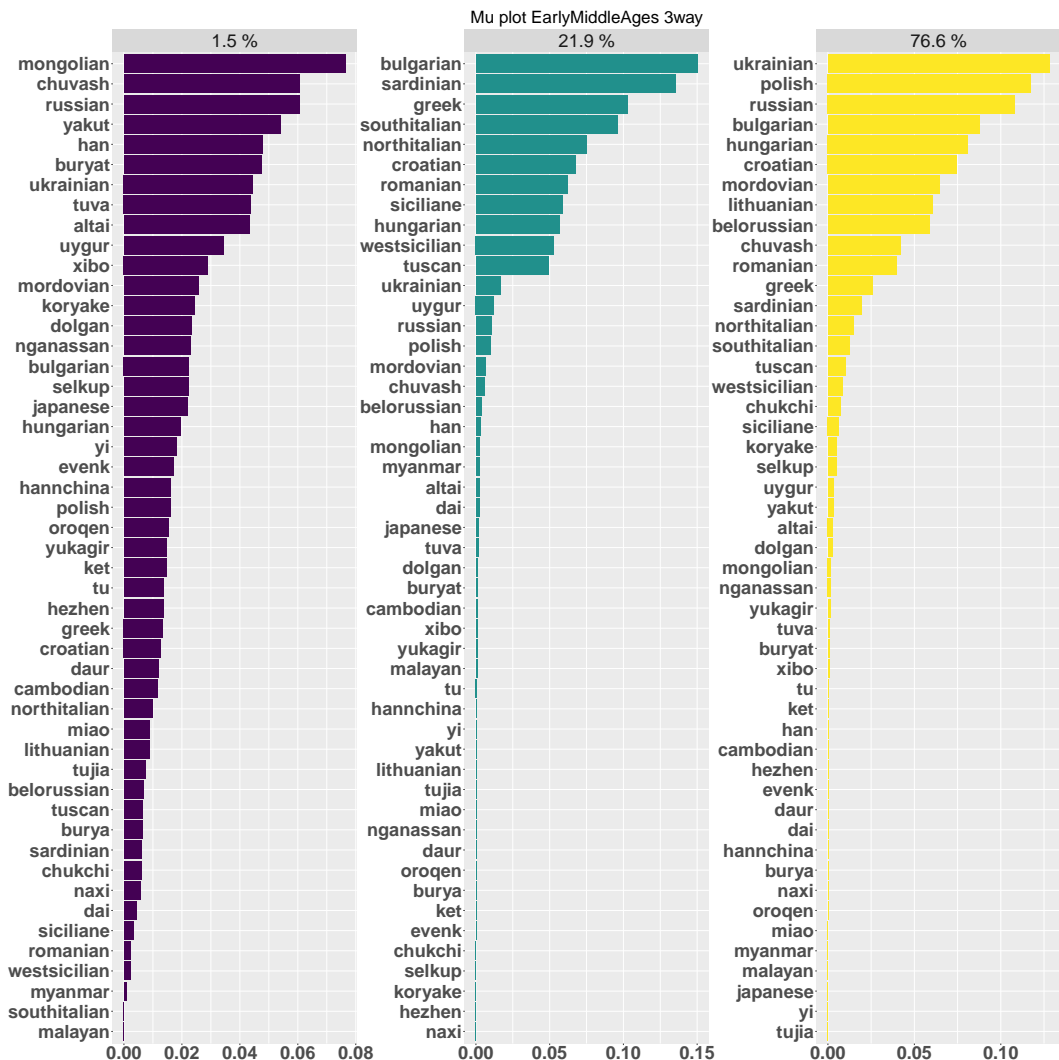


Figure 5.3: Copying matrix plot for sources in 3-way admixture event for Early Middle Age ancient Slavic samples. Each panel represents one of the 3 putative mixing sources. Labels above each panel give the proportion that mixing source contributed to the Early Middle Age samples. Length of the bars within each panel represent the amount that putative mixing source copied from a particular population.

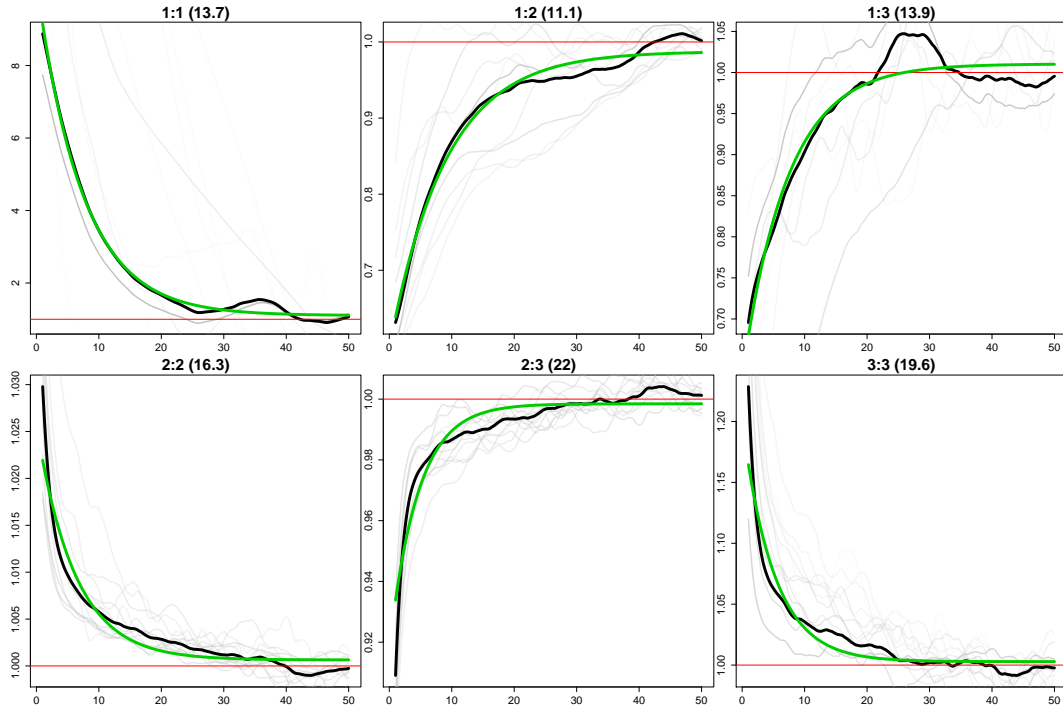


Figure 5.4: Inferred Coancestry Curves obtained from modeling Early Middle Age samples as a 3-way mixture of present-day individuals. Black lines are empirical coancestry curves across all target individuals, light grey are per individual, green is the fitted single-event coancestry curve. Note to self - need to figure out what the numbers mean but doesn't say in the manual anywhere.

iterations where $TVD_{mp,ema}^{rand} > TVD_{mp,ema}$. This test supported clustering the samples into their respective groups ($p = 0.0013$).

This is in agreement with the fineSTRUCTURE results which grouped together all of the Early Middle Age samples together to the exclusion of the Migration Period samples.

5.4.4 Interactions between the two groups

The previous section suggested that individuals from the Migration Period and Early Middle Ages had differing ancestry signals.

To determine the extend of mixture and continuity between the Migration Period and Early Middle Ages, I modeled each Early Middle Ages sample as a

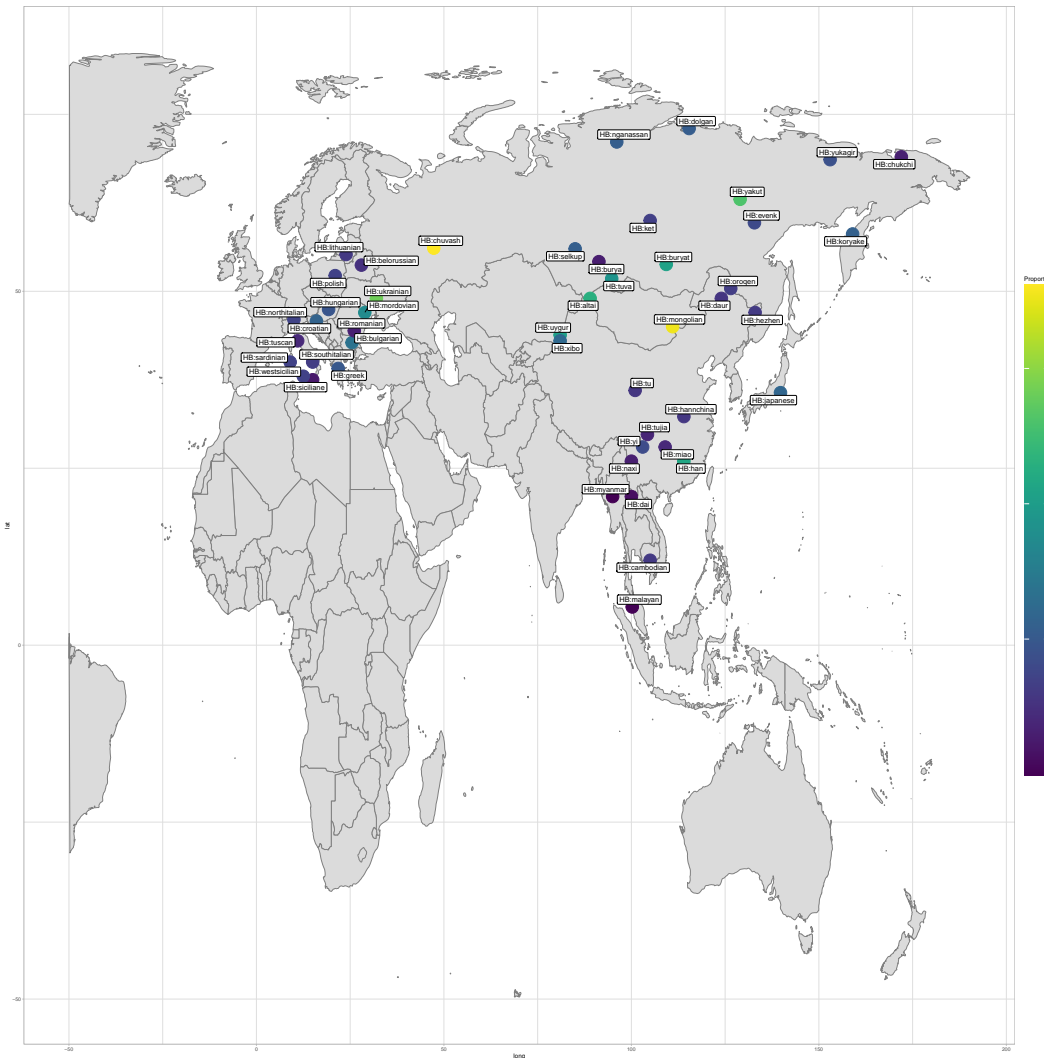


Figure 5.5: Distribution of East-Asian minor ancestry component in Early Middle Age samples.

mixture of other ancients, including individuals from the preceding Migration Period. The proportion of ancestry the individuals derive from the Migration Period clusters could be used as a proxy for the degree of continuity. The proportion of ancestry derived from the Migration Period was low (mean 3.4% , range 0.4% - 12.5%), suggesting that there was a relatively large scale population replacement between the two different time periods.

Note - I could do something like admixture f3 to see if Early Middle Age is admixed between Middle Age and any other pop instead as a more explicit test.

5.4.5 Legacy of Slavic migrations in present-day individuals

To understand the genetic legacy the newly sequenced Slavic samples left in different European populations, I painted each sample using the HellBus dataset of present-day individuals. This dataset contains a diverse set of European populations - particularly those from present-day Slavic speaking countries (Polish, Croatian, Bulgarian, Belorussian, Ukrainian, Russian) but also neighbouring non-Slavic speaking countries (Romanian, Lithuanian, Germany and Mordovia).

Principle component analysis (PCA) of the chunklengths matrix, where present-day European samples acted as donors, reveals genetic similarity between ancient Slavic samples from the Early Middle Ages and present-day Slavic speaking people (Fig. 5.6). The samples primarily cluster with present-day Polish and Belorussian individuals, but appear to fall on a cline of genetic similarity between Russians and Southern Europeans. This cline could be mediated by the possible historical admixture event between a source closest to present-day East Asians and a second closest present-day Southern Europeans, with the position of the samples along the cline dependent on the level of admixture from the different sources.

As with previous analyses, Migration Era Slavs are spread across the PCA. 3 samples, LIB3, LIB4, and LIB5 cluster with present-day Italians, consistent with deriving a substantial ancestry component from Neolithic-like sources. LIB4 and LIB5 appear to be positioned closer to Southern Italians and Greeks, whereas LIB3 is closer to Northern Italian and Tuscan populations.

LIB2 shows a strong affinity to present-day Norwegians, suggesting it may be a recent migrant from Viking regions.

The same pattern can be observed on the raw copyvector output matrix

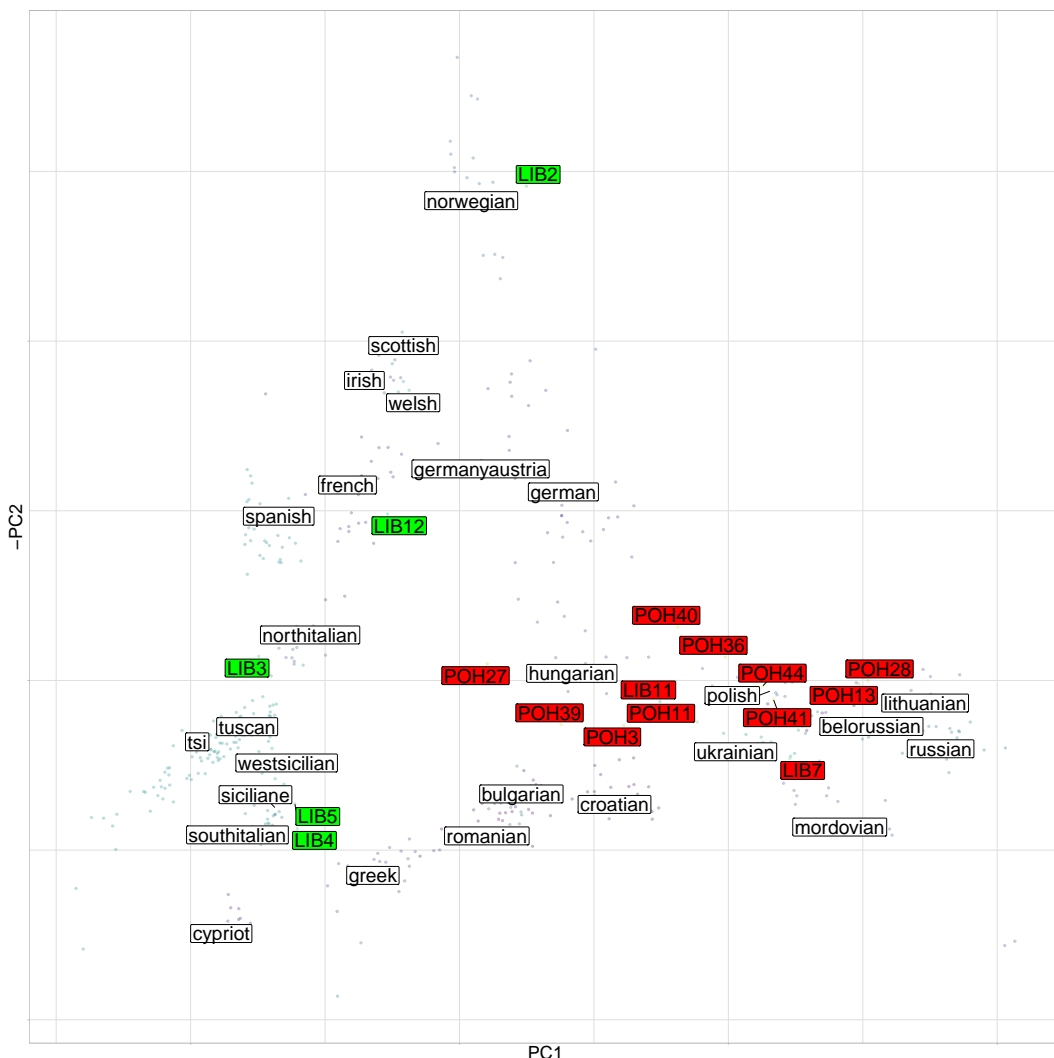


Figure 5.6: Principle component plot of newly sequenced ancient samples and reference modern individuals performed using the finestructure library. Green labels correspond to Migration Era samples, red labels correspond to Early Middle Age samples and white labels correspond to reference populations. The position of each reference label is the mean PC coordinates of all individuals within that population. Transparent coloured points correspond to present-day individuals.

(Fig. 5.7). The Migration Era samples appear not to show any excess affinity to present-day day Slavic populations. The two samples who in previous analysis showed a strong genetic relationship to the Neolithic, LIB4 and LIB5, shared the most haplotypes with present-day day Greek individuals. This should not be surprising given present-day day Greeks have a relatively high proportion of Neolithic ancestry relative to other European populations [93].

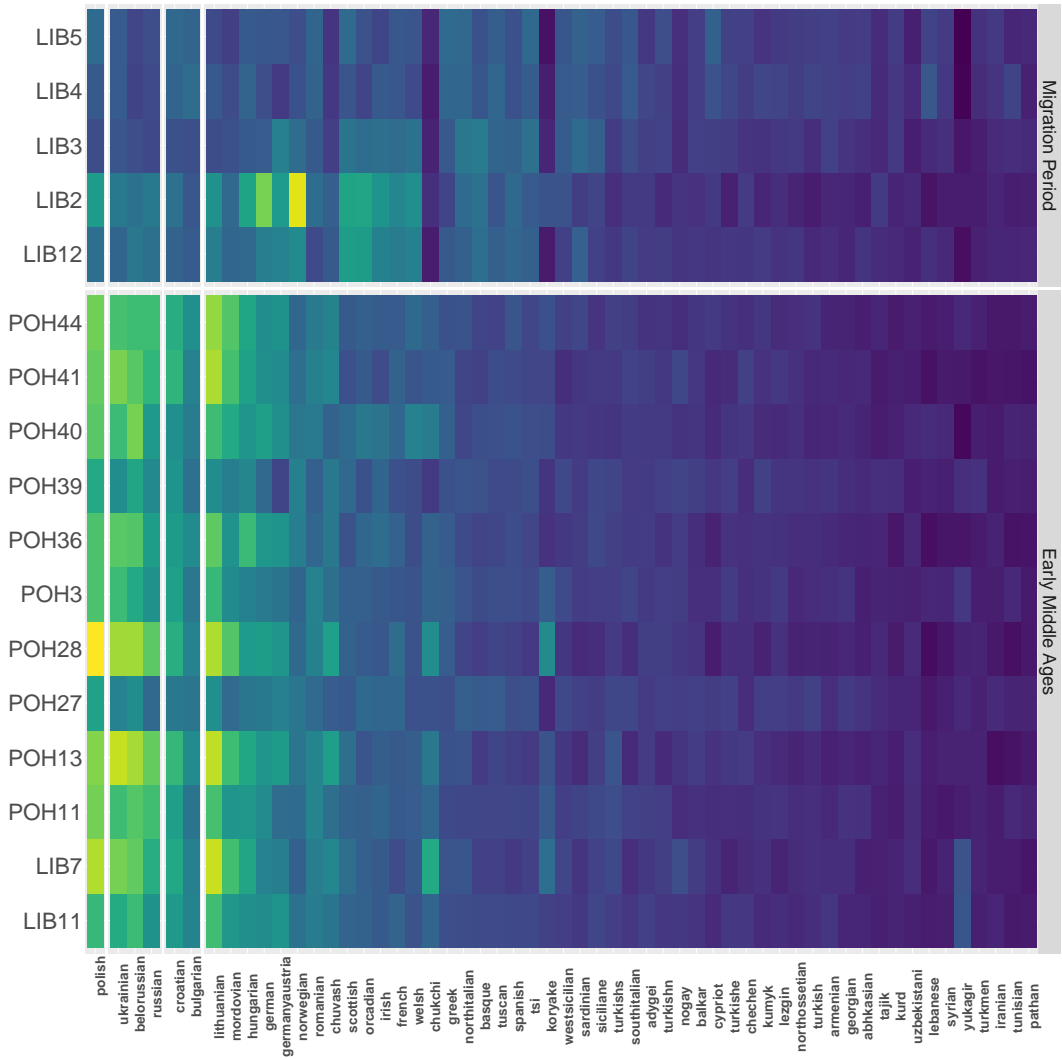


Figure 5.7: Raw chunklengths matrix from the ‘present-day’ painting. Rows correspond to different ancient recipient individuals, grouped into Migration Period and Early Middle Age period, and columns to different donor populations. Colour of cells corresponds to the total length of genome that a given donor individuals donates to that recipient, with dark/blue indicating less sharing and light/yellow colours indicating more sharing.

In contrast, the Early Middle Age samples showed a strong affinity to

present-day day Slavic populations. In particular, we find that samples copy many more haplotypes from present-day day Polish individuals than they do from other populations. This is consistent with previous findings based on uniparental markers. There was also a strong affinity to several non-Slavic speaking present-day populations - notably Lithuania and Mordovian.

To confirm that the observed results were not a result of phasing or imputing ancient individuals using present-day samples, I performed analysis f_3 statistics. Specifically, I calculated f_3 , or the branch length / amount of shared drift, between a set of present-day test populations and the grouped Early Middle Age samples. The results are qualitatively similar to those obtained using haplotype-based methods, with Early Middle Age ancient Slavic individuals being closest to samples from Eastern Europe (Fig. 5.8). However, the f_3 results do not appear to show the same degree of geographical structure; for example, Early Middle Age have a more positive f_3 with present-day Irish individuals than with present-day Croatians.

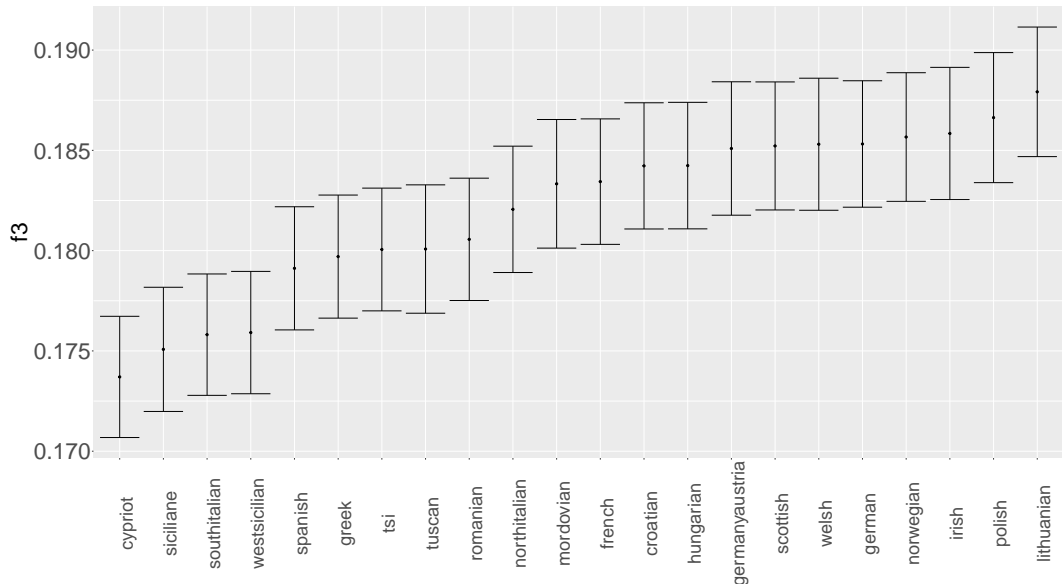


Figure 5.8: f_3 statistics in the form of $f_3(EMA, present-day; mbutipygmy)$, where *present-day* is different present-day European population. Error bars represent ± 2 stderr.

5.4.6 Continuity with present-day Slavs

The previous section strongly suggests at least some degree of continuity between Early Middle Age samples and present day Slavic populations that is not shared with the samples from the Migration Period, as the Early Middle Age samples share many more haplotypes with present-day Slavs compared to Migration Period.

To explicitly test the hypothesis that the Early Middle Age samples were continuous with the present-day Slavic populations, I used *qpWave*, which tests the number of streams of ancestry from a set of *right* populations into a set of *left* populations, $qpWave(left = croatian, lithuanian, polish, ukrainian, right = middleage, migration)$. The matrix with rank $r = 0$ can be rejected ($p = 0.112$). Note - not sure how to interpret this.

5.4.7 Genetic structure and admixture events of present-day Slavic people

As described in the introduction, several studies have looked at the structure of present-day Slavic populations, but none have integrated autosomal DNA from present-day and ancient samples and analysed them jointly with haplotype-based methods. I performed an all-v-all painting of a selection of present-day European populations and all newly sequenced ancient Slavic samples and applied the fineSTRUCTURE algorithm to the resulting chunkcounts matrix, inferring 32 clusters.

As a whole, present-day Slavs do not form a monophyletic group within the fineSTRUCTURE dendrogram to the exclusion of non-Slavic populations (Fig. 5.10), as several non-Slavic speaking populations such as German, Irish and Scottish cluster in the main clade containing Slavic speakers. However, some structure is apparent; speakers of ‘Southern’ Slavic languages from Croatia and Bulgaria form a group to the exclusion of ‘Eastern’ Slavic speaking pop-

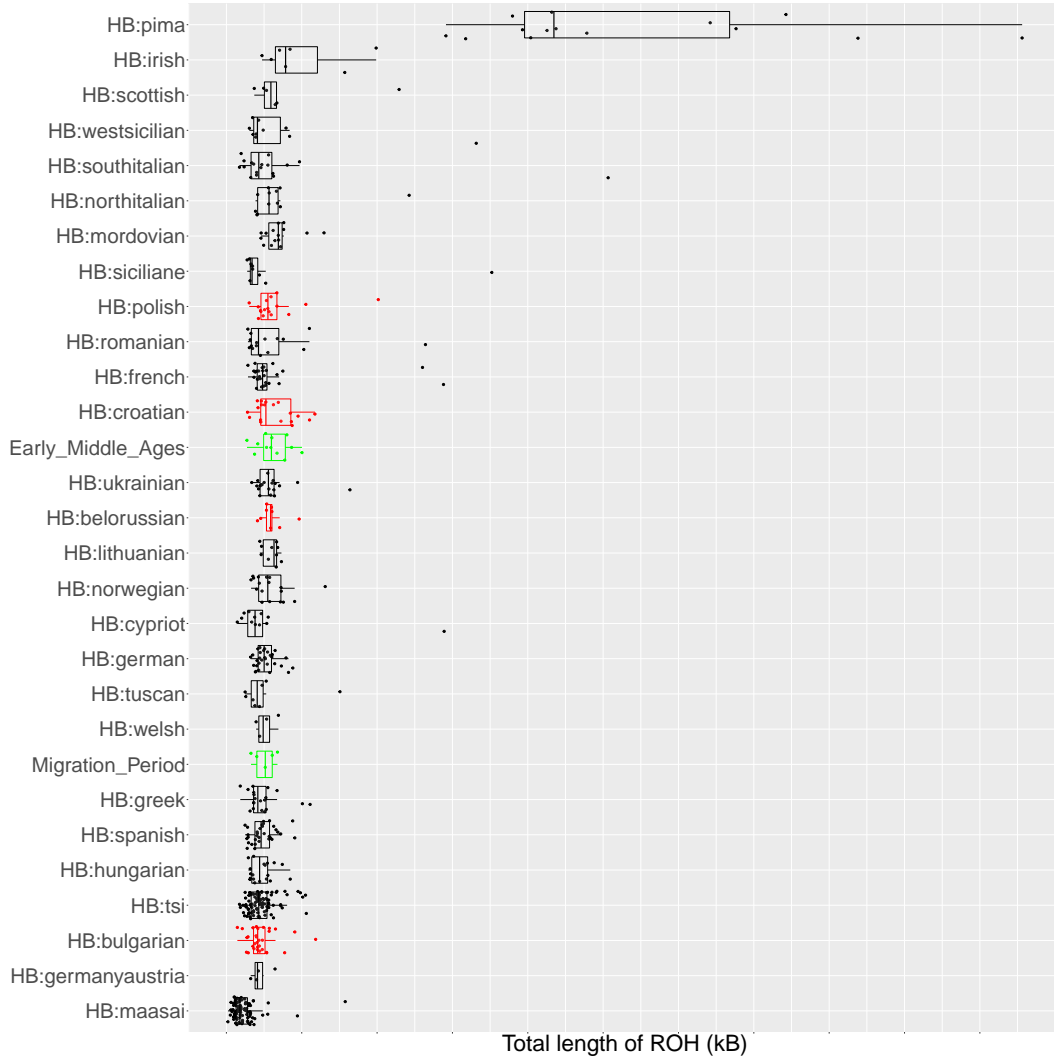


Figure 5.9: Total length of runs-of-homozygosity (ROH) in different present-day and ancient populations. Each point is the total length of ROH (kB) within an individual in that population. Points given jitter to aid visualisation. HB:pima and HB:masasai included to display extremes of ROH in different present-day human populations.

ulations from Belarus, Russia and Ukraine. Individuals from Poland cluster with ‘Eastern’ Slavic speakers, suggesting the principle axis of variation splits populations into ‘North-West’ and ‘South-East’ groups.

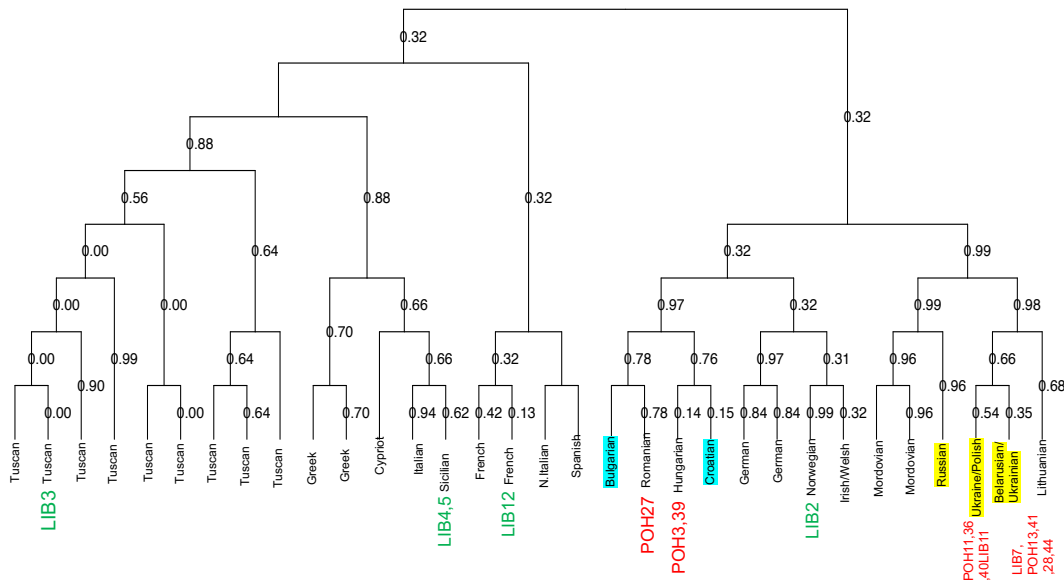


Figure 5.10: Population dendrogram generated by the fineSTRUCTURE tree building algorithm. Labeled tips refer to the primary population(s) represented in that clade. present-day non-Slavic populations shown in black. ‘South-East’ Slavs highlighted in cyan and ‘North-West’ Slavs highlighted in yellow. Migration period individuals superimposed in green and Early Middle Age samples superimposed in red. Read fineSTRUCTURE paper for description of edge values. Note: some tips contained more than one population but were not included as labels to save space.

Of the Early Middle Age samples, 3 samples (POH3, POH39, POH27) were present in the ‘South-East’ Slavic cluster, falling into a group composed of Bulgarian and Romanian samples. The remaining 7 samples are found in the ‘North-West’ cluster containing samples from Lithuania, Poland, Ukraine and Belarus. Painting the samples using present-day individuals has thus uncovered structure that was not able to be detected by looking only at ancient samples. It also suggests the structure of Slavic populations into was present at least as early as the date of these samples.

Previous studies have identified admixture events in present-day Slavic

populations involving an East Asian source approximately xx years ago [50, 94]. In previous sections, I showed that this signal exists in the Early Middle Age ancient samples, best characterised by populations from present-day Mongolia (Fig. 5.3).

I employed MOSAIC to replicate these results and determine whether a similar admixing source is present in the ancient populations.

When considering 2-way admixture event, all of the tested populations, bar the Migration Period Slavs, showed evidence of an admixture event involving a minor source which has the lowest Fst with present-day Uygurs. The dates and bootstrapped confidence intervals are given in Fig. 5.11.

Interestingly, most present-day Slavic speaking populations, such as present-day Polish, show evidence of a 3-way admixture event, where the middle component has the lowest F_{st} with Migration Era ancient samples (Fig. 5.12). The major component has a low F_{st} with Early Middle Age Slavs. This suggests that the formation of present-day Slavic populations could have occurred via an admixture event(s) involving Migration Era individuals with high levels of Southern European ancestry, Middle Age Era samples which show a strong affinity to present day Eastern Europeans, and a small but significant East Asian source best represented by present-day Uygurs.

5.5 Discussion

The combined results from the Migration Period suggest the individuals living in Czechia during this time period were of mixed ancestry and did not originate from the same source population. The diverse set of ancestries, spanning from Scandinavia to Southern Europe imply that the Migration Period was truly a period of Migration where individuals from distal ends of Europe lived among one another. I identified ancestry sources from Southern Europe and Scandinavia.

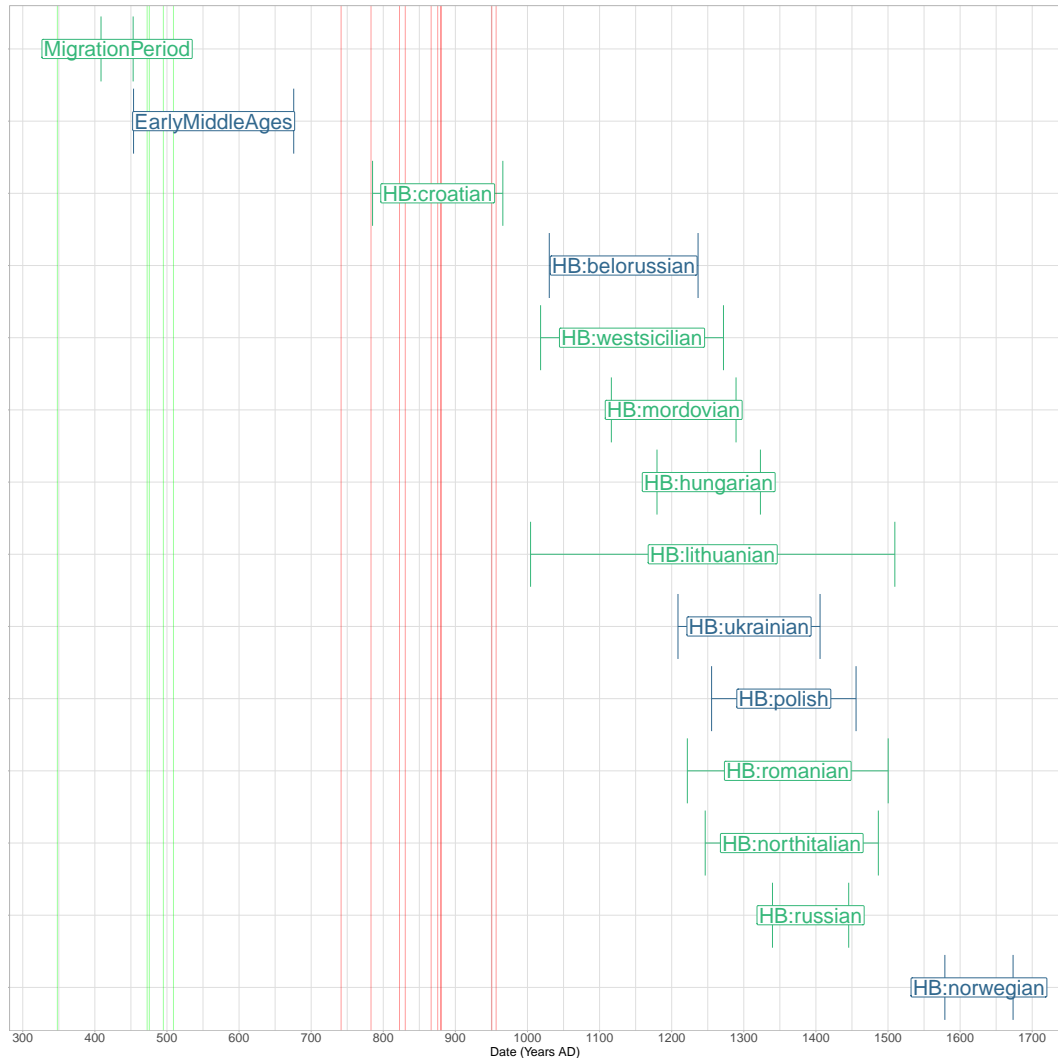


Figure 5.11: MOSAIC inferred 2-way admixture dates with bootstrapped 97.5% and 2.5% CI. Vertical green lines correspond to radiocarbon estimated dates of Migration Period samples and red lines equivalent for Early Middle Age samples.

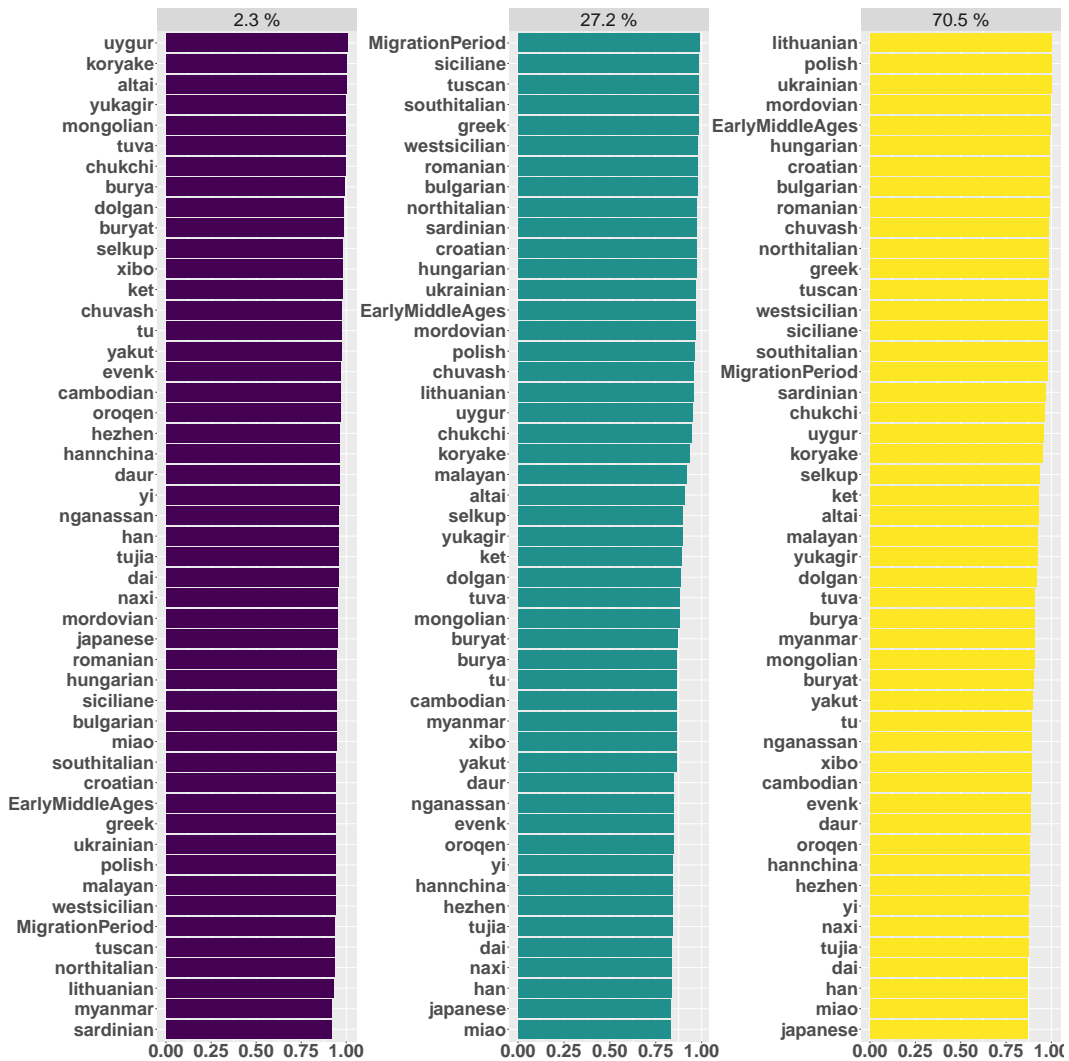


Figure 5.12: $1 - F_{st}$ between 3 inferred mixing sources for present-day Belorussians. Each panel represent a different mixing source. Each bar gives the value $1 - F_{st}$ between that samples population and the mixing source. Higher values of $1 - F_{st}$ suggest that source is well represented by a particular population.

The results from the analysis of combined ancient and present-day genomes are consistent with those from Kushniarevich et al (2015) [80] who determined that Eastern (Russia, Belarus, Ukraine) and Western (Polish) central European Slavs form a cluster to the exclusion of Southern Slavs (Croatia, Bulgaria), whilst also remaining distinct from geographically proximate Germanic (German/Austrian) and Baltic (Lithuanian) populations. This is also consistent with results from Veeramah et al 2011, who showed that Sorbs, a west-Slavic population found between Poland and Germany, have a much stronger affinity to more distant Slavic populations from Czechia than to more proximate Germans [95]. Similarly, I found that the Slavisation of the Balkan peninsula doesn't extend beyond Croatia; the cluster of Croatian individuals only derives 1.2% of their ancestry from nearby Greek sources. However, admixture modeling suggested that Southern Slavs show signals of a historic admixture event where the minor source is related to present-day Mediterranean populations. An admixture event with a similar minor source is found in Migration period samples, albeit dated further in the past.

I recapitulated a previously described admixture event into not only present day Slavic speaking populations, but also Southern Europeans (e.g. North Italians). The source of this East-Asian admixture is most closest to present-day Uygurs. However, the true ancient population that was responsible to transmitting East-Asian ancestry into Europe is yet to be determined. It seems likely that the ancestry was brought to Europe via an intermediate population containing East Asian ancestry, such as the Huns or Turkic peoples.

Chapter 6

General Conclusions

Lorem ipsum dolor sit amet, consectetuer adipiscing elit. Etiam lobortis facilisis sem. Nullam nec mi et neque pharetra sollicitudin. Praesent imperdiet mi nec ante. Donec ullamcorper, felis non sodales commodo, lectus velit ultrices augue, a dignissim nibh lectus placerat pede. Vivamus nunc nunc, molestie ut, ultricies vel, semper in, velit. Ut porttitor. Praesent in sapien. Lorem ipsum dolor sit amet, consectetuer adipiscing elit. Duis fringilla tristique neque. Sed interdum libero ut metus. Pellentesque placerat. Nam rutrum augue a leo. Morbi sed elit sit amet ante lobortis sollicitudin. Praesent blandit blandit mauris. Praesent lectus tellus, aliquet aliquam, luctus a, egestas a, turpis. Mauris lacinia lorem sit amet ipsum. Nunc quis urna dictum turpis accumsan semper.

Appendix A

Datasets used

This appendix described the different datasets used in analyses performed in this thesis. It includes datasets of both modern and ancient genomes

A.1 Antonio et al 2019

Samples from Antonio et al (2019) [7]. Looking at the population genomics of ancient Rome.

This dataset consists of 134 shotgun-sequenced individuals from 12,000 years ago to the present day. Coverage ranges from 0.4x - 4x (median 1.05x).

Aligned reads in .bam format were downloaded from the ENA under accession number PRJEB32566.

A.2 Margaryan et al 2020

Samples from Margaryan et al 2020 [96], looking at the population genomics of Vikings.

This dataset consists of 442 shotgun-sequenced individuals from the Bronze Age to Medieval and Early Modern ages. Mean coverage of 1x. X individuals

did not have enough data to estimate recalibration parameters and were excluded from the rest of the analysis.

Aligned reads in .bam format were downloaded from the ENA under accession number PRJEB37976.

A.3 Rivollat et al 2020

Samples from Rivollat et al (2020) [53]. Looking at the population genomics of France and Germany.

This dataset consists of 101 captured individuals from 7000–3000 BCE. years ago to the present day.

Aligned reads in .bam format were downloaded from the ENA under accession number PRJEB36208.

A.4 Brunel et al 2018

Samples from Brunel et al (2018) [66]. Looking at the population genomics of France.

This dataset consists of 52 shotgun sequenced individuals from Mesolithic to the Iron Age.

Aligned reads in .bam format were downloaded from the ENA under accession number PRJEB36208.

A.5 Allentoft et al 2015

Samples from Allentoft et al 2015 [97]. Looking at the population genomics Bronze Age Eurasia.

This dataset consists of 20 shotgun sequenced individuals.

Aligned reads in .bam format were downloaded from the ENA under accession number PRJEB9021.

A.6 Broushaki et al 2016

Samples from Broushaki et al 2016 [98]. Looking at the population genomics Bronze Age Eurasia.

This dataset consists of 1 shotgun sequenced individual.

Aligned reads in .bam format were downloaded from the ENA under accession number xxxx.

A.7 Cassidy et al 2016

Samples from Cassidy et al 2016 [99]. Looking at the population genomics of the Neolithic and Bronze Age migrations to Ireland.

This dataset consists of 4 shotgun sequenced individuals.

Aligned reads in .bam format were downloaded from the ENA under accession number PRJEB11995.

A.8 de Barros Damgaard et al 2018a

The first horse herders and the impact of early Bronze Age steppe expansions into Asia.

Samples from de Barros Damgaard et al 2018a [19].

This dataset consists of 34 shotgun sequenced individuals.

Aligned reads in .bam format were downloaded from the ENA under accession number PRJEB26349.

A.9 de Barros Damgaard et al 2018b

137 ancient human genomes from across the Eurasian steppes

Samples from de Barros Damgaard et al 2018b [100].

This dataset consists of 58 shotgun sequenced individuals.

Aligned reads in .bam format were downloaded from the ENA under accession number PRJEB20658.

A.10 Gamba et al 2014

Genome flux and stasis in a five millennium transect of European prehistory

Samples from Gamba et al 2014 [62].

This dataset consists of 10 shotgun sequenced individuals.

Aligned reads in .bam format were downloaded from the Sequence Read Archive (SRA) under the accession code SRP039766.

A.11 Gunther et al 2015

Genomic diversity and admixture differs for Stone-Age Scandinavian foragers and farmers

Samples from Gunther et al 2015 [101].

This dataset consists of 2 shotgun sequenced individuals.

Aligned reads in .bam format were downloaded from the ENA under acces-

sion number PRJEB9783.

A.12 Hofmanová et al 2016

Early farmers from across Europe directly descended from Neolithic Aegeans

Samples from Hofmanová et al 2016 [55].

This dataset consists of 5 shotgun sequenced individuals.

Aligned reads in .bam format were downloaded from the ENA under accession number PRJEB11848.

A.13 Jones et al 2015

Upper Palaeolithic genomes reveal deep roots of modern Eurasians

Samples from Jones et al 2015 [102].

This dataset consists of 2 shotgun sequenced individuals.

Aligned reads in .bam format were downloaded from the ENA under accession number PRJEB11364.

A.14 Marchi et al 2020

The mixed genetic origin of the first farmers of Europe

Samples from Marchi et al 2020 [103].

This dataset consists of 4 shotgun sequenced individuals.

Aligned reads in .bam format were downloaded from the ENA under accession number PRJEB11364.

A.15 Olalde et al 2014

Derived immune and ancestral pigmentation alleles in a 7,000-year-old Mesolithic European

Samples from Olalde et al 2014 [104].

This dataset consists of 1 shotgun sequenced individual.

Aligned reads in .bam format were downloaded from the ENA under accession number PRJNA230689.

A.16 Sánchez-Quinto et al 2019

Megalithic tombs in western and northern Neolithic Europe were linked to a kindred society

Samples from Sánchez-Quinto et al 2019 [105].

This dataset consists of 7 shotgun sequenced individuals.

Aligned reads in .bam format were downloaded from the ENA accession number PRJNA230689.

A.17 Seguin-Orlando et al 2014

Genomic structure in Europeans dating back at least 36,200 years

Samples from Seguin-Orlando et al 2014 [106].

This dataset consists of 1 shotgun sequenced individual.

Aligned reads in .bam format were downloaded from the ENA under accession number PRJNA230689.

A.18 30x 1000 genomes dataset

Samples from [28].

This dataset consists of 3,202 modern individuals from 26 worldwide populations, sequenced to a targeted depth of 30x coverage. The downloaded dataset was aligned to the gr38 reference genome.

Samples were downloaded to the UCL Computer Science cluster by myself from the ftp mirror.

The following steps were taken to process the data before being used as an imputation reference.

1. Filtered such that SNPs with only 2 alleles were retained
2. Performed a liftover to hg19 using LiftOverVcf from picard tools [22]
3. Filter again for SNPs with only 2 alleles
4. Phase using shapeit4, using the ‘sequencing’ parameter and setting –pbwt-depth 4.
5. Remove duplicated SNPs using bcftools norm [46]
6. Use Beagle’s conform-gt utility to ensure reference alleles were consistent with the previous 1000 genomes build. This was done because all previous datasets I have compiled were also conformed to the previous 1000 genomes build.

A.19 Human Origins dataset

Samples from various studies.

This dataset consists of 560,420 SNPs and 5998 individuals from 509 worldwide populations.

A.20 MS POBI HellBus dataset

??

Multiple Sclerosis (MS), People of the British Isles (POBI), Hellenthal and Busby (HB) / MS POBI HellBus

Samples from Sawcer et al (2011) [107], Leslie et al 2015 [42] and

Appendix B

Another Appendix About Things

(things)

Appendix C

Colophon

This is a description of the tools you used to make your thesis. It helps people make future documents, reminds you, and looks good.

(example) This document was set in the Times Roman typeface using L^AT_EX and BibT_EX, composed with a text editor.

Bibliography

- [1] H.A. Green, R.E., Krause, J., Briggs, A., W., Maricic, T., Stenzel, U., Kircher, M., Patterson, N., Li, H., Zhai, W., Fritz, M.H., Hansen, N.F., Durand, E., Y., Malaspinas, A., Jensen, J., D., Marques-Bonet, T., Alkan, C., Prüfer, K., Meyer, M., Burbano. A Draft Sequence of the Neandertal Genome. *Science (New York, N.Y.)*, 328(5979):710–22, 2010.
- [2] Nick Patterson, Priya Moorjani, Yontao Luo, Swapan Mallick, Nadin Rohland, Yiping Zhan, Teri Genschoreck, Teresa Webster, and David Reich. Ancient admixture in human history. *Genetics*, 192(3):1065–1093, 2012.
- [3] Benjamin M Peter. Admixture, population structure, and f-statistics. *Genetics*, 202(4):1485–1501, 2016.
- [4] Alkes L Price, Nick J Patterson, Robert M Plenge, Michael E Weinblatt, Nancy A Shadick, and David Reich. Principal components analysis corrects for stratification in genome-wide association studies. *Nature genetics*, 38(8):904–909, 2006.
- [5] Iosif Lazaridis, Nick Patterson, Alissa Mittnik, Gabriel Renaud, Swapan Mallick, Karola Kirsanow, Peter H. Sudmant, Joshua G. Schraiber, Sergi Castellano, Mark Lipson, Bonnie Berger, Christos Economou, Ruth Bollongino, Qiaomei Fu, Kirsten I. Bos, Susanne Nordenfelt, Heng Li, Cesare De Filippo, Kay Prüfer, Susanna Sawyer, Cosimo Posth, Wolfgang Haak, Fredrik Hallgren, Elin Fornander, Nadin Rohland, Dominique

Delsate, Michael Francken, Jean Michel Guinet, Joachim Wahl, George Ayodo, Hamza A. Babiker, Graciela Bailliet, Elena Balanovska, Oleg Balanovsky, Ramiro Barrantes, Gabriel Bedoya, Haim Ben-Ami, Judit Bene, Fouad Berrada, Claudio M. Bravi, Francesca Brisighelli, George B.J. J Busby, Francesco Cali, Mikhail Churnosov, David E.C. C Cole, Daniel Corach, Larissa Damba, George Van Driem, Stanislav Dryomov, Jean Michel Dugoujon, Sardana A. Fedorova, Irene Gallego Romero, Marina Gubina, Michael Hammer, Brenna M. Henn, Tor Hervig, Ugur Hodoglugil, Aashish R. Jha, Sena Karachanak-Yankova, Rita Khusainova, Elza Khusnudinova, Rick Kittles, Toomas Kivisild, William Klitz, Vaidutis Kučinskas, Alena Kushniarevich, Leila Laredj, Sergey Litvinov, Theologos Loukidis, Robert W. Mahley, Béla Melegh, Ene Metspalu, Julio Molina, Joanna Mountain, Klemetti Näkkäläjärvi, Desislava Nesheva, Thomas Nyambo, Ludmila Osipova, Jüri Parik, Fedor Platonov, Olga Posukh, Valentino Romano, Francisco Rothhammer, Igor Rudan, Ruslan Ruizbakiev, Hovhannes Sahakyan, Antti Sajantila, Antonio Salas, Elena B. Starikovskaya, Ayele Tarekegn, Draga Toncheva, Shahlo Turdikulova, Ingrida Uktveryte, Olga Utevska, René Vasquez, Mercedes Villena, Mikhail Voevoda, Cheryl A. Winkler, Levon Yepiskoposyan, Pierre Zalloua, Tatjana Zemunik, Alan Cooper, Cristian Capelli, Mark G. Thomas, Andres Ruiz-Linares, Sarah A. Tishkoff, Lalji Singh, Kumarasamy Thangaraj, Richard Villemans, David Comas, Rem Sukernik, Mait Metspalu, Matthias Meyer, Evan E. Eichler, Joachim Burger, Montgomery Slatkin, Svante Pääbo, Janet Kelso, David Reich, and Johannes Krause. Ancient human genomes suggest three ancestral populations for present-day Europeans. *Nature*, 513(7518):409–413, 2014.

- [6] Rui Martiniano, Lara M. Cassidy, Ros Ó'Maoldúin, Russell McLaughlin, Nuno M. Silva, Licinio Manco, Daniel Fidalgo, Tania Pereira, Maria J. Coelho, Miguel Serra, Joachim Burger, Rui Parreira, Elena Moran, Antonio C. Valera, Eduardo Porfirio, Rui Boaventura, Ana M. Silva, Daniel G.

- Bradley, Maoldú In, Russell McLaughlin, Nuno M. Silva, Licinio Manco, Daniel Fidalgo, Tania Pereira, Maria J. Coelho, Miguel Serra, Joachim Burger, Rui Parreira, Elena Moran, Antonio C. Valera, Eduardo Porfirio, Rui Boaventura, Ana M. Silva, Daniel G. Bradley, Ros Ó'Maoldúin, Russell McLaughlin, Nuno M. Silva, Licinio Manco, Daniel Fidalgo, Tania Pereira, Maria J. Coelho, Miguel Serra, Joachim Burger, Rui Parreira, Elena Moran, Antonio C. Valera, Eduardo Porfirio, Rui Boaventura, Ana M. Silva, and Daniel G. Bradley. The population genomics of archaeological transition in west Iberia: Investigation of ancient substructure using imputation and haplotype-based methods. *PLoS Genetics*, 13(7):1–24, 2017.
- [7] Margaret L Antonio, Ziyue Gao, Hannah M Moots, Michaela Lucci, Francesca Candilio, Susanna Sawyer, Victoria Oberreiter, Diego Calderon, Katharina Devitofranceschi, Rachael C Aikens, et al. Ancient rome: a genetic crossroads of europe and the mediterranean. *Science*, 366(6466):708–714, 2019.
- [8] Guy S. Jacobs, Georgi Hudjashov, Lauri Saag, Pradiptajati Kusuma, Chelzie C. Darusallam, Daniel J. Lawson, Mayukh Mondal, Luca Pagani, François-Xavier Ricaut, Mark Stoneking, Mait Metspalu, Herawati Sudoyo, J. Stephen Lansing, and Murray P. Cox. Multiple deeply divergent denisovan ancestries in papuans. *Cell*, 177(4):1010–1021.e32, 2019.
- [9] João C Teixeira, Guy S Jacobs, Chris Stringer, Jonathan Tuke, Georgi Hudjashov, Gludhug A Purnomo, Herawati Sudoyo, Murray P Cox, Raymond Tobler, Chris SM Turney, et al. Widespread denisovan ancestry in island southeast asia but no evidence of substantial super-archaic hominin admixture. *Nature Ecology & Evolution*, 5(5):616–624, 2021.
- [10] Donald F Conrad, Mattias Jakobsson, Graham Coop, Xiaoquan Wen, Jeffrey D Wall, Noah A Rosenberg, and Jonathan K Pritchard. A

- worldwide survey of haplotype variation and linkage disequilibrium in the human genome. *Nature genetics*, 38(11):1251–1260, 2006.
- [11] Yun S Song. Na li and matthew stephens on modeling linkage disequilibrium. *Genetics*, 203(3):1005–1006, 2016.
- [12] Garrett Hellenthal, Adam Auton, and Daniel Falush. Inferring human colonization history using a copying model. *PLoS genetics*, 4(5):e1000078, 2008.
- [13] Daniel John Lawson, Garrett Hellenthal, Simon Myers, and Daniel Falush. Inference of population structure using dense haplotype data. *PLoS Genetics*, 8(1):11–17, 2012.
- [14] Vivian Link, Athanasios Kousathanas, Krishna Veeramah, Christian Sell, Amelie Scheu, and Daniel Wegmann. ATLAS: Analysis Tools for Low-depth and Ancient Samples. *bioRxiv*, page 105346, 2017.
- [15] Simone Rubinacci, Diogo M Ribeiro, Robin J Hofmeister, and Olivier Delaneau. Efficient phasing and imputation of low-coverage sequencing data using large reference panels. *Nature Genetics*, 53(1):120–126, 2021.
- [16] Juan C. Chacon-Duque, Kaustubh Adhikari, Macarena Fuentes-Guajardo, Javier Mendoza-Revilla, Victor Acuna-Alonso, Rodrigo Barquera Lozano, Mirsha Quinto-Sanchez, Jorge Gomez-Valdes, Paola Everardo Martinez, Hugo Villamil-Ramirez, Tabita Hunemeier, Virginia Ramallo, Caio C. Silva de Cerqueira, Malena Hurtado, Valeria Villegas, Vanessa Granja, Mercedes Villena, Rene Vasquez, Elena Llop, Jose R. Sandoval, Alberto A. Salazar-Granara, Maria-Laura Parolin, Karla Sandoval, Rosenda I. Penalosa-Espinosa, Hector Rangel-Villalobos, Cheryl Winckler, William Klitz, Claudio Bravi, Julio Molina, Daniel Corach, Ramiro Barrantes, Veronica Gomes, Carlos Resende, Leonor Gusmao, Antonio Amorim, Yali Xue, Jean-Michel Dugoujon, Pedro Moral, Rolando

- Gonzalez-Jose, Lavinia Schuler-Faccini, Francisco M. Salzano, Maria-Catira Bortolini, Samuel Canizales-Quinteros, Giovanni Poletti, Carla Gallo, Gabriel Bedoya, Francisco Rothhammer, David Balding, Garrett Hellenthal, and Andres Ruiz-Linares. Latin Americans show wide-spread Converso ancestry and the imprint of local Native ancestry on physical appearance. *Nature Communications*, page 252155, 2018.
- [17] Na Li and Matthew Stephens. Modeling Linkage Disequilibrium and Identifying Recombination Hotspots Using Single-Nucleotide Polymorphism Data. *Genetics*, 165(4):2213–2233, 2003.
- [18] G. A. Watterson. On the number of segregating sites in genetical models without recombination. *Theoretical Population Biology*, 1975.
- [19] Peter de Barros Damgaard, Rui Martiniano, Jack Kamm, J. Víctor Moreno-Mayar, Guus Kroonen, Michaël Peyrot, Gojko Barjamovic, Simon Rasmussen, Claus Zacho, Nurbol Baimukhanov, Victor Zaibert, Victor Merz, Arjun Biddanda, Ilja Merz, Valeriy Loman, Valeriy Evdokimov, Emma Usmanova, Brian Hemphill, Andaine Seguin-Orlando, Fulya Eylem Yediay, Inam Ullah, Karl-Göran Sjögren, Katrine Højholt Iversen, Jeremy Choin, Constanza de la Fuente, Melissa Ilardo, Hannes Schroeder, Vyacheslav Moiseyev, Andrey Gromov, Andrei Polyakov, Sachihiro Omura, Süleyman Yücel Senyurt, Habib Ahmad, Catriona McKenzie, Ashot Margaryan, Abdul Hameed, Abdul Samad, Nazish Gul, Muhammad Hassan Khokhar, O. I. Goriunova, Vladimir I. Bazaliiskii, John Novembre, Andrzej W. Weber, Ludovic Orlando, Morten E. Allentoft, Rasmus Nielsen, Kristian Kristiansen, Martin Sikora, Alan K. Outram, Richard Durbin, and Eske Willerslev. The first horse herders and the impact of early bronze age steppe expansions into asia. *Science*, 360(6396), 2018.
- [20] Qiaomei Fu, Heng Li, Priya Moorjani, Flora Jay, Sergey M. Slepchenko, Aleksei A. Bondarev, Philip L.F. Johnson, Ayinuer Aximu-Petri, Kay

- Prüfer, Cesare De Filippo, Matthias Meyer, Nicolas Zwyns, Domingo C. Salazar-García, Yaroslav V. Kuzmin, Susan G. Keates, Pavel A. Kosintsev, Dmitry I. Razhev, Michael P. Richards, Nikolai V. Peristov, Michael Lachmann, Katerina Douka, Thomas F.G. Higham, Montgomery Slatkin, Jean Jacques Hublin, David Reich, Janet Kelso, T. Bence Viola, and Svante Pääbo. Genome sequence of a 45,000-year-old modern human from western Siberia. *Nature*, 2014.
- [21] Torsten Günther, Helena Malmström, Emma M. Svensson, Ayça Omrak, Federico Sánchez-Quinto, Gülsah M. Kılınç, Maja Krzewińska, Gunilla Eriksson, Magdalena Fraser, Hanna Edlund, Arielle R. Munters, Alexandra Coutinho, Luciana G. Simões, Mário Vicente, Anders Sjölander, Berit Jansen Sellevold, Roger Jørgensen, Peter Claes, Mark D. Shriver, Cristina Valdiosera, Mihai G. Netea, Jan Apel, Kerstin Lidén, Birgitte Skar, Jan Storå, Anders Götherström, and Mattias Jakobsson. Population genomics of Mesolithic Scandinavia: Investigating early postglacial migration routes and high-latitude adaptation. *PLoS Biology*, 2018.
- [22] Broad Institute. Picard tools. <http://broadinstitute.github.io/picard/>, 2018. Accessed: 2018-MM-DD; version X.Y.Z.
- [23] 1000 Genomes Project Consortium, Adam Auton, Lisa D. Brooks, Richard M. Durbin, Erik P. Garrison, Hyun Min Kang, Jan O. Korbel, Jonathan L. Marchini, Shane McCarthy, Gil A. McVean, Gonçalo R. Abecasis, David M. Altshuler, Richard M. Durbin, David R. Bentley, Aravinda Chakravarti, Andrew G. Clark, Peter Donnelly, Evan E. Eichler, Paul Flicek, Stacey B. Gabriel, Richard A. Gibbs, Eric D. Green, Matthew E. Hurles, Bartha M. Knoppers, Jan O. Korbel, Eric S. Lander, Charles Lee, Hans Lehrach, Elaine R. Mardis, Gabor T. Marth, Gil A. McVean, Deborah A. Nickerson, Jeanette P. Schmidt, Stephen T. Sherry, Jun Wang, Richard K. Wilson, Eric Boerwinkle, Harsha Doddapaneni, Yi Han, Viktoriya Korchina, Christie Kovar, Sandra Lee, Donna Muzny,

Jeffrey G. Reid, Yiming Zhu, Yuqi Chang, Qiang Feng, Xiaodong Fang, Xiaosen Guo, Min Jian, Hui Jiang, Xin Jin, Tianming Lan, Guoqing Li, Jingxiang Li, Yun Yingrui Li, Shengmao Liu, Xiaoming Liu, Yao Lu, Xuedi Ma, Meifang Tang, Bo Wang, Guangbiao Wang, Honglong Wu, Renhua Wu, Xun Xu, Ye Yin, Dandan Zhang, Wenwei Zhang, Jiao Zhao, Meiru Zhao, Xiaole Zheng, Namrata Gupta, Neda Gharani, Lorraine H. Toji, Norman P. Gerry, Alissa M. Resch, Jonathan Barker, Laura Clarke, Laurent Gil, Sarah E. Hunt, Gavin Kelman, Eugene Kulesha, Rasko Leinonen, William M. McLaren, Rajesh Radhakrishnan, Asier Roa, Dmitriy Smirnov, Richard E. Smith, Ian Streeter, Anja Thormann, Iliana Toneva, Brendan Vaughan, Xiangqun Zheng-Bradley, Russell Grocock, Sean Humphray, Terena James, Zoya Kingsbury, Ralf Sudbrak, Marcus W. Albrecht, Vyacheslav S. Amstislavskiy, Tatiana A. Borodina, Matthias Lienhard, Florian Mertes, Marc Sultan, Bernd Timmermann, Marie Laure Yaspo, Lucinda Fulton, Victor Ananiev, Zinaida Belaia, Dimitriy Beloslyudtsev, Nathan Bouk, Chao Chen, Deanna Church, Robert Cohen, Charles Cook, John Garner, Timothy Hefferon, Mikhail Kimelman, Chunlei Liu, John Lopez, Peter Meric, Chris O'Sullivan, Yuri Ostapchuk, Lon Phan, Sergiy Ponomarov, Valerie Schneider, Eugene Shekhtman, Karl Sirotkin, Douglas Slotta, Hua Zhang, Senduran Balasubramaniam, John Burton, Petr Danecek, Thomas M. Keane, Anja Kolb-Kokocinski, Shane McCarthy, James Stalker, Michael Quail, Christopher J. Davies, Jeremy Gollub, Teresa Webster, Brant Wong, Yiping Zhan, Christopher L. Campbell, Yu Kong, Anthony Marcketta, Fuli Yu, Lilian Antunes, Matthew Bainbridge, Aniko Sabo, Zhuoyi Huang, Lachlan J.M. Coin, Lin Fang, Qibin Li, Zhenyu Li, Haoxiang Lin, Binghang Liu, Ruibang Luo, Haojing Shao, Yinlong Xie, Chen Ye, Chang Yu, Fan Zhang, Hancheng Zheng, Hongmei Zhu, Can Alkan, Elif Dal, Fatma Kahveci, Erik P. Garrison, Deniz Kural, Wan Ping Lee, Wen Fung Leong, Michael Stromberg, Alastair N. Ward, Jiantao Wu, Mengyao Zhang, Mark J. Daly, Mark A.

DePristo, Robert E. Handsaker, Eric Banks, Gaurav Bhatia, Guillermo Del Angel, Giulio Genovese, Heng Li, Seva Kashin, Steven A. McCarroll, James C. Nemesh, Ryan E. Poplin, Seungtai C. Yoon, Jayon Lihm, Vladimir Makarov, Srikanth Gottipati, Alon Keinan, Juan L. Rodriguez-Flores, Tobias Rausch, Markus H. Fritz, Adrian M. Stütz, Kathryn Beal, Avik Datta, Javier Herrero, Graham R.S. Ritchie, Daniel Zerbino, Paridis C. Sabeti, Ilya Shlyakhter, Stephen F. Schaffner, Joseph Vitti, David N. Cooper, Edward V. Ball, Peter D. Stenson, Bret Barnes, Markus Bauer, R. Keira Cheetham, Anthony Cox, Michael Eberle, Scott Kahn, Lisa Murray, John Peden, Richard Shaw, Eimear E. Kenny, Mark A. Batzer, Miriam K. Konkel, Jerilyn A. Walker, Daniel G. MacArthur, Monkol Lek, Ralf Herwig, Li Ding, Daniel C. Koboldt, David Larson, Kai Kenny Ye, Simon Gravel, Anand Swaroop, Emily Chew, Tuuli Lappalainen, Yaniv Erlich, Melissa Gymrek, Thomas Frederick Willems, Jared T. Simpson, Mark D. Shriver, Jeffrey A. Rosenfeld, Carlos D. Bustamante, Stephen B. Montgomery, Francisco M. De La Vega, Jake K. Byrnes, Andrew W. Carroll, Marianne K. DeGorter, Phil Lacroix, Brian K. Maples, Alicia R. Martin, Andres Moreno-Estrada, Suyash S. Shringarpure, Fouad Zakaria, Eran Halperin, Yael Baran, Eliza Cerveira, Jaeho Hwang, Ankit Malhotra, Dariusz Plewczynski, Kamen Radew, Mallory Romanovitch, Chengsheng Zhang, Fiona C.L. Hyland, David W. Craig, Alexis Christofides, Nils Homer, Tyler Izatt, Ahmet A. Kurdoglu, Shripad A. Sinari, Kevin Squire, Chunlin Xiao, Jonathan Sebat, Danny Antaki, Madhusudan Gujral, Amina Noor, Kai Kenny Ye, Esteban G. Burchard, Ryan D. Hernandez, Christopher R. Gignoux, David Haussler, Sol J. Katzman, W. James Kent, Bryan Howie, Andres Ruiz-Linares, Emmanouil T. Dermitzakis, Scott E. Devine, Hyun Min Kang, Jeffrey M. Kidd, Tom Blackwell, Sean Caron, Wei Chen, Sarah Emery, Lars Fritzsche, Christian Fuchsberger, Goo Jun, Bingshan Li, Robert Lyons, Chris Scheller, Carlo Sidore, Shiya Song, Elzbieta Sliwerska, Daniel Taliun, Adrian Tan,

Ryan Welch, Mary Kate Wing, Xiaowei Zhan, Philip Awadalla, Alan Hodgkinson, Yun Yingrui Li, Xinghua Shi, Andrew Quitadamo, Gerton Lunter, Jonathan L. Marchini, Simon Myers, Claire Churchhouse, Olivier Delaneau, Anjali Gupta-Hinch, Warren Kretzschmar, Zamin Iqbal, Iain Mathieson, Androniki Menelaou, Andy Rimmer, Dionysia K. Xifara, Taras K. Oleksyk, Yunxin Yao Fu, Xiaoming Liu, Momiao Xiong, Lynn Jorde, David Witherspoon, Jinchuan Xing, Brian L. Browning, Sharon R. Browning, Fereydoun Hormozdiari, Peter H. Sudmant, Ekta Khurana, Chris Tyler-Smith, Cornelis A. Albers, Qasim Ayub, Yuan Chen, Vincenza Colonna, Luke Jostins, Klaudia Walter, Yali Xue, Mark B. Gerstein, Alexej Abyzov, Suganthi Balasubramanian, Jieming Chen, Declan Clarke, Yunxin Yao Fu, Arif O. Harmanci, Mike Jin, Donghoon Lee, Jeremy Liu, Xinmeng Jasmine Mu, Jing Zhang, Yan Yujun Zhang, Chris Hartl, Khalid Shakir, Jeremiah Degenhardt, Sascha Meiers, Benjamin Raeder, Francesco Paolo Casale, Oliver Stegle, Eric Wubbo Lameijer, Ira Hall, Vineet Bafna, Jacob Michaelson, Eugene J. Gardner, Ryan E. Mills, Gargi Dayama, Ken Chen, Xian Fan, Zechen Chong, Tenghui Chen, Mark J. Chaisson, John Huddleston, Maika Malig, Bradley J. Nelson, Nicholas F. Parrish, Ben Blackburne, Sarah J. Lindsay, Zemin Ning, Yan Yujun Zhang, Hugo Lam, Cristina Sisu, Danny Challis, Uday S. Evani, James Lu, Uma Nagaswamy, Jin Yu, Wangshen Li, Lukas Habegger, Haiyuan Yu, Fiona Cunningham, Ian Dunham, Kasper Lage, Jakob Berg Jespersen, Heiko Horn, Donghoon Kim, Rob Desalle, Apurva Narechania, Melissa A. Wilson Sayres, Fernando L. Mendez, G. David Poznik, Peter A. Underhill, David Mittelman, Ruby Banerjee, Maria Cerezo, Thomas W. Fitzgerald, Sandra Louzada, Andrea Massaia, Fengtang Yang, Divya Kalra, Walker Hale, Xu Dan, Kathleen C. Barnes, Christine Beiswanger, Hongyu Cai, Hongzhi Cao, Brenna Henn, Danielle Jones, Jane S. Kaye, Alastair Kent, Angeliki Kerasidou, Rasika A. Mathias, Pilar N. Ossorio, Michael Parker, Charles N. Rotimi, Charmaine D. Royal, Karla San-

- doval, Yeyang Su, Zhongming Tian, Sarah Tishkoff, Marc Via, Yuhong Wang, Huanming Yang, Ling Yang, Jiayong Zhu, Walter Bodmer, Gabriel Bedoya, Zhiming Cai, Yang Gao, Jiayou Chu, Leena Peltonen, Andres Garcia-Montero, Alberto Orfao, Julie Dutil, Juan C. Martinez-Cruzado, Rasika A. Mathias, Anselm Hennis, Harold Watson, Colin McKenzie, Firdausi Qadri, Regina LaRocque, Xiaoyan Deng, Danny Asogun, Onikepe Folarin, Christian Happi, Omonwunmi Omoniwa, Matt Stremlau, Ridhi Tariyal, Muminatou Jallow, Fatoumatta Sisay Joof, Tumani Corrah, Kirk Rockett, Dominic Kwiatkowski, Jaspal Kooner, Tran Tinh Hien, Sarah J. Dunstan, Nguyen ThuyHang, Richard Fonnlie, Robert Garry, Lansana Kanneh, Lina Moses, John Schieffelin, Donald S. Grant, Carla Gallo, Giovanni Poletti, Danish Saleheen, Asif Rasheed, Lisa D. Brooks, Adam L. Felsenfeld, Jean E. McEwen, Yekaterina Vaydylevich, Audrey Duncanson, Michael Dunn, Jeffery A. Schloss, 1000 Genomes Project Consortium, Adam Auton, Lisa D. Brooks, Richard M. Durbin, Erik P. Garrison, Hyun Min Kang, Jan O. Korbel, Jonathan L. Marchini, Shane McCarthy, Gil A. McVean, and Gonçalo R. Abecasis. A global reference for human genetic variation. *Nature*, 526(7571):68–74, 2015.
- [24] Olivier Delaneau, Jean-François Zagury, Matthew Robinson, Jonathan Marchini, and Emmanouil Dermitzakis. Integrative haplotype estimation with sub-linear complexity. *bioRxiv*, page 493403, 2018.
- [25] Lucy Huang, Yun Li, Andrew B. Singleton, John A. Hardy, Gonçalo Abecasis, Noah A. Rosenberg, and Paul Scheet. Genotype-imputation accuracy across worldwide human populations. *The American Journal of Human Genetics*, 84(2):235–250, 2009.
- [26] Shane McCarthy, Sayantan Das, Warren Kretzschmar, Olivier Delaneau, Andrew R Wood, Alexander Teumer, Hyun Min Kang, Christian Fuchsberger, Petr Danecek, Kevin Sharp, et al. A reference panel of 64,976 haplotypes for genotype imputation. *Nature genetics*, 48(10):1279, 2016.

- [27] Sharon R. Browning and Brian L. Browning. Rapid and Accurate Haplotype Phasing and Missing-Data Inference for Whole-Genome Association Studies By Use of Localized Haplotype Clustering. *The American Journal of Human Genetics*, 81(5):1084–1097, 2007.
- [28] Marta Byrska-Bishop, Uday S Evani, Xuefang Zhao, Anna O Basile, Haley J Abel, Allison A Regier, André Corvelo, Wayne E Clarke, Rajeeva Musunuri, Kshithija Nagulapalli, et al. High coverage whole genome sequencing of the expanded 1000 genomes project cohort including 602 trios. *bioRxiv*, 2021.
- [29] Heng Li. A statistical framework for snp calling, mutation discovery, association mapping and population genetical parameter estimation from sequencing data. *Bioinformatics*, 27(21):2987–2993, 2011.
- [30] John G Cleary, Ross Braithwaite, Kurt Gaastra, Brian S Hilbush, Stuart Inglis, Sean A Irvine, Alan Jackson, Richard Littin, Sahar Nohzadeh-Malakshah, Mehul Rathod, et al. Joint variant and de novo mutation identification on pedigrees from high-throughput sequencing data. *Journal of Computational Biology*, 21(6):405–419, 2014.
- [31] James Baglama and Lothar Reichel. Augmented implicitly restarted lanczos bidiagonalization methods. *SIAM Journal on Scientific Computing*, 27(1):19–42, 2005.
- [32] Martyn Plummer, Nicky Best, Kate Cowles, and Karen Vines. Coda: convergence diagnosis and output analysis for mcmc. *R News*, 6(1):7–11, March 2006.
- [33] Wolfgang Haak, Iosif Lazaridis, Nick Patterson, Nadin Rohland, Swapan Mallick, Bastien Llamas, Guido Brandt, Susanne Nordenfelt, Eadaoin Harney, Kristin Stewardson, Qiaomei Fu, Alissa Mitnik, Eszter Bánffy, Christos Economou, Michael Francken, Susanne Friederich, Rafael Garrido Pena, Fredrik Hallgren, Valery Khartanovich, Aleksandr Khokhlov,

- Michael Kunst, Pavel Kuznetsov, Harald Meller, Oleg Mochalov, Vayacheslav Moiseyev, Nicole Nicklisch, Sandra L. Pichler, Roberto Risch, Manuel A. Rojo Guerra, Christina Roth, Anna Szécsényi-Nagy, Joachim Wahl, Matthias Meyer, Johannes Krause, Dorcas Brown, David Anthony, Alan Cooper, Kurt Werner Alt, and David Reich. Massive migration from the steppe was a source for Indo-European languages in Europe. *Nature*, 522(7555):207–211, 2015.
- [34] W Haak, P Forster, B Bramanti, S Matsumura, G Brandt, M Tänzer, R Villem, C Renfrew, D Gronenborn, K W Alt, and J Burger. Ancient DNA from the first European farmer in 750-year-old Neolithic sites. *Science*, 310(November):1016–1019, 2005.
- [35] Kay Prüfer, Fernando Racimo, Nick Patterson, Flora Jay, Sriram Sankararaman, Susanna Sawyer, Anja Heinze, Gabriel Renaud, Peter H. Sudmant, Cesare De Filippo, Heng Li, Swapan Mallick, Michael Dannemann, Qiaomei Fu, Martin Kircher, Martin Kuhlwilm, Michael Lachmann, Matthias Meyer, Matthias Ongyerth, Michael Siebauer, Christoph Theunert, Arti Tandon, Priya Moorjani, Joseph Pickrell, James C. Mullikin, Samuel H. Vohr, Richard E. Green, Ines Hellmann, Philip L.F. F Johnson, Hélène Blanche, Howard Cann, Jacob O. Kitzman, Jay Shendure, Evan E. Eichler, Ed S. Lein, Trygve E. Bakken, Liubov V. Golovanova, Vladimir B. Doronichev, Michael V. Shunkov, Anatoli P. Derevianko, Bence Viola, Montgomery Slatkin, David Reich, Janet Kelso, and Svante Pääbo. The complete genome sequence of a Neanderthal from the Altai Mountains. *Nature*, 505(7481):43–49, 2014.
- [36] Augustine Kong, Gisli Masson, Michael L Frigge, Arnaldur Gylfason, Pasha Zusmanovich, Gudmar Thorleifsson, Pall I Olason, Andres Ingason, Stacy Steinberg, Thorunn Rafnar, et al. Detection of sharing by descent, long-range phasing and haplotype imputation. *Nature genetics*, 40(9):1068–1075, 2008.

- [37] Laurent Excoffier and Stefan Schneider. Why hunter-gatherer populations do not show signs of pleistocene demographic expansions. *Proceedings of the National Academy of Sciences*, 96(19):10597–10602, 1999.
- [38] Qiaomei Fu, Cosimo Posth, Mateja Hajdinjak, Martin Petr, Swapan Mallick, Daniel Fernandes, Anja Furtwängler, Wolfgang Haak, Matthias Meyer, Alissa Mittnik, Birgit Nickel, Alexander Peltzer, Nadin Rohland, Viviane Slon, Sahra Talamo, Iosif Lazaridis, Mark Lipson, Iain Mathieson, Stephan Schiffels, Pontus Skoglund, Anatoly P. Derevianko, Nikolai Drovzov, Vyacheslav Slavinsky, Alexander Tsybankov, Renata Grifoni Cremonesi, Francesco Mallegni, Bernard Gély, Eli-gio Vacca, Manuel R. González Morales, Lawrence G. Straus, Christine Neugebauer-Maresch, Maria Teschler-Nicola, Silviu Constantin, Oana Teodora Moldovan, Stefano Benazzi, Marco Peresani, Donato Coppola, Martina Lari, Stefano Ricci, Annamaria Ronchitelli, Frédérique Valentin, Corinne Thevenet, Kurt Wehrberger, Dan Grigorescu, Hélène Rougier, Isabelle Crevecoeur, Damien Flas, Patrick Semal, Marcello A. Mannino, Christophe Cupillard, Hervé Bocherens, Nicholas J. Conard, Katerina Harvati, Vyacheslav Moiseyev, Dorothée G. Drucker, Jiří Svo-boda, Michael P. Richards, David Caramelli, Ron Pinhasi, Janet Kelso, Nick Patterson, Johannes Krause, Svante Pääbo, and David Reich. The genetic history of Ice Age Europe. *Nature*, 534(7606):200–205, 2016.
- [39] Brian L. Browning and Sharon R. Browning. Genotype Imputation with Millions of Reference Samples. *American Journal of Human Genetics*, 98(1):116–126, 2016.
- [40] Ruoyun Hui, Eugenia D’Atanasio, Lara M Cassidy, Christiana L Scheib, and Toomas Kivisild. Evaluating genotype imputation pipeline for ultra-low coverage ancient genomes. *Scientific reports*, 10(1):1–8, 2020.
- [41] David H Alexander, John Novembre, and Kenneth Lange. Fast model-based estimation of ancestry in unrelated individuals. *Genome research*,

- 19(9):1655–1664, 2009.
- [42] Stephen Leslie, Bruce Winney, Garrett Hellenthal, Dan Davison, Abdelhamid Boumertit, Tammy Day, Katarzyna Hutnik, Ellen C. Rorvik, Barry Cunliffe, Daniel J. Lawson, Daniel Falush, Colin Freeman, Matti Pirinen, Simon Myers, Mark Robinson, Peter Donnelly, and Walter Bodmer. The fine-scale genetic structure of the British population. *Nature*, 519(7543):309–314, 2015.
- [43] Shaun Purcell, Benjamin Neale, Kathe Todd-Brown, Lori Thomas, Manuel AR Ferreira, David Bender, Julian Maller, Pamela Sklar, Paul IW De Bakker, Mark J Daly, et al. Plink: a tool set for whole-genome association and population-based linkage analyses. *The American journal of human genetics*, 81(3):559–575, 2007.
- [44] 1000 Genomes Project Consortium et al. A map of human genome variation from population-scale sequencing. *Nature*, 467(7319):1061, 2010.
- [45] Clare Bycroft, Colin Freeman, Desislava Petkova, Gavin Band, Lloyd T Elliott, Kevin Sharp, Allan Motyer, Damjan Vukcevic, Olivier Delaneau, Jared O’Connell, et al. The uk biobank resource with deep phenotyping and genomic data. *Nature*, 562(7726):203–209, 2018.
- [46] Heng Li, Bob Handsaker, Alec Wysoker, Tim Fennell, Jue Ruan, Nils Homer, Gabor Marth, Goncalo Abecasis, and Richard Durbin. The sequence alignment/map format and samtools. *Bioinformatics*, 25(16):2078–2079, 2009.
- [47] Steven J Micheletti, Kasia Bryc, Samantha G Ancona Esselmann, William A Freyman, Meghan E Moreno, G David Poznik, Anjali J Shastri, M Agee, S Aslibekyan, A Auton, et al. Genetic consequences of the transatlantic slave trade in the americas. *The American Journal of Human Genetics*, 107(2):265–277, 2020.

- [48] Nicholas J Conard. A female figurine from the basal aurignacian of hohle fels cave in southwestern germany. *Nature*, 459(7244):248–252, 2009.
- [49] Nicholas J Conard, Maria Malina, and Susanne C Münzel. New flutes document the earliest musical tradition in southwestern germany. *Nature*, 460(7256):737–740, 2009.
- [50] Michael Salter-Townshend and Simon Myers. Fine-Scale Inference of Ancestry Segments Without Prior Knowledge of Admixing Groups. *Genetics*, 212(3):869–889, 05 2019.
- [51] Garrett Hellenthal, George B.J. J. Busby, Gavin Band, James F. Wilson, Cristian Capelli, Daniel Falush, and Simon Myers. A Genetic Atlas of Human Admixture History. *Science*, 343(6172):747–751, 2014.
- [52] Éadaoin Harney, Nick Patterson, David Reich, and John Wakeley. Assessing the performance of qpAdm: a statistical tool for studying population admixture. *Genetics*, 217(4), 01 2021. iyaa045.
- [53] Maïté Rivollat, Choongwon Jeong, Stephan Schiffels, İşil Küçükkalıpçı, Marie-Hélène Pemonge, Adam Benjamin Rohrlach, Kurt W. Alt, Didier Binder, Susanne Friederich, Emmanuel Ghesquière, Detlef Gronenborn, Luc Laporte, Philippe Lefranc, Harald Meller, Hélène Réveillas, Eva Rosenstock, Stéphane Rottier, Chris Scarre, Ludovic Soler, Joachim Wahl, Johannes Krause, Marie-France Deguilloux, and Wolfgang Haak. Ancient genome-wide dna from france highlights the complexity of interactions between mesolithic hunter-gatherers and neolithic farmers. *Science Advances*, 6(22), 2020.
- [54] Mark Lipson, Anna Szécsényi-Nagy, Swapan Mallick, Annamária Pósa, Balázs Stégmár, Victoria Keerl, Nadin Rohland, Kristin Stewardson, Matthew Ferry, Megan Michel, Jonas Oppenheimer, Nasreen Broomand-khoshbacht, Eadaoin Harney, Susanne Nordenfelt, Bastien Llamas,

Balázs Mende Gusztáv, Kitti Köhler, Krisztián Oross, Mária Bondár, Tibor Marton, Anett Osztás, János Jakucs, Tibor Paluch, Ferenc Horváth, Piroska Csengeri, Judit Koós, Katalin Sebok, Alexandra Anders, Pál Raczky, Judit Regenye, Judit P. Barna, Szilvia Fábián, Gábor Serlegi, Zoltán Toldi, Emese Gyöngyvér Nagy, János Dani, Erika Molnár, György Pálfi, László Márk, Béla Melegh, Zsolt Bánfai, László Domboróczki, Javier Fernández-Eraso, José Antonio Mujika-Alustiza, Carmen Alonso Fernández, Javier Jiménez Echevarría, Ruth Bollongino, Jörg Orschiedt, Kerstin Schierhold, Harald Meller, Alan Cooper, Joachim Burger, Eszter Bánffy, Kurt W. Alt, Carles Lalueza-Fox, Wolfgang Haak, and David Reich. Parallel palaeogenomic transects reveal complex genetic history of early European farmers. *Nature*, 551(7680):368–372, 2017.

- [55] Zuzana Hofmanová, Susanne Kreutzer, Garrett Hellenthal, Christian Sell, Yoan Diekmann, David Díez-del Molino, Lucy van Dorp, Saioa López, Athanasios Kousathanas, Vivian Link, Karola Kirsanow, Lara M. Cassidy, Rui Martiniano, Melanie Strobel, Amelie Scheu, Kostas Kotakis, Paul Halstead, Sevi Triantaphyllou, Nina Kyparissi-Apostolika, Dushka Urem-Kotsou, Christina Ziota, Fotini Adaktylou, Shyamalika Gopalan, Dean M. Bobo, Laura Winkelbach, Jens Blöcher, Martina Unterländer, Christoph Leuenberger, Çiler Çilingiroğlu, Barbara Horejs, Fokke Gerritsen, Stephen J. Shennan, Daniel G. Bradley, Mathias Currat, Krishna R. Veeramah, Daniel Wegmann, Mark G. Thomas, Christina Papseorgopoulou, and Joachim Burger. Early farmers from across Europe directly descended from Neolithic Aegeans. *Proceedings of the National Academy of Sciences*, 2016.
- [56] Wolfgang Haak, Oleg Balanovsky, Juan J. Sanchez, Sergey Koshel, Valery Zaporozhchenko, Christina J. Adler, Clio S.I. I der Sarkissian, Guido Brandt, Carolin Schwarz, Nicole Nicklisch, Veit Dresely, Barbara Fritsch, Elena Balanovska, Richard Villem, Harald Meller, Kurt W. Alt, and

- Alan Cooper. Ancient DNA from European early Neolithic farmers reveals their near eastern affinities. *PLoS Biology*, 8(11), 2010.
- [57] Wolfgang Haak, Peter Forster, Barbara Bramanti, Shuichi Matsumura, Guido Brandt, Marc Tänzer, Richard Villems, Colin Renfrew, Detlef Gronenborn, Kurt Werner Alt, et al. Ancient dna from the first european farmers in 7500-year-old neolithic sites. *Science*, 310(5750):1016–1018, 2005.
- [58] Barbara Bramanti, Mark G Thomas, Wolfgang Haak, Martina Unterländer, Pia Jores, Kristiina Tambets, Indre Antanaitis-Jacobs, Miriam N Haidle, Rimantas Jankauskas, C-J Kind, et al. Genetic discontinuity between local hunter-gatherers and central europe's first farmers. *science*, 326(5949):137–140, 2009.
- [59] Eva Fernández, Alejandro Pérez-Pérez, Cristina Gamba, Eva Prats, Pedro Cuesta, Josep Anfruns, Miquel Molist, Eduardo Arroyo-Pardo, and Daniel Turbón. Ancient dna analysis of 8000 bc near eastern farmers supports an early neolithic pioneer maritime colonization of mainland europe through cyprus and the aegean islands. *PLoS genetics*, 10(6):e1004401, 2014.
- [60] Iosif Lazaridis, Dani Nadel, Gary Rollefson, Deborah C. Merrett, Nadin Rohland, Swapan Mallick, Daniel Fernandes, Mario Novak, Beatriz Gamarra, Kendra Sirak, Sarah Connell, Kristin Stewardson, Eadaoin Harney, Qiaomei Fu, Gloria Gonzalez-Fortes, Eppie R. Jones, Songül Alpaslan Roodenberg, György Lengyel, Fanny Bocquentin, Boris Gasparian, Janet M. Monge, Michael Gregg, Vered Eshed, Ahuva Sivan Mizrahi, Christopher Meiklejohn, Fokke Gerritsen, Luminita Bejenaru, Matthias Blüher, Archie Campbell, Gianpiero Cavalleri, David Comas, Philippe Froguel, Edmund Gilbert, Shona M. Kerr, Peter Kovacs, Johannes Krause, Darren McGettigan, Michael Merrigan, D. Andrew Merriwether, Seamus O'Reilly, Martin B. Richards, Ornella Semino, Michel Shamoony-Pour, Gheorghe Stefanescu, Michael Stumvoll, Anke Tönjes, Antonio Torroni,

- James F. Wilson, Loic Yengo, Nelli A. Hovhannisyan, Nick Patterson, Ron Pinhasi, and David Reich. Genomic insights into the origin of farming in the ancient Near East. *Nature*, 536(7617):419–424, 2016.
- [61] Iain Mathieson, Iosif Lazaridis, Nadin Rohland, Swapan Mallick, Nick Patterson, Songül Alpaslan Roodenberg, Eadaoin Harney, Kristin Stewardson, Daniel Fernandes, Mario Novak, Kendra Sirak, Cristina Gamba, Eppie R. Jones, Bastien Llamas, Stanislav Dryomov, Joseph Pickrell, Juan Luís Arsuaga, José María Bermúdez De Castro, Eudald Carbonell, Fokke Gerritsen, Aleksandr Khokhlov, Pavel Kuznetsov, Marina Lozano, Harald Meller, Oleg Mochalov, Vyacheslav Moiseyev, Manuel A.Rojo Guerra, Jacob Roodenberg, Josep Maria Vergès, Johannes Krause, Alan Cooper, Kurt W. Alt, Dorcas Brown, David Anthony, Carles Lalueza-Fox, Wolfgang Haak, Ron Pinhasi, and David Reich. Genome-wide patterns of selection in 230 ancient Eurasians. *Nature*, 528(7583):499–503, 2015.
- [62] Cristina Gamba, Eppie R. Jones, Matthew D. Teasdale, Russell L. McLaughlin, Gloria Gonzalez-Fortes, Valeria Mattiangeli, László Dom-boróczki, Ivett Kővári, Ildikó Pap, Alexandra Anders, Alasdair Whittle, János Dani, Pál Raczkay, Thomas F. G. Higham, Michael Hofreiter, Daniel G. Bradley, and Ron Pinhasi. Genome flux and stasis in a five millennium transect of European prehistory. *Nature Communications*, 5:5257, 2014.
- [63] Mark Lipson, Anna Szécsényi-Nagy, Swapan Mallick, Annamária Pósa, Balázs Stégmár, Victoria Keerl, Nadin Rohland, Kristin Stewardson, Matthew Ferry, Megan Michel, Jonas Oppenheimer, Nasreen Broomand-khoshbacht, Eadaoin Harney, Susanne Nordenfelt, Bastien Llamas, Balázs Gusztáv Mende, Kitti Köhler, Krisztián Oross, Mária Bondár, Tibor Marton, Anett Osztás, János Jakucs, Tibor Paluch, Ferenc Horváth, Piroska Csengeri, Judit Koós, Katalin Sebok, Alexandra Anders, Pál Raczkay, Judit Regenye, Judit P. Barna, Szilvia Fábián, Gábor Serlegi,

Zoltán Toldi, Emese Gyöngyvér Nagy, János Dani, Erika Molnár, György Pálfi, László Márk, Béla Melegh, Zsolt Bátfai, Javier Fernández-Eraso, José Antonio Mujika-Alustiza, Carmen Alonso Fernández, Javier Jiménez Echevarría, Ruth Bollongino, Jörg Orschiedt, Kerstin Schierhold, Harald Meller, Alan Cooper, Joachim Burger, Eszter Bánffy, Kurt W. Alt, Carles Lalueza-Fox, Wolfgang Haak, and David Reich. Parallel ancient genomic transects reveal complex population history of early European farmers. *Nature*, page 114488, 2017.

- [64] Fernando Racimo, Jessie Woodbridge, Ralph M. Fyfe, Martin Sikora, Karl-Göran Sjögren, Kristian Kristiansen, and Marc Vander Linden. The spatiotemporal spread of human migrations during the european holocene. *Proceedings of the National Academy of Sciences*, 117(16):8989–9000, 2020.
- [65] Christine Keyser, Caroline Bouakaze, Eric Crubézy, Valery G Nikolaev, Daniel Montagnon, Tatiana Reis, and Bertrand Ludes. Ancient dna provides new insights into the history of south siberian kurgan people. *Human genetics*, 126(3):395–410, 2009.
- [66] Samantha Brunel, E. Andrew Bennett, Laurent Cardin, Damien Garraud, Hélène Barrand Emam, Alexandre Beylier, Bruno Boulestin, Fanny Chenal, Elsa Ciesielski, Fabien Convertini, Bernard Dedet, Stéphanie Desbrosse-Degobertiere, Sophie Desenne, Jérôme Dubouloz, Henri Duday, Gilles Escalon, Véronique Fabre, Eric Gailledrat, Muriel Gandelin, Yves Gleize, Sébastien Goepfert, Jean Guilaine, Lamys Hachem, Michael Ilett, François Lambach, Florent Maziere, Bertrand Perrin, Suzanne Plouin, Estelle Pinard, Ivan Praud, Isabelle Richard, Vincent Riquier, Réjane Roure, Benoit Sendra, Corinne Thevenet, Sandrine Thiol, Elisabeth Vauquelin, Luc Vergnaud, Thierry Grange, Eva-Maria Geigl, and Mélanie Pruvost. Ancient genomes from present-day france unveil 7,000 years of

- its demographic history. *Proceedings of the National Academy of Sciences*, 117(23):12791–12798, 2020.
- [67] authors. Genetic structure of europeans: a view from the north–east. *PloS one*, 4(5):e5472, 2009.
- [68] Paul M Barford and Paul M Barford. *The early Slavs: culture and society in early medieval Eastern Europe*. Cornell University Press, 2001.
- [69] Paul Fouracre, Rosamond McKitterick, David Abulafia, Timothy Reuter, David Edward Luscombe, CT Allmand, Michael CE Jones, Jonathan Riley-Smith, Michael Jones, et al. *The New Cambridge Medieval History: Volume 1, C. 500-c. 700*. Number 1. Cambridge University Press, 1995.
- [70] Florin Curta, Paul Stephenson, et al. *Southeastern Europe in the middle ages, 500-1250*. Cambridge University Press, 2006.
- [71] Guy Halsall. *Barbarian migrations and the Roman West, 376–568*. Cambridge University Press, 2007.
- [72] Sebastian Brather. *Archäologie der westlichen Slawen: Siedlung, Wirtschaft und Gesellschaft im früh-und hochmittelalterlichen Ostmitteleuropa*, volume 61. Walter de Gruyter, 2008.
- [73] Patrick J Geary. *The myth of nations: the medieval origins of Europe*. Princeton University Press, 2003.
- [74] Martin Gojda. *The ancient Slavs: settlement and society*, volume 1989. Edinburgh University Press, 1991.
- [75] Roland Sussex and Paul Cubberley. *The slavic languages*. Cambridge University Press, 2006.
- [76] Anna Juras, Miroslawa Dabert, Alena Kushniarevich, Helena Malmström, Maanasa Raghavan, Jakub Z. Kosicki, Ene Metspalu, Eske Willerslev, and

- Janusz Piontek. Ancient dna reveals matrilineal continuity in present-day poland over the last two millennia. *PLOS ONE*, 9(10):1–9, 10 2014.
- [77] Kerry L. Shaw. Conflict between nuclear and mitochondrial dna phylogenies of a recent species radiation: What mtDNA reveals and conceals about modes of speciation in hawaiian crickets. *Proceedings of the National Academy of Sciences*, 99(25):16122–16127, 2002.
- [78] Daniel Rubinoff and Brenden S. Holland. Between Two Extremes: Mitochondrial DNA is neither the Panacea nor the Nemesis of Phylogenetic and Taxonomic Inference. *Systematic Biology*, 54(6):952–961, 12 2005.
- [79] Cosimo Posth, Christoph Wißing, Keiko Kitagawa, Luca Pagani, Laura van Holstein, Fernando Racimo, Kurt Wehrberger, Nicholas J Conard, Claus Joachim Kind, Hervé Bocherens, et al. Deeply divergent archaic mitochondrial genome provides lower time boundary for african gene flow into neanderthals. *Nature communications*, 8(1):1–9, 2017.
- [80] Alena Kushniarevich, Olga Utevska, Marina Chuhryaeva, Anastasia Agdzhoyan, Khadizhat Dibirova, Ingrida Uktveryte, Märt Möls, Lejla Mulahasanovic, Andrey Pshenichnov, Svetlana Frolova, Andrey Shanko, Ene Metspalu, Maere Reidla, Kristiina Tambets, Erika Tamm, Sergey Koshel, Valery Zaporozhchenko, Lubov Atramentova, Vaidutis Kučinskas, Oleg Davydenko, Olga Goncharova, Irina Evseeva, Michail Churnosov, Elvira Pocheshchova, Bayazit Yunusbayev, Elza Khusnutdinova, Damir Marjanović, Pavao Rudan, Siiri Roots, Nick Yankovsky, Phillip Endicott, Alexei Kassian, Anna Dybo, The Genographic Consortium, Chris Tyler-Smith, Elena Balanovska, Mait Metspalu, Toomas Kivisild, Richard Villems, and Oleg Balanovsky. Genetic heritage of the balto-slavic speaking populations: A synthesis of autosomal, mitochondrial and y-chromosomal data. *PLOS ONE*, 10(9):1–19, 09 2015.

- [81] Jiří Macháček, Robert Nedoma, Petr Dresler, Ilektra Schulz, Elias Lagonik, Stephen M. Johnson, Ludmila Kaňáková, Alena Slámová, Bastien Llamas, Daniel Wegmann, and Zuzana Hofmanová. Runes from lány (czech republic) - the oldest inscription among slavs. a new standard for multidisciplinary analysis of runic bones. *Journal of Archaeological Science*, 127:105333, 2021.
- [82] Vasili Pankratov, Sergei Litvinov, Alexei Kassian, Dzmitry Shulhin, Lieve Tchepotarev, Bayazit Yunusbayev, Märt Möls, Hovhannes Sahakyan, Levon Yepiskoposyan, Siiri Roots, et al. East eurasian ancestry in the middle of europe: genetic footprints of steppe nomads in the genomes of belarusian lipka tatars. *Scientific reports*, 6(1):1–11, 2016.
- [83] BA Maliarchuk, MA Perkova, and MV Derenko. Origin of the mongoloid component in the mitochondrial gene pool of slavs. *Genetika*, 44(3):401–406, 2008.
- [84] Pengfei Qin, Ying Zhou, Haiyi Lou, Dongsheng Lu, Xiong Yang, Yuchen Wang, Li Jin, Yeun-Jun Chung, and Shuhua Xu. Quantitating and dating recent gene flow between european and east asian populations. *Scientific reports*, 5(1):1–8, 2015.
- [85] Peter Ralph and Graham Coop. The geography of recent genetic ancestry across europe. *PLOS Biology*, 11(5):1–20, 05 2013.
- [86] Hussein Al-Asadi, Desislava Petkova, Matthew Stephens, and John Novembre. Estimating recent migration and population-size surfaces. *PLoS genetics*, 15(1):e1007908, 2019.
- [87] Harald Ringbauer, Graham Coop, and Nicholas H Barton. Inferring recent demography from isolation by distance of long shared sequence blocks. *Genetics*, 205(3):1335–1351, 2017.

- [88] Martin Petr, Benjamin Vernot, and Janet Kelso. admixr—R package for reproducible analyses using ADMIXTOOLS. *Bioinformatics*, 35(17):3194–3195, 01 2019.
- [89] Wladyslaw Duczko. *Viking Rus: studies on the presence of Scandinavians in Eastern Europe*. Brill, 2004.
- [90] Gary Dean Peterson. *Vikings and Goths: A History of Ancient and Medieval Sweden*. McFarland, 2016.
- [91] Krishna R. Veeramah, Andreas Rott, Melanie Groß, Lucy van Dorp, Saioa López, Karola Kirsanow, Christian Sell, Jens Blöcher, Daniel Wegmann, Vivian Link, Zuzana Hofmanová, Joris Peters, Bernd Trautmann, Anja Gairhos, Jochen Haberstroh, Bernd Päffgen, Garrett Hellenthal, Brigitte Haas-Gebhard, Michaela Harbeck, and Joachim Burger. Population genomic analysis of elongated skulls reveals extensive female-biased immigration in Early Medieval Bavaria. *Proceedings of the National Academy of Sciences*, 2018.
- [92] F Lotter. Völkerverschiebungen im ostalpen-mitteldonau-raum zwischen antike und mittelalter (365–600). *Gra Ergänzungsband*, 39, 2003.
- [93] Iosif Lazaridis, Alissa Mitnik, Nick Patterson, Swapan Mallick, Nadin Rohland, Saskia Pfrengle, Anja Furtwängler, Alexander Peltzer, Cosimo Posth, Andonis Vasilakis, et al. Genetic origins of the minoans and mycenaeans. *Nature*, 548(7666):214–218, 2017.
- [94] Garrett Hellenthal, Daniel Falush, Simon Myers, David Reich, George B.J. Busby, Mark Lipson, Cristian Capelli, and Nick Patterson. The Kalash Genetic Isolate? the Evidence for Recent Admixture. *American Journal of Human Genetics*, 98(2):396–397, 2016.
- [95] Krishna R Veeramah, Anke Tönjes, Peter Kovacs, Arnd Gross, Daniel Wegmann, Patrick Geary, Daniela Gasperikova, Iwar Klimes, Markus

- Scholz, John Novembre, et al. Genetic variation in the sorbs of eastern germany in the context of broader european genetic diversity. *European Journal of Human Genetics*, 19(9):995–1001, 2011.
- [96] Ashot Margaryan, Daniel J Lawson, Martin Sikora, Fernando Racimo, Simon Rasmussen, Ida Moltke, Lara M Cassidy, Emil Jørsboe, Andrés Ingason, Mikkel W Pedersen, et al. Population genomics of the viking world. *Nature*, 585(7825):390–396, 2020.
- [97] Morten E. Allentoft, Martin Sikora, Karl Göran Sjögren, Simon Rasmussen, Morten Rasmussen, Jesper Stenderup, Peter B. Damgaard, Hannes Schroeder, Torbjörn Ahlström, Lasse Vinner, Anna Sapfo Malaspinas, Ashot Margaryan, Tom Higham, David Chivall, Niels Lynnerup, Lise Harvig, Justyna Baron, Philippe Della Casa, Paweł Dąbrowski, Paul R. Duffy, Alexander V. Ebel, Andrey Epimakhov, Karin Frei, Mirosław Furmanek, Tomasz Gralak, Andrey Gromov, Stanisław Gronkiewicz, Gisela Grupe, Tamás Hajdu, Radosław Jarysz, Valeri Kharlanovich, Alexandr Khokhlov, Viktória Kiss, Jan Kolář, Aivar Kriiska, Irena Lasak, Cristina Longhi, George McGlynn, Algimantas Merkevicius, Inga Merkyte, Mait Metspalu, Ruzan Mkrtchyan, Vyacheslav Moiseyev, László Paja, György Pálfi, Dalia Pokutta, Łukasz Pospieszny, T. Douglas Price, Lehti Saag, Mikhail Sablin, Natalia Shishlina, Václav Smrčka, Vasili I. Soenov, Vajk Szeverényi, Gusztáv Tóth, Synaru V. Trifanova, Lívia Varul, Magdolna Vicze, Levon Yepiskoposyan, Vladislav Zhitenev, Ludovic Orlando, Thomas Sicheritz-Pontén, Søren Brunak, Rasmus Nielsen, Kristian Kristiansen, and Eske Willerslev. Population genomics of Bronze Age Eurasia. *Nature*, 2015.
- [98] Farnaz Broushaki, Mark G. Thomas, Vivian Link, Saioa López, Lucy van Dorp, Karola Kirsanow, Zuzana Hofmanová, Yoan Diekmann, Lara M. Cassidy, David Díez-del Molino, Athanasios Kousathanas, Christian Sell, Harry K. Robson, Rui Martiniano, Jens Blöcher, Amelie Scheu,

- Susanne Kreutzer, Ruth Bollongino, Dean Bobo, Hossein Davoudi, Olivia Munoz, Mathias Currat, Kamyar Abdi, Fereidoun Biglari, Oliver E. Craig, Daniel G. Bradley, Stephen Shennan, Krishna R. Veeramah, Marjan Mashkour, Daniel Wegmann, Garrett Hellenthal, and Joachim Burger. Early Neolithic genomes from the eastern Fertile Crescent. *Science*, 2016.
- [99] Lara M. Cassidy, Rui Martiniano, Eileen M. Murphy, Matthew D. Teasdale, James Mallory, Barrie Hartwell, and Daniel G. Bradley. Neolithic and bronze age migration to ireland and establishment of the insular atlantic genome. *Proceedings of the National Academy of Sciences*, 113(2):368–373, 2016.
- [100] Peter de Barros Damgaard, Nina Marchi, Simon Rasmussen, Michaël Peyrot, Gabriel Renaud, Thorfinn Korneliussen, J Víctor Moreno-Mayar, Mikkel Winther Pedersen, Amy Goldberg, Emma Usmanova, et al. 137 ancient human genomes from across the eurasian steppes. *Nature*, 557(7705):369–374, 2018.
- [101] Torsten Günther, Cristina Valdiosera, Helena Malmström, Irene Ureña, Ricardo Rodriguez-Varela, Óddny Osk Sverrisdóttir, Evangelia A Daskalaki, Pontus Skoglund, Thijessen Naidoo, Emma M Svensson, et al. Ancient genomes link early farmers from atapuerca in spain to modern-day basques. *Proceedings of the National Academy of Sciences*, 112(38):11917–11922, 2015.
- [102] Eppie R. Jones, Gloria Gonzalez-Fortes, Sarah Connell, Veronika Siska, Anders Eriksson, Rui Martiniano, Russell L. McLaughlin, Marcos Gallego Llorente, Lara M. Cassidy, Cristina Gamba, Tengiz Meshveliani, Ofer Bar-Yosef, Werner Müller, Anna Belfer-Cohen, Zinovi Matskevich, Nino Jakeli, Thomas F.G. Higham, Mathias Currat, David Lordkipanidze, Michael Hofreiter, Andrea Manica, Ron Pinhasi, and Daniel G. Bradley. Upper Palaeolithic genomes reveal deep roots of modern Eurasians. *Nature Communications*, 6:1–8, 2015.

- [103] Nina Marchi, Laura Winkelbach, Ilektra Schulz, Maxime Brami, Zuzana Hofmanová, Jens Blocher, Carlos S Reyna-Blanco, Yoan Diekmann, Alexandre Thiéry, Adamandia Kapopoulou, et al. The mixed genetic origin of the first farmers of europe. *bioRxiv*, 2020.
- [104] Inigo Olalde, Morten E Allentoft, Federico Sánchez-Quinto, Gabriel Santpere, Charleston WK Chiang, Michael DeGiorgio, Javier Prado-Martinez, Juan Antonio Rodríguez, Simon Rasmussen, Javier Quilez, et al. Derived immune and ancestral pigmentation alleles in a 7,000-year-old mesolithic european. *Nature*, 507(7491):225–228, 2014.
- [105] Federico Sánchez-Quinto, Helena Malmström, Magdalena Fraser, Linus Girdland-Flink, Emma M Svensson, Luciana G Simões, Robert George, Nina Hollfelder, Göran Burenhult, Gordon Noble, et al. Megalithic tombs in western and northern neolithic europe were linked to a kindred society. *Proceedings of the National Academy of Sciences*, 116(19):9469–9474, 2019.
- [106] Andaine Seguin-Orlando, Thorfinn S. Korneliussen, Martin Sikora, Anna-sapfo Malaspinas, Andrea Manica, Ida Moltke, Michael Westaway, David Lambert, Valeri Khartanovich, Jeffrey D Wall, Philip R Nigst, and Robert A Foley. Genomic structure in Europeans dating back at least 36 , 200 years. *Science*, 346(6213):1113–1118, 2014.
- [107] Stephen Sawcer, Garrett Hellenthal, Matti Pirinen, Chris C.A. Spencer, Nikolaos A. Patsopoulos, Loukas Moutsianas, Alexander Dilthey, Zhan Su, Colin Freeman, Sarah E. Hunt, Sarah Edkins, Emma Gray, David R. Booth, Simon C. Potter, An Goris, Gavin Band, Annette Bang Oturai, Amy Strange, Janna Saarela, Céline Bellenguez, Bertrand Fontaine, Matthew Gillman, Bernhard Hemmer, Rhian Gwilliam, Frauke Zipp, Alagurevathi Jayakumar, Roland Martin, Stephen Leslie, Stanley Hawkins, Eleni Giannoulatou, Sandra D’Alfonso, Hannah Blackburn, Filippo Martinelli Boneschi, Jennifer Liddle, Hanne F. Harbo, Marc L.

Perez, Anne Spurkland, Matthew J. Waller, Marcin P. Mycko, Michelle Ricketts, Manuel Comabella, Naomi Hammond, Ingrid Kockum, Owen T. McCann, Maria Ban, Pamela Whittaker, Anu Kemppinen, Paul Weston, Clive Hawkins, Sara Widaa, John Zajicek, Serge Dronov, Neil Robertson, Suzannah J. Bumpstead, Lisa F. Barcellos, Rathi Ravindrarajah, Roby Abraham, Lars Alfredsson, Kristin Ardlie, Cristin Aubin, Amie Baker, Katharine Baker, Sergio E. Baranzini, Laura Bergamaschi, Roberto Bergamaschi, Allan Bernstein, Achim Berthele, Mike Boggild, Jonathan P. Bradfield, David Brassat, Simon A. Broadley, Dorothea Buck, Helmut Butzkueven, Ruggero Capra, William M. Carroll, Paola Cavalla, Elisabeth G. Celius, Sabine Cepok, Rosetta Chiavacci, Françoise Clerget-Darpoux, Kathleen Clysters, Giancarlo Comi, Mark Cossburn, Isabelle Cournu-Rebeix, Mathew B. Cox, Wendy Cozen, Bruce A.C. Cree, Anne H. Cross, Daniele Cusi, Mark J. Daly, Emma Davis, Paul I.W. De Bakker, Marc Debouverie, Marie Beatrice D'Hooghe, Katherine Dixon, Rita Dobosi, Bénédicte Dubois, David Ellinghaus, Irina Elovaara, Federica Esposito, Claire Fontenille, Simon Foote, Andre Franke, Daniela Galimberti, Angelo Ghezzi, Joseph Glessner, Refujia Gomez, Olivier Gout, Colin Graham, Struan F.A. Grant, Franca Rosa Guerini, Hakon Hakonarson, Per Hall, Anders Hamsten, Hans Peter Hartung, Rob N. Heard, Simon Heath, Jeremy Hobart, Muna Hoshi, Carmen Infante-Duarte, Gillian Ingram, Wendy Ingram, Talat Islam, Maja Jagodic, Michael Kabesch, Allan G. Kermode, Trevor J. Kilpatrick, Cecilia Kim, Norman Klopp, Keijo Koivisto, Malin Larsson, Mark Lathrop, Jeannette S. Lechner-Scott, Maurizio A. Leone, Virpi Leppä, Ulrika Liljedahl, Izaura Lima Bomfim, Robin R. Lincoln, Jenny Link, Jianjun Liu, Aslaug R. Lorentzen, Sara Lupoli, Fabio MacCiardi, Thomas MacK, Mark Marriott, Vittorio Martinelli, Deborah Mason, Jacob L. McCauley, Frank Mentch, Inger Lise Mero, Tania Mihalova, Xavier Montalban, John Mottershead, Kjell Morten Myhr, Paola Naldi, William Ollier, Alison Page, Aarno

Palotie, Jean Pelletier, Laura Piccio, Trevor Pickersgill, Fredrik Piehl, Susan Pobywajlo, Hong L. Quach, Patricia P. Ramsay, Mauri Reunanen, Richard Reynolds, John D. Rioux, Mariaemma Rodegher, Sabine Roesner, Justin P. Rubio, Ina Maria Rückert, Marco Salvetti, Erika Salvi, Adam Santaniello, Catherine A. Schaefer, Stefan Schreiber, Christian Schulze, Rodney J. Scott, Finn Sellebjerg, Krzysztof W. Selmaj, David Sexton, Ling Shen, Brigid Simms-Acuna, Sheila Skidmore, Patrick M.A. Sleiman, Cathrine Smestad, Per Soelberg Sørensen, Helle Bach Søndergaard, Jim Stankovich, Richard C. Strange, Anna Maija Sulonen, Emilie Sundqvist, Ann Christine Syvänen, Francesca Taddeo, Bruce Taylor, Jenefer M. Blackwell, Pentti Tienari, Elvira Bramon, Ayman Tourbah, Matthew A. Brown, Ewa Tronczynska, Juan P. Casas, Niall Tubridy, Aiden Corvin, Jane Vickery, Janusz Jankowski, Pablo Viloslada, Hugh S. Markus, Kai Wang, Christopher G. Mathew, James Wason, Colin N.A. Palmer, Erich Wichmann, Robert Plomin, Ernest Willoughby, Anna Rautanen, Juliane Winkelmann, Michael Wittig, Richard C. Trembath, Jacqueline Yaouancq, Ananth C. Viswanathan, Haitao Zhang, Nicholas W. Wood, Rebecca Zuvich, Panos Deloukas, Cordelia Langford, Audrey Duncanson, Jorge R. Oksenberg, Margaret A. Pericak-Vance, Jonathan L. Haines, Tomas Ols-son, Jan Hillert, Adrian J. Ivinson, Philip L. De Jager, Leena Peltonen, Graeme J. Stewart, David A. Hafler, Stephen L. Hauser, Gil McVean, Peter Donnelly, and Alastair Compston. Genetic risk and a primary role for cell-mediated immune mechanisms in multiple sclerosis, 2011.